Dirección de Formación Académica

Programa de Doctorado en Ciencias (Óptica)

Metodologías para el Diseño Óptico de Instrumentos de Imaginología Retiniana con Óptica Adaptativa.

Tesis como requisito para obtener el grado de:

Doctor en Ciencias (Óptica)

Presenta

M.C. Armando Gómez Vieyra

Asesor:

Dr. Daniel Malacara Hernández

León, Guanajuato, México. Diciembre 2010

Dirección de Formación Académica

Programa de Doctorado en Ciencias (Óptica)

Metodologías para el Diseño Óptico de Instrumentos de Imaginología Retiniana con Óptica Adaptativa.

Tesis como requisito para obtener el grado de:

Doctor en Ciencias (Óptica)

Presenta

M.C. Armando Gómez Vieyra

Asesor:

Dr. Daniel Malacara Hernández

León, Guanajuato, México. Diciembre 2010

Leer y entender es algo;
leer y sentir es mucho;
leer y pensar es cuanto puede desearse.
Anónimo

Qué cada paso sea una meta,
sin dejar de ser paso.
Goethe

Contenido

Lista de Tablas

Lista de Figuras

Abstract

The development of retinal imaging has taken place during the last 25 years, since the invention of scanning laser ophthalmoscopes (SLO) by Webb and his colleagues at MIT in 1980, and the incorporation of optical coherence tomographers (OCT) to study ocular structures. Unfortunately, one of the major limitations in the resolution of these instruments is the effect of eye aberrations, which were no fully understood. Subsequently, active optics was used to compensate for the astigmatism of a person and the development of the Shack-Hartmann sensor to measure ocular aberrations in real time. With these tools, it was possible to start working with ophthalmic systems based on adaptive optics. The incorporation of adaptive optics (AO) to ophthalmic imaging instruments such as fundus cameras, SLOs and OCTs, increased axial and lateral resolution of these instruments.

Scanning instruments with adaptive optics are typically based on optical reflection in order to eliminate unwanted reflections produced by the refractive elements, which can become comparable in magnitude to the light reflected or scattered by the retina. Current clinical instruments use different parts of the eye pupil to illuminate and capture the image in order to avoid these problems, but this is not possible in AO instruments, because they limit axial and lateral resolution, wasting the capabilities of the instruments. Current AO scanning instruments use spherical mirrors (in off-axis arrangements to access the conjugate planes of the pupil of the eye), mainly because their low cost and easy alignment. Typical configurations used in these systems are afocal telescopes and simple mirrors in an Abbe aplanatic configuration to get the conjugate planes of both the pupil of the eye and the retinal image.

Most of these systems have a high degree of astigmatism in their design, and even Webb suggested folding a plane in the optical system to compensate the astigmatism. An analytical approach to systematize the design of these instruments had not been proposed. In this study, we analytically demonstrate Webb's proposal by breaking the symmetry plane of afocal telescopes. It was found that with the union of two telescopes, one can compensate for the two conjugate planes (eye pupil and retina).

Furthermore, we show that it is possible to compensate for the astigmatism at the retinal image plane, using only mirrors as relays in the Abbe aplanatic configuration, but without the compensation of astigmatism in the pupil of the eye. This demonstrates that you can make mixed designs, i.e. afocal telescopes and aplanatic configurations mirrors are used together in order to obtain systems under the diffraction limit.

To understand all aberrations present in the systems that are not centered, off-axis, non symmetric and reflective, the coefficients of the wavefront aberration of an off-axis spherical mirror are analyzed based on the Fermat principle. The results presented in this thesis can also be applied to laser resonators and spectrographs

Resumen

El desarrollo de la imaginología retiniana ha tenido un gran avance en los últimos 25 años, desde la aparición de los oftalmoscopios por escaneo laser (SLO), creado por Webb y sus colaboradores en el MIT en 1980, así como la incorporación de los tomógrafos por coherencia óptica (OCT) al estudio de las estructuras oculares. Desafortunadamente una de las mayores limitantes en resolución de estos instrumentos son los efectos de las aberraciones propias del ojo, que no eran comprendidas completamente. Posteriormente, se empleo de óptica activa para compensar el astigmatismo propio de cada individuo y se desarrollo el sensor Hartmann-Shack para medición de aberraciones oculares en tiempo real. Con estas dos herramientas fue posible iniciar el trabajo con sistemas oftálmicos basados en óptica adaptativa. La incorporación de la óptica adaptativa (AO) a los instrumentos de imaginología oftálmica, como las cámaras de fondo de ojo, los SLOs y los OCTs, ha incrementado la resolución axial y lateral de estos instrumentos.

Los instrumentos de escaneo con óptica adaptativa están basados típicamente en óptica de reflexión con el fin de eliminar reflejos indeseables que producen los elementos refractivos, que pueden llegar a ser comparables en magnitud con la luz reflejada o esparcida por la retina. Los instrumentos clínicos actuales usan diferentes partes de la pupila del ojo para iluminar y capturar la imagen con el propósito de evitar estos problemas. Pero esto no es posible en los instrumentos de AO, debido a que limitaríamos nuestra resolución axial y lateral, desaprovechando las capacidades de los instrumentos. Los instrumentos actuales de escaneo con AO usan espejos esféricos (en arreglos fuera de eje para tener acceso los planos conjugados de la pupila de ojo), principalmente por su bajo costo y su fácil alineamiento. Las configuraciones típicas empleadas en estos sistemas son los telescopios afocales y espejos simples en configuración de Abbe para obtener los planos conjugados, tanto de la pupila del ojo, como de la imagen retiniana.

La mayoría de estos sistemas presenta un alto grado de astigmatismo al ser diseñados, y aunque Webb sugirió compensar el astigmatismo sacando del plano algún elemento óptico del sistema, no se tenía un tratamiento analítico que permitiera sistematizar el diseño de estos instrumentos. En esta investigación demostramos analíticamente lo propuesto por Webb, rompiendo el plano de simetría en telescopios afocales. Encontrando que con la unión de dos telescopios es posible compensar dos planos conjugados a la vez.

Además demostramos que es posible compensar el astigmatismo en el plano de la imagen retiniana, empleando como relevadores únicamente espejos en configuración aplanática de Abbe, pero sin la compensación de astigmatismo en la pupila del ojo. Se demuestra que se pueden realizar diseños mixtos, es decir, donde se emplean telescopios afocales y espejos en configuraciones de Abbe para poder obtener diseños bajo limite de difracción.

Para lograr entender todas las aberraciones presentes en los sistemas no centrados, no simétricos y fuera de eje reflexivos, se analizan los coeficientes de aberración del frente de onda de un espejo esférico fuera de eje basados en el principio de Fermat. Los resultados presentados pueden ser aplicados también en resonadores láser y espectrógrafos.

Agradecimientos

Este es el final de un largo camino académico que no he recorrido solo, donde muchas personas me han apoyado y acompañado a través de estos 25 años de vida, es un triunfo compartido. Me permitiré mencionar brevemente a las personas que han tenido más influencia en mi educación durante estos últimos seis años de mi vida (dos de maestría y cuatro de doctorado). De antemano pido una disculpa a cualquier persona que haya sido omitida.

Primeramente, agradezco al Dr. Daniel Malacara Hernández por haber aceptado ser mi asesor, tanto de maestría como de doctorado, cuando yo era un completo ignorante de maravilloso mundo de la óptica. El Dr. Malacara ha compartido su vasta experiencia, me ha tenido una paciencia infinita, me ha apoyado y soportado constantemente durante mi estancia en el Centro de Investigaciones en Óptica (CIO), mostrándome sobre todo que en la sencillez engrandece aun más nuestra persona y nuestro trabajo. A quien le debo la mayor parte de mi formación en el campo de la óptica, así como todas las facilidades proporcionadas por él, la Dirección de Formación Académica del CIO, y el Consejo de Ciencia y Tecnología para desarrollar mi investigación en México y en el extranjero.

Me gustaría agradecer muy en especial a los Drs. Zacarías Malacara Hernández y Ricardo Benjamín Flores Hernández por tomarse el tiempo de apoyarme y resolver mis constantes dudas sobre el campo de la óptica. Además debo agradecer al Dr. Rufino Díaz Uribe, por tener la amabilidad y paciencia de ser evaluador de mi trabajo doctoral.

Al Dr. Luis Carlos Álvarez Núñez, Dr. Julio Cesar Estrada, Dr. Jorge Luis Márquez, Dr. Jesús Rafael Moya Cessa y M.C. José Enrique A. Landgrave Manjarez por todas las discusiones y experiencias que enriquecieron mi trabajo y formación.

Al laboratorio de Óptica de la Universidad de Murcia (LOUM), dirigido por el Dr. Pablo Artal, por los cuatro meses que pase con ustedes, donde me introduje al fascinante mundo del estudio del ojo (ciencias de la visión) y la óptica adaptativa. Agradezco el apoyo desinteresado de Pablo Artal, Pedro Prieto (gracias por responder todas mis dudas sobre el sensor Hartman-Shack), Juan Bueno (gracias por tu explicación de los efectos de polarización en el ojo y los extraordinarios momentos a la hora de la comida), Brian Vohnsen (ahora en Irlanda), Linda Lundström (en Suecia), Joshua Fernández, Juan Tabernero, Esther Berrio, Elloy Villegas, Antonio Benito, Carmen Cánovas, Encarna Alarcón, Guillermo Pérez, Diego Ayala, Alejandro Mira, Astrid Duque, Bart Jaequen y Silvestre Manzanares (por todo el intercambio de información tanto escrita como oral).

Y como olvidar mi estancia en la Universidad de Rochester:

It has been a privilege to have the opportunity to work with many talented individuals at the University of Rochester. David Williams, my host advisor, has been an incredible mentor, teacher and friend during my stay. I would like to thank the Williams family for many enjoyable parties and summer camp. Interactions with fellow students and postgraduates at the University of Rochester have also been invaluable; many thanks to Melissa (Ying Geng), Ben Marsella, Lu Yin, Yusufu Salai, Zach Harvey, Jen Hunter, and Jen Norris for all your time and knowledge. The staff at the Center for Visual Science was an incredible resource, literally supporting all aspects of my visit (Debbi Shannon, Marina Fabian, Teresa Williams). And finally, I've been fortunate to have a strong collaboration with Alfredro Dubra Suarez, who suggest the subject for this work and whom I appreciate as a teacher and a friend (aunque no la pasemos peleando la mitad del tiempo, en verdad admire cuanto amas tu trabajo, y como buscas cosas e ideas nuevas, aunque no las entiendas completamente en lo que te metes, pero es admirable).

Es importante darle un reconocimiento especial Luis Díaz Santana por la sugerencia del estudio de configuraciones aplanáticas de Abbe para este trabajo. También tengo que agradecer a una persona con la que conviví muchos fines de semana en Rochester, que ha tenido el gran gesto de leer y opinar sobre la escritura de la tesis y mucho de mi trabajo, gracias Aixa Alarcón (Universidad de Granada).

Además quisiera agradecer a las autoridades y empleados el CIO con los que conviví durante mis estudios. En especial, en el departamento de formación académica, a la Lic. Guillermina Muñiz Palancares y todas sus muchachas, por el apoyo recibido durante todos estos años, a la Dra. Reina Duarte, al personal de Biblioteca y centro de cómputo. En vinculación y desarrollo tecnológico, me gustaría agradecer a nuestros compañeros de taller óptico y mecánico por todo su apoyo y enseñanzas. En el área de investigación, tengo mucho que agradecer a todos los miembros de la comunidad de Investigadores del CIO de los cuales he aprendido a valorar el esfuerzo personal y colectivo. También me gustaría agradecer a la Srita. Marissa Vázquez por todo el tiempo, trabajo y apoyo proporcionado durante mi estancia con el Dr. Malacara, así como a todas las personas que han pasado por el Laboratorio de Interferometría. Es importante agradecer al personal de servicios generales y área de sistemas (sin ellos se caería esta institución). Al Lic. Mario Ruiz por las revisiones de mis textos en ingles, así como la resolución de mis frecuentes dudas gramaticales.

Mi respeto y amistad a todos mis compañeros de posgrado con quienes he crecido como persona, he pasado momentos inolvidables durante mi estancia en esta institución. En especial me gustaría agradecer a Irma L. Villegas, Dinora Guzmán, Susana Vargas, Jose Luis Cabellos, Jesús Jiménez, Cornelio Álvarez, Haggeo Dessirena, Mauricio Flores, Claudio Ramírez, Daniel Aguayo, Edgar Saucedo, David Solís, Victor Arellano, Guillermo Huerta, Flavio Ruiz, Adonaí Gonzales, Tonatihu Rangel, Miguel Vallejo, Jorge Parra, Lelio de la Cruz, Octavio Meza, Guillermo Cárdenas, Luis Adán, Luis Escalante, Maximiliano Galán, Marco Escobar, Jorge Oliva, Rubén Grajales, y muchos más. Además debo agradecer Raymundo Mendoza y su familia, Isidro Saldaña, Aron Serrano y Martin Olmos, por todo el tiempo que me permitieron compartir con ellos y hacer más agradable mi estancia en León.

A mis amigos que siempre han estado ahí para oírme, alentarme y regañarme.

Al CONACYT por la beca para realizar mis estudios de posgrado.

Finalmente no tengo palabras para agradecer a mis padres, a mis abuelos, a mi hermana y el resto de mi familia por estar ahí siempre. Y a quienes dedico este trabajo.

CAPÍTULO 1

Introducción a la imaginología retiniana.

Uno de los aspectos más relevantes en la supervivencia de cada especie animal es el sistema ocular. El interés por el estudio del sistema ocular, ha llevado al desarrollo de instrumentos cada vez más avanzados, que permitan analizar sus diversas estructuras celulares, tanto en-vivo como ex-vivo. Una rama de estos instrumentos son los sistemas de imaginología retiniana, que permiten estudiar las estructuras celulares que componen la retina en-vivo. En el presente capítulo expondremos brevemente la historia y los aspectos básicos que han llevado al desarrollo de los instrumentos de última generación en este campo, los cuales emplean óptica adaptativa como núcleo principal para su funcionamiento. Describiremos sus características generales y los retos actuales en el diseño e implementación de estos instrumentos.

1.1 EL SISTEMA OCULAR

El ojo (humano o animal), uno de los órganos biológicos más exquisitamente desarrollados en toda la naturaleza [Horridge, 1977; Land y Nilsson, 2002; Rodieck, R.W., 1998], transmite información del mundo que lo rodea al cerebro para poder realizar la detección de la intensidad de luz, la discriminación del color y la interpretación de los objetos observados. La complejidad de la estructura y funcionamiento depende de cada especie del reino animal y el hábitat que lo rodea [Land y Nilsson, 2002]. Pero como todo sistema óptico, el ojo presenta imperfecciones. Durante mucho tiempo, se ha tenido la inquietud de entender los procesos físico-químico-biológicos que se desarrollan durante el proceso de la visión, en especial en el ojo humano (Fig. 1.1). Esto ha marcado al trabajo de innumerables investigadores de todas las áreas del conocimiento a través de los siglos.

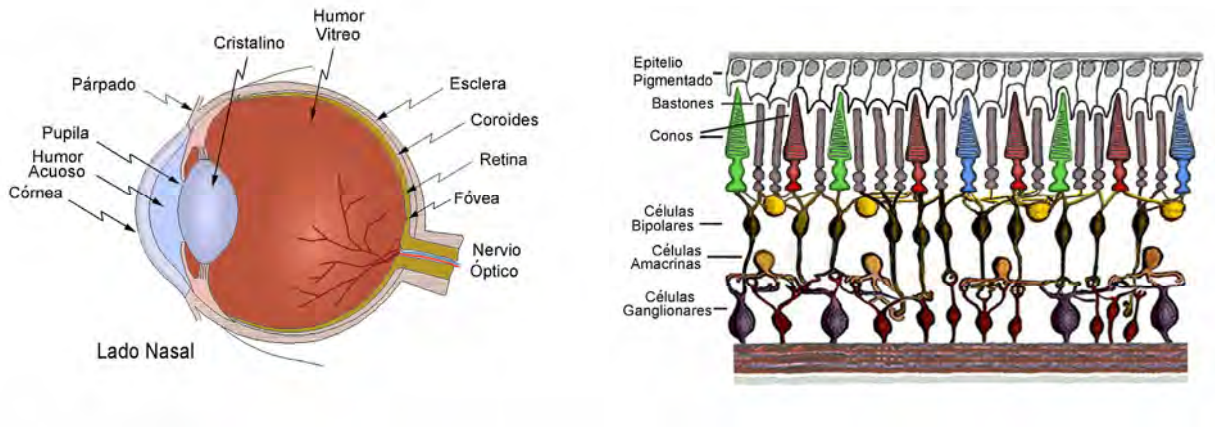

Figura 1.1.- Estructura interna del ojo humano (izquierda) y capa retiniana (derecha). Cortesía del Dr. Daniel Malacara.

Los instrumentos empleados en el estudio del sistema ocular son muy diversos, descritos en forma general por Smith y Atchinson [1997]. Estos instrumentos presentan características y cualidades diversas, debido a que el sistema ocular (Fig. 1.1) tiene una gran complejidad. Las propiedades del sistema ocular humano pueden ser encontradas en diversos textos, como el escrito por Atchison y Smith [2000], así como sus implicaciones en la optometría [Rabbetts, 2006]. Una introducción al campo de la percepción visual es presentada por Schwartz [2004],

descrito desde un punto de vista interdisciplinario. Si se desea una visión más general puede revisarse el Handbook of Optics Vol. 3 [2010], editado por la Optical Society of America, que exploran todas las áreas que constituyen el campo de Ciencias de la Visión.

El estudio de las estructuras oculares es complejo debido a que el ojo presenta propiedades fisicoquímicas muy específicas dadas por su naturaleza biológica. Estas estructuras y propiedades del tejido ocular han sido estudiadas principalmente en especímenes ex-vivo; como consecuencia se conocen muchas de las propiedades fisicoquímicas que permiten el estudio de los tejidos, tanto independientemente como en conjunto. Sin embargo existen propiedades que limitan los estudios en-vivo, como son las aberraciones ópticas del ojo [Howland y Howland, 1977; Campbell, 1966; Artal y Navarro, 1994; Artal et al., 1993; Guirao et al., 1993; McLellan et al., 2002; Artal et al., 2002]. En años recientes se ha incrementado el interés en la interacción de diversos factores ópticos en el proceso de la percepción visual, así como la implementación de metodologías adecuadas para el estudio a nivel biológico in-vivo. Diversos grupos de investigación se han orientado a desarrollar las metodologías, instrumentos y software necesario para poder estudiar en-vivo las estructuras retinianas compensando las aberraciones del ojo en cada sujeto. Una de estas metodologías es la integración de la óptica adaptativa a los sistemas de imaginología retiniana, implementada por primera vez en la Universidad de Rochester hacia mediados de los 90s. A continuación revisaremos brevemente la evolución de la imaginología retiniana.

1.2 IMAGINOLOGÍA RETINIANA

El mayor obstáculo para obtener la imagen del interior del ojo en-vivo es la fracción de luz que se refleja en el interior del ojo y llega al detector. La reflectancia de salida del ojo es del orden de 0.1% al 10% dependiendo la longitud de onda (400 a700 μm) [van Norren y Tiemei, 1986; Delori y Pflibsen, 1989] y las restricciones impuestas por la pupila del ojo en la cantidad de luz que puede salir del interior, afectan en un factor de 100, aproximadamente. Estos dos factores reducen la luz que retorna a través de la pupila a ordenes de 10^{-3} – 10^{-5} dependiendo de la

longitud de onda. Punkinje observó que sobre ciertas condiciones la pupila del ojo podía dar un aspecto más luminoso que oscuro [Purkinje, 1823; Kruta, 1969]. Brücke [1847] demostró que el brillo en la pupila producido por la luz de la flama de una vela que apuntaba hacia el ojo podía ser estudiado a través de un tubo. Helmholtz [1851] revolucionó el campo de la oftalmología con la invención del oftalmoscopio. El llamó a su invención el "Augenspiegel" (espejo del ojo). Jackman y Webster [1886] obtuvieron las primeras fotografías de una retina humana en vivo al instalar la cámara fotográfica en la cabeza del paciente para reducir el movimiento de la imagen durante la exposición de 2.5 minutos requerida para obtener la imagen. Subsecuentemente, las cámaras de fondo de ojo fueron mejorándose mediante el bloqueo de los reflejos no deseados de la superficie de la córnea, aumentando la sensibilidad de la película fotográfica y la integración de una lámpara electrónica de flash, que permitió que las exposiciones fueran lo suficientemente breves para evitar el movimiento del ojo, evitando así imágenes borrosas.

El oftalmoscopio por escaneo laser (scanning laser ophtalmoscope, SLO) inventado por Robert Webb et al. [1980] permitió el uso de detectores, como fotodiodos de avalancha y tubos fotomultiplicadores, lo que incrementó la sensibilidad de los sistemas de imaginología retiniana mas allá de lo que podía lograrse con las películas fotográficas. El uso del barrido láser en estos instrumentos, en lugar de iluminación con flash, proporcionó la ventaja adicional de obtener imágenes en tiempo real. Por otra parte, el instrumento pudo ser equipado con un pinhole confocal para seleccionar la imagen del plano de interés y eliminar la luz proveniente de otras estructuras, proporcionando la capacidad de selección óptica. La aplicación de la tomografía por coherencia óptica (optical coherence tomography, OCT) permitió mejorar la resolución axial [Fercher et al., 1988; Huang et al., 1991], obteniendo resoluciones axiales tan altas como de 1 a 3µm en-vivo [Drexler et al., 2001].

Miller et al. [1996] construyeron una cámara de fondo de ojo de alta amplificación capaz de iluminar la retina con luz incoherente, siendo la primera vez que pudieron observar estructuras celulares retinianas en-vivo, aunque este instrumento sólo funcionaba con ojos jóvenes y de buena calidad óptica. Dando paso al desarrollo de sistemas de imaginología con óptica

adaptativa.

1.3 LA ÓPTICA ADAPTATIVA

La óptica adaptativa (adaptive optics, AO) fue desarrollada en astrónomia, con la finalidad de compensar las distorsiones atmosféricas debidas a las variaciones de las condiciones climatológicas que limitaban la resolución de los telescopios (fluctuaciones en el índice de refracción atmosférico). Diversas técnicas fueron evolucionando tanto para medir las aberraciones atmosféricas como para compensarlas, lográndose una mayor resolución angular y un aumento en la resolución de las imágenes estelares al mitigar los efectos de la turbulencia atmosférica. El primero en proponer la corrección en tiempo real usando OA fue Babcock [1953]. Sin embargo, mucha de esta tecnología fue mantenida en secreto por el gobierno estadunidense, hasta 1978 cuando la fuerza aérea estadunidense lo dió a conocer por primera vez. El lector puede consultar los libros de Tyson [2000], Hardy [1998] o Roddier [1999] para mayor profundidad en el tema.

Un sistema de óptica adaptativa es un sistema que es capaz de medir, calcular y compensar las aberraciones en lazo cerrado para poder obtener la mejor imagen posible. Un esquema general es mostrado en la Fig. 1.2. En esta se puede observar que consta de un compensador del frente de onda, que por lo general es un espejo deformable; un sensor de frente de onda, que dependiendo de la aplicación puede ser un sensor piramidal (basado en la prueba de Foucault), una prueba de la estrella o un sensor Hartmann-Shack (ampliamente usado en ciencias de la visión), además de un sistema de control lazo cerrado (no mostrado en la figura) que es el cerebro del sistema y finalmente el sistema de imaginología que puede ser una cámara CCD, un sistema de tomografía óptica, un espectroscopio o un microscopio confocal dependiendo de la aplicación.

Pese a su origen militar, los sistemas de óptica adaptativa se han integrado a los sistemas de microscopia óptica aplicados a biología [Booth, 2002; Kam, 2001], a los oftalmoscopios, a las

cámaras de fondo de ojo [Liang et al., 1997, Roorda et al., 2002],a los sistemas de tomografía por coherencia óptica [Hermann et al., 2004; Miller et al., 2005],a los láseres [Kudryashov et al., 2005], y a los sistemas de imaginología multifocal [Johnson, 1994]. Esta gran integración conlleva a problemas específicos para el diseño e ingeniería de estos sistemas.

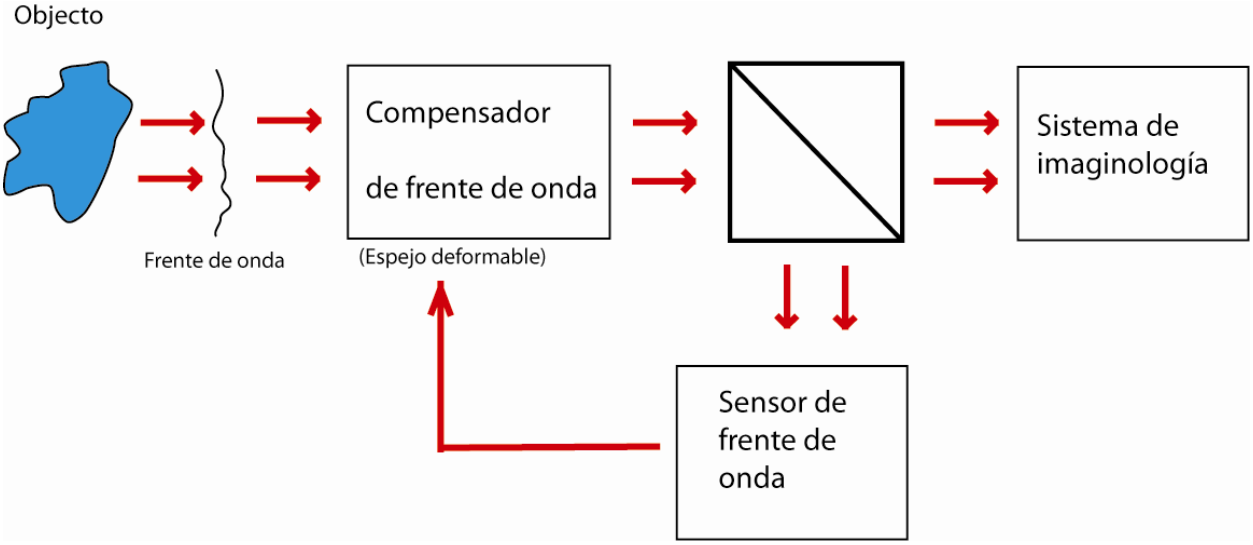

Figura 1.2.- Diagrama a bloques de un sistema de óptica adaptativa.

1.4 LA ÓPTICA ADAPTATIVA EN CIENCIAS DE LA VISION

Una aplicación especialmente promisoria de la óptica adaptativa (OA) es la imaginología de alta resolución retiniana en-vivo [Porter et al., 2006]. Los investigadores en visión y los oftalmólogos han estado interesados por largo tiempo en la imaginología de estructuras celulares retinianas vivas para examinar sus propiedades en-vivo y poder caracterizar más eficazmente las degeneraciones maculares. Pero el ojo humano sufre de aberraciones de alto orden, introducidas principalmente por la córnea y el cristalino, que degradan la calidad de la imagen retiniana y limitan la visión espacial. Smirnov[1965] fue el primero en sugerir la corrección de las aberraciones de alto orden para mejorar la calidad del ojo humano.

En 1989, Dreher et al. fueron los primeros en usar un espejo deformable para mejorar la calidad

de las imágenes retinianas, con la corrección del astigmatismo del ojo mediante un método subjetivo. Además, como se mencionó anteriormente, las primeras imágenes de estructuras celulares retinianas simples en un ojo humano en-vivo fueron obtenidas por Miller et al. [1996], corrigiendo únicamente aberraciones de bajo orden. La limitación de estas primeras investigaciones era la falta de un sensor que permitiera caracterizar las aberraciones de alto orden con la precisión adecuada y en tiempo real. La situación cambió abruptamente cuando Junhong Liang [1994], trabajando como estudiante de doctorado en el laboratorio de Joseph Bille, en la Universidad de Heidelberg, demostró que era posible adaptar un sensor Hartmann-Shack (Shack-Hartmann, SH) para medir aberraciones hasta décimo orden dependiente del número de microlentes que contenga. El sensor SH es típicamente usado en metrología óptica, en la medición de las aberraciones de frente de onda. La simplicidad de la prueba de Hartmann-Shack y su popularidad en sistemas AO astronómica dio por consecuencia su traslado a la medición de las aberraciones en sistemas oculares.

Esta innovación, adaptada a una cámara de fondo de ojo de alta resolución, permitió corregir las aberraciones del ojo en tiempo real mediante un espejo deformable y obtener un aumento substancial en la resolución de las imágenes retinianas en-vivo [Liang et al., 1997]. Esta tecnología ha evolucionado desde las cámaras de fondo de ojo con AO, dependiente del desarrollo de otras tecnologías de óptica activa, hasta integrarse a otro tipo de instrumentos oftalmológicos ya existentes, los oftalmoscopios confocales por escaneo láser y los tomógrafos de coherencia óptica, dando lugar al AOSLO [Roorda et al., 2002] y el AOOCT [Hermann et al., 2004; Miller et al., 2005]. Además, recientemente se han integrado técnicas de fluorescencia y auto-fluorescencia que han permitido observar estructuras celulares ganglionares [Gray et al., 2006] y pigmento retino epiteliales [Morgan et al., 2008]. Sin embargo, como discutiremos más adelante, estos instrumentos presentan algunos problemas, de tipo científico-tecnológicos, para poder ser integrados al ámbito clínico.

Las ventajas que ofrece la AOSLO sobre las AO cámaras de fondo de ojo son la mayor eficiencia en la colección de la luz y el aumento en la velocidad de captura de imágenes. Adicionalmente,

si se agrega un módulo de detección confocal, resultan imágenes de mayor contraste. La incorporación de la AO al SLO incrementa tanto la resolución axial como lateral. Por otro lado, de todos los aparatos imaginológicos, el OCT es quizás el de más rápido desarrollo. Estos instrumentos tienen un poder de resolución de aproximadamente 25µm lateral y 10 µm axial, pero presentan un nivel pobre de resolución para cualquier estructura retiniana. Como se mencionó anteriormente, investigadores de la universidad de Viena y Murcia combinaron el OCT con OA en lazo cerrado [Hermann y otros, 2004] para obtener resoluciones de 5 a 10 µm lateral y 3µm axiales. De esta forma, se logró recrear visualizaciones de imágenes en 3D de la estructura retiniana, donde las limitaciones son la estructura biológica de la retina y los movimientos naturales e involuntarios del ojo.

Adicionalmente, se ha creado una tecnología híbrida entre imaginología con AO y la imaginología por procesamiento de imágenes (teoría de la deconvolución) que proporciona una mejora en la razón señal a ruido [Arines y Bara, 2003], obteniendo un mayor factor de contraste y un incremento en la visibilidad [Christou y otros, 2004].

1.5 PRINCIPALES PROBLEMAS EN EL DISEÑO DE SISTEMAS DE IMAGINOLOGÍA RETINIANA CON OPTICA ADAPTATIVA

Como se ha descrito anteriormente, el desarrollo de las cámaras de fondo de ojo con AO, AOSLO y AOOCT lleva poco más de 15 años de investigación. Pero todavía existen limitantes tecnológicas e ingenieriles para poder llevar esta tecnología a la siguiente etapa, el uso clínico. Existen diversos factores que influyen, pero desde nuestro punto de vista los principales son:

- Los estudios oftalmológicos requieren múltiples longitudes de onda y/o múltiples planos imagen. Es necesario, por lo tanto, el empleo de distintos láseres, algunos no existentes en el mercado, así como diseños ópticos eficientes que permitan la integración de subsistemas por módulos (un diseño óptico flexible).

- Aumentar la sensibilidad de los sensores de frente de onda y la corrección de los sistemas de óptica adaptativa. Este es un problema de dependencia tecnológica, presente principalmente en los dispositivos ópticos, electro-ópticos y optoelectrónicos.

- Además de los problemas en el diseño óptico de estos sistemas, que constituyen un problema por la presencia de un gran astigmatismo.

Tomando este último punto, hemos realizado una investigación en colaboración con la Universidad de Rochester y el Colegio Universitario de Londres, para entender las aberraciones presentes en las configuraciones más empleadas en estos sistemas y desarrollar métodos sistemáticos para el diseño óptico de estos instrumentos. Los resultados obtenidos de esta investigación son presentados en las secciones subsecuentes. Por último nos gustaría agregar, que en esta área existen otras limitantes impuestas por la velocidad de procesamiento de imágenes y la estructura biológica de los pacientes, como tendencia a síndrome de ojo seco, cataratas o los movimientos involuntarios de los ojos (microsacadas). Estas limitaciones no han sido incluidas en este trabajo.

1.6 REFERENCIAS

Arines, J., Bara, S., "Hybrid technique for high resolution imaging of the eye fundus," *Opt. Express.* **11** (2003) 761-766.

Artal, P., Berrio, E., Guirao, A., Piers, P., "Contribution of the Cornea and Internal Surfaces to the Change of Ocular Aberrations with Age," *J. Opt. Soc. Am. A.* **19** (2002) 137-143.

Artal, P., Ferro, M., Miranda, I., Navarro, R., "Effects of Aging in Retinal Image Quality," *J. Opt. Soc. Am. A.* **10** (1993) 1656-1662.

Artal, P., Navarro, R., "Monochromatic Modulation Transfer Function of the Human Eye for Different Pupil Diameters: An Analytical Expression," *J. Opt. Soc. Am. A.* **11** (1994) 246-249.

Atchinson, D.A. y Smith, G. (2000), *Optics of the Human Eye.* USA: Butterworth Heinemann

Babcock, H.W., "The Possibility of Compensating Astronomical Seeing," *Pub. Astr. Soc. Pac.* **65** (1953) 229–236.

Bass, M., Enoch, J.M., Lakshminarayanan, V. (2010), *Handbook of Optics Volumen III Vision and Vision Optics.* USA: Mc Graw Hill.

Booth, M.J., Neil, M.A.A., Juskaitis, R., Wilson, T., "Adaptive aberration correction in a confocal microscope," *Proc. Natl Acad. Sci.* **99** (2002) 5789-5792.

Brücke E.W. (1847), Anatomische Beschreibung des Menschlichen Augapfels. Berlin: G. Reimer.

Campbell, F.W., Gubisch, R.W., "Optical Quality of the Human Eye," *J. Physiol.* **186** (1966) 558–578.

Christou, J.C., Roorda, A., Williams, D.R., "Deconvolution of Adaptive Optics Retinal Images," *J. Opt. Soc. Am. A.* **21** (2004) 1393-1401.

Delori, F.C., Pflibsen, K.P., "Spectral Reflectance of the Human Ocular Fundus," *Appl. Opt.* **28** (1989) 1061-1077.

Dreher, A.W., Bille, J.F., Weinreb, R.N., "Active Optical Depth Resolution Improvement of the Laser Tomographic Scanner," *Appl. Opt.* **28** (1989) 804-808.

Drexler, W, Morgner U, Ghanta RK, Kärtner FX, Schuman JS, Fujimoto JG. "Ultrahigh-Resolution Ophthalmic Optical Coherence Tomography," *Nat. Med.***7** (2001) 502–507.

Fercher, A.F., Mengedoht, K., Werner W., "Eye Length Measurement by Interferometry with Partially Coherent Light," *Opt. Lett.* **13** (1988) 186-188.

Gray, D., Merigan, W., Wolfing, J., Gee, B., Porter, J., Dubra, A., Twietmeyer, T., Ahmad, K., Tumbar, R., Reinholz, F., Williams, D.R., "In vivo fluorescence imaging of primate retinal ganglion cells and retinal pigment epithelial cells," *Opt. Express.* **14** (2006) 7144-7158.

Guirao, A., Gonzalez, C., Redondo, M., Geraghty, E., Norrby, S., Artal, P., "Average Optical Performance of the Human Eye as a Function of Age in a Normal Population," *Invest. Ophthalmol. Vis. Sci.* **40** (1999) 203–213.

Hardy, J.W. (1998), *Adaptive Optics for Astronomical Telescopes.* USA: Oxford

Hardy, W.H. (1998), *Adaptive Optics for Astronomical Telescopes.* USA: Oxford University Press.

Helmholtz, H. L. F. (1851) *Beschreibung eines Augen-Spiegels zur Untersuchung der Netzhaut im lebenden Auge* [Description of an eye mirror for the investigation of the retina of the living eye]. Berlin: A Förstner'sche Verlagsbuchhandlung.

Hermann, B., Fernandez, E.J., Unterhuber, A., et al., "Adaptive-Optics Ultrahigh-Resolution Optical Coherence Tomography," *Opt. Lett.* **29** (2004) 2142–2144.

Horridge, G. A., "The Compound Eye of Insects," *Sci. Am.* (Julio, 1977) 108–120.

Howland, H.C. y Howland, B. A., “Subjective Method for the Measurement of Monochromatic Aberrations of the Eye,” *J. Opt. Soc. Am. A.* **67** (1977) 1508–1518.

Huang, D., Swanson, E.A., Lin C.P., et al. “Optical Coherence Tomography,” *Science.* **254** (1991) 1178–1181.

Jackman, W.T., Webster, J.D., “On Photographing the Retina of the Living Human Eye,” *Philadelphia Photographer*. **23** (1886) 340–341.

Johnston, D.C., Welsh, B. M., "Analysis of multiconjugate adaptive optics," *J. Opt. Soc. Am. A* **11** (1994) 394-408.

Kam, Z., Hanser, B., Gustafsson, M.G., Agard, D. A., Sedat, J.W. “Computational adaptive optics for live three-dimensional biological imaging.” Proc. Natl Acad. Sci. **98** (2001) 3790-3795.

Kruta, V. (1969) *J.E. Purkyne (1787–1869) Physiologist A Short Account of His Contributions to the Progress of Physiology with a Bibliography of His Works*. Prague: Academia, Publishing House of the Czechoslovak Academy of Sciences.

Kudryashov, A., Samarkin, V., Alexandrov, A., Rukosuev, A., Zavalova, V. (2005) Adaptive Optics for High-Power Laser Beam Control, Germany: Springer.

Land, M. F. y Nilsson, D.E. (2002), *Animal Eyes.* UK: Oxford.

Liang, J., Williams, D.R., “Aberrations and Retinal Image Quality of the Normal Human Eye,” *J. Opt. Soc. Am. A.* **14** (1997) 2873–2883.

Liang, J., Williams, D.R., Miller, D., “Supernormal Vision and High-Resolution Retinal Imaging through Adaptive Optics,” *J. Opt. Soc. Am. A.* **14** (1997) 2884–2892.

McLellan, J.S., Marcos, S., Prieto, P.M., Burns, S.A., “Imperfect Optics May Be the Eye’s Defense Against Chromatic Blur,” *Nature* **417** (2002) 174–176.

Miller, D.T., Williams, D.R., Morris, G.M., Liang, J., “Images of Cone Photoreceptors in the Living Human Eye,” *Vision Res.* **36** (1996) 1067–1079.

Morgan, J.I.W., Hunter, J.J., Masella, B., Wolfe, R., Gray, D.C., Merigan, W.H., Delori, F.C., William, D.R., “Light induced retinal changes observed with high resolution autofluorescence imaging of the retinal pigment epithelium,” *IOVS* **49** (2008) 3715-3729.

Porter, J, et al. (2006), *Adaptive optics for vision science: principles, practices, design and applications*. USA; Wiley.

Purkinje J. (1823) *Beobachtungen und Versuche zur Physiologie der Sinne* [Observations and Experiments Investigating the Physiology of Senses]. Erstes Bändchen. Beiträge zur Kenntniss des Sehens in subjectiver Hinsicht. Prague: Calve.

Rabbetts, R. B. (2006), *Bennett and Rabbetts’ Clinical Visual Optics.* USA: Butterworth Heinemann

Roddier, F. (1999), *Adaptive optics in astronomy.* UK: Cambridge University Press.

Rodieck, R. W. (1998), *The first steps in seeing.* USA: Sinauer Associates

Roorda, A., Romero-Borja, F., Donnelly, W.J., et al., "Adaptive Optics Laser Scanning Ophthalmoscopy," *Opt. Express.* **10** (2002) 405–412.

Schwartz, S. H. (2004), *Visual Perception a Clinical Orientation.* USA: McGraw-Hill

Smirnov, M.S., "Measurement of the Wave Aberration of the Human Eye," *Biophysics.* **6** (1961) 776–795.

Smith, G. y Atchinson, D.A. (1996), *The Eye and the Visual Optical Instruments.* USA: Cambridge University Press

Tyson, R.K. (2000), *Adaptive Optics Engineering Handbook.* USA: Marcel Dekker.

van Norren, D., Tiemeijer, L.F., "Spectral Reflectance of the Human Eye," *Vision Res.* **26** (1986) 313–320.

Webb, R.H., Hughes, G.W., Pomerantzeff, O., "Flying Spot TV Ophthalmoscope," *Appl. Opt.* **19** (1980) 2991–2997.

Zhang, Y., Rha, J., Jonnal, R.S., Miller D.T., "Adaptive Optics Parallel Spectral Domain Optical Coherence Tomography for Imaging the Living Retina," *Opt. Express.* **13** (2005) 4792-4811.

CAPÍTULO 2

Representación de aberraciones de frente de onda.

Las aberraciones de los sistemas ópticos son usualmente analizadas por la descomposición de las aberraciones de frente de onda en la pupila, en términos de series polinómicas. Existen diversas familias de polinomios empleadas en la representación de las aberraciones de onda, de las cuales nos centraremos en Seidel, Zernike, Stephenson y una propuesta por nosotros. En este capítulo exploraremos los conceptos esenciales de las aberraciones ópticas y analizaremos las características de las diversas representaciones de las aberraciones de frente de onda.

Un sistema óptico es un conjunto de componentes (espejos, lentes, prismas, etc.) dispuestas de tal manera que modifican la trayectoria de la luz. La Fig. 2.1 muestra un sistema óptico como una caja negra donde ocurren una serie de interacciones representadas por una función de transferencia $G(x,y)$. Al pasar la luz emitida por un objeto o fuente luminosa $(F(x,y))$ por el sistema óptico, se obtendrá una imagen $H(x,y)$ de éste, como resultado de la interacción de la luz con el sistema óptico.

El descubrimiento de la fotografía en 1839 por Daguerre fue el principal impulso para extender la teoría gaussiana, concentrando el interés de las investigaciones en la construcción de objetivos de telescopio, con la finalidad de producir objetivos que tuvieran una gran apertura numérica y amplios campos de visión. Petzval, impulsó el empleo de métodos y cálculos matemáticos en el diseño de sistemas ópticos; desafortunadamente, la mayor parte de su trabajo se perdió. Posteriormente, Seidel presentó un tratamiento sistemático para el análisis de aberraciones geométricas de primer orden [Born y Wolf, 1999]. Desde esa época muchos investigadores han contribuido en el desarrollo de la teoría de las aberraciones geométricas y sus efectos en la calidad de las imágenes ópticas.

2.1 FORMACIÓN DE IMÁGENES

Un sistema óptico forma una imagen perfecta cuando todos los rayos procedentes del mismo punto en el plano objeto, llegan a un solo punto en el plano imagen, equivalentemente, cuando el frente de onda geométrico en la pupila de salida tiene forma esférica centrada en el punto imagen (Fig. 2.2).

Figura 2.1 Representación esquemática de un sistema óptico

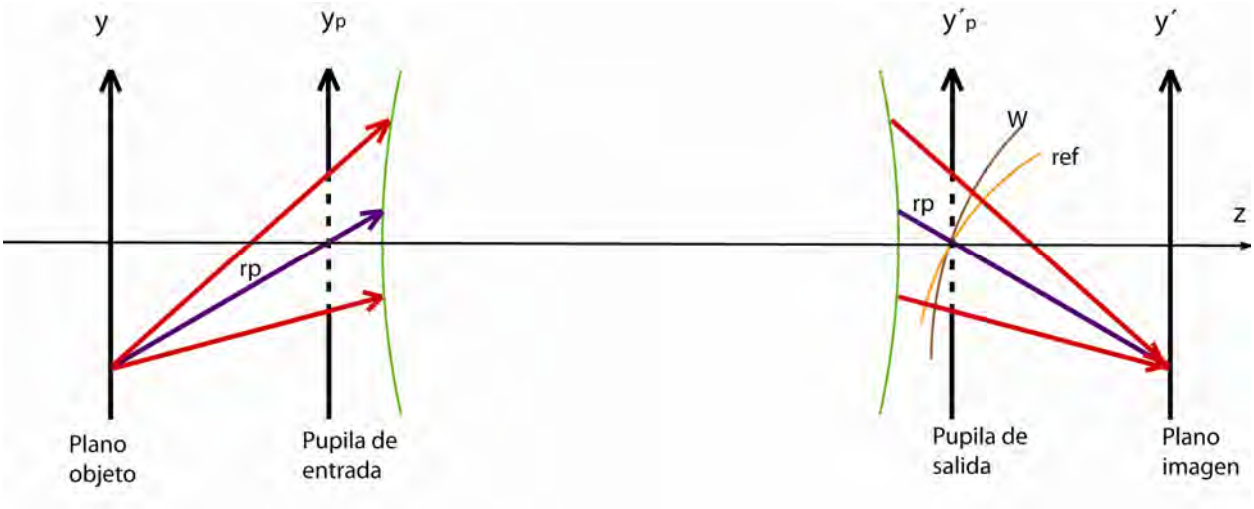

Figura 2.2.- Proceso de la formación de imágenes.

Lord Rayleigh presentó una prueba matemática que deberían cumplir los sistemas ópticos que producen una imagen perfecta, es decir, los caminos ópticos (CO) para cada uno de los rayos que conectan un punto del objeto a su correspondiente punto en la imagen (puntos conjugados) deben ser iguales (principio de Fermat). Las únicas superficies que pueden satisfacer esta condición rigurosamente son el óvalo cartesiano y las secciones cónicas en pares conjugados. Esta situación nunca se satisface para un sistema óptico real con superficies ópticas esféricas, con excepción de los puntos aplanáticos de Abbe en arreglos centrados y en eje, o para las secciones ovales y cónicas fuera de su par de puntos conjugados (el único elemento óptico que exhibe la imagen ideal, estigmática, para todos los pares de puntos conjugados es el espejo plano, que tiene su distancia focal en el infinito). Esto nos lleva considerar las desviaciones de la imagen estigmática, llamadas aberraciones. Las aberraciones reducen la calidad de la imagen en un sistema óptico, por esta razón, el propósito principal en el proceso del diseño óptico es reducir las aberraciones a un nivel satisfactorio para el sistema óptico, lo que lleva a comprender la naturaleza de las aberraciones y conocer sus propiedades.

2.2 FRENTE DE ONDA DE REFERENCIA

El frente de onda de referencia es un frente de onda idealizado matemáticamente, donde su centro de curvatura se encuentra centrado en la intersección del plano imagen con el rayo principal. Además, el frente de onda de referencia debe contener el punto donde el rayo principal cruza la pupila de salida. Las características empleadas para definir el frente de onda esférico de referencia son definidas por la distancia a lo largo del rayo principal, de la pupila de salida al plano imagen, define el radio de curvatura de la esfera de referencia. Si la forma del frente de onda real es igual a la esfera de referencia, el sistema óptico formará una imagen perfecta sobre cualquier punto del plano imagen, es decir, una imagen estigmática.

2.3 LA FUNCIÓN DE ABERRACIÓN

Posiblemente la forma más elegante para derivar la teoría de las aberraciones sea a través la función característica del sistema, en otras palabras el empleo de la óptica hamiltoniana. Pero también se pueden aplicar métodos geométricos y trigonométricos que son los más empleados en la actualidad, en el campo de la óptica, para la descripción de la teoría de aberraciones.

La desviación del frente de onda real, en la pupila de salida, respecto a la esfera o frente de onda de referencia se describe matemáticamente por un conjunto de funciones conocidas como aberraciones. La desviación Δy puede determinarse con ayuda de la Fig. 2.3. El radio de la esfera de referencia (R) es la distancia a lo largo del rayo principal de la pupila de salida a la superficie de la imagen. Todos los rayos normales a la esfera de referencia deberán converger a este punto y formar una imagen geométrica ideal del punto objeto. En cambio, si el rayo es normal al frente de onda real (W) en algún punto en la pupila de salida no formará una imagen geométrica ideal. En general, un rayo arbitrario no será normal al mismo tiempo a la esfera de la referencia y al frente de onda real. Es decir, el punto de intersección del rayo arbitrario en la

superficie de la imagen no estará en el punto de la imagen ideal. Δy indica la distancia del punto de intersección del rayo real respecto de la posición ideal en el plano *y*-*x*. La aberración es descrita por Rayces [Born y Wolf, 1999] como:

$$\Delta y = \frac{R}{n}\frac{dW}{dy}\frac{\cos\theta}{\cos(\theta+\alpha)} \tag{2.1}$$

Donde el término W representa la aberración de frente de onda, Δy representan las aberraciones transversales y R representa el radio de la esfera de referencia. El índice de refracción *n* puede aproximarse a 1(1.00029 en condiciones normales) en el aire.

Una medida similar se realiza en el plano *x*-*y*. En las regiones donde las aberraciones son pequeñas, el ángulo α es pequeño; $\cos\theta$ y $\cos(\theta+\alpha)$ son casi iguales (Fig. 2.3), por lo que las aberraciones son aproximadamente:

$$\Delta y = -\frac{R}{n}\frac{dW}{dy} \quad \text{y} \quad \Delta x = -\frac{R}{n}\frac{dW}{dx} \tag{2.2}$$

Las Ecs. 2.2 muestran que hay dos componentes de las aberraciones, siendo éstas cantidades vectoriales. Por lo tanto, las aberraciones se definen completamente cuando consideramos las direcciones x y y, llamadas aberraciones transversales (Δ). De forma que

$$\Delta = -\frac{R}{n}\nabla\overline{W} \tag{2.3}$$

Una propiedad muy importante de las aberraciones de frente de onda es su característica aditiva en sistemas multielementos, sin embargo, esta propiedad no se extrapola a las aberraciones de rayo.

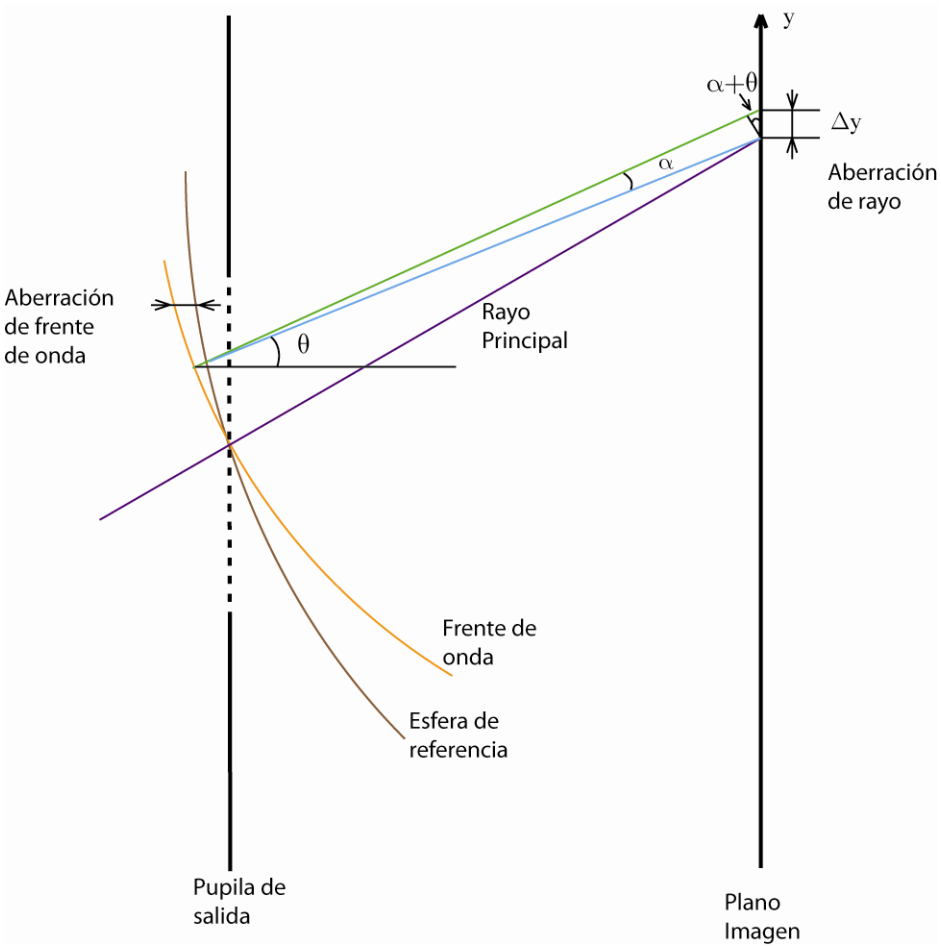

Figura 2.3. Aberración de rayo y de frente de onda.

Las aberraciones longitudinales (Δl), aberraciones axiales de rayo, describen la separación entre imágenes diferentes formadas por rayos diferentes y medidas a lo largo del eje óptico; están definidas por:

$$\Delta l \cong \frac{1}{nu^2}\nabla\overline{W}, \tag{2.4}$$

Donde u es el seno del ángulo del rayo marginal paraxial.

Después de haber definido las relaciones entre las distintas formas de establecer las aberraciones de un sistema óptico, es conveniente hablar de las imágenes que son más

representativas y sus características cuando el objeto y la imagen están fuera de eje. Por simplicidad consideremos un solo espejo como se muestra en la Fig 2.4, donde se forma una imagen puntual. Si el espejo fuera un elipsoide de revolución, el objeto y su imagen perfecta se encontrarán en los focos del elipsoide.

Pero si el espejo en la Fig. 2.4, es esférico, formara diversas imágenes, que definen diversas superficies dependientes del ángulo de incidencia. La superficie imagen más simple de hallar es el plano gaussiano determinado por la teoría gaussiana. La imagen gaussiana para configuraciones fuera de eje sufre un pequeño defoco con respecto a la mejor imagen obtenida (suponiendo que solo tenemos aberración esférica), sin embargo la superficie de Petzval es introducida para compensar este error. Pero si consideramos una pupila pequeña donde sólo tenemos presente aberración esférica y astigmatismo, se pueden definir claramente diversas superficies definidas por los distintos haces marginales, donde las más importantes son las superficies formadas a partir de los rayos tangenciales y sagitales, como se muestra en la Fig 2.5.

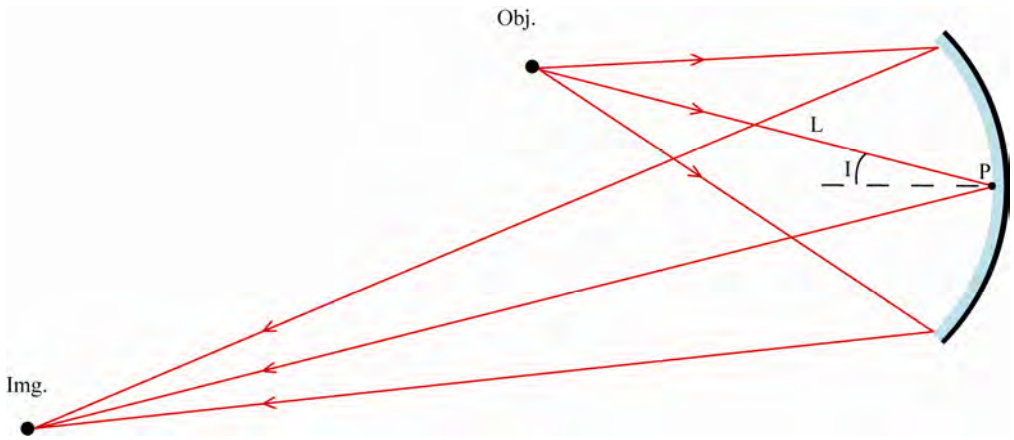

Figura 2.4.- Espejo fuera de eje, caso ideal.

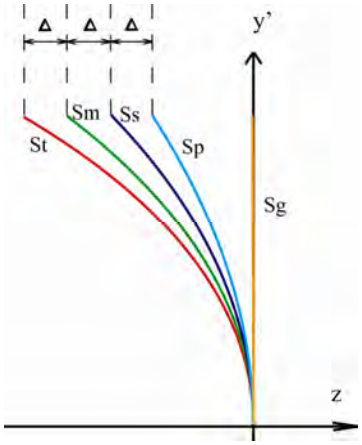

Figura 2.5.- Superficies de las imágenes gaussiana (*Sg*), Petzval (*Sp*), sagital (*Ss*), media(*Sm*) y tangencial (*St*)

A partir de estas superficies se pueden analizar las diversas representaciones de las aberraciones de frente de onda, debido a que cada una de las representaciones se define por la localización del centro de la esfera de referencia, definiendo así los términos individuales de cada aberración.

De forma general, sin considerar ninguna simetría, el frente de onda puede ser descrito por

$$W = T_1 + T_2 x + T_3 y + T_4 x^2 + T_5 xy + T_6 y^2 + T_7 x^3 + T_8 x^2 y + T_9 xy^2 + T_{10} y^3 + T_{11} x^4 + T_{12} x^3 y + T_{13} x^2 y^2 + T_{14} xy^3 + T_{15} y^4 + \text{aberraciones de alto orden} \quad (2.5)$$

Donde x y y son las coordenadas en la pupila de salida. Esta descripción del frente de onda en monomios nos permite clasificar los coeficientes de aberración en las subcategorías enunciadas en la Tabla 2.1.

Es decir, la tabla anterior nos muestra los coeficientes de las componentes de aberración de un sistema asimétrico, donde algunos de estos coeficientes son cero si el sistema óptico es simétrico. Si fuera necesario, la función W puede ser representado en coordenadas polares mediante la sustitución:

$$x = \rho \sin\theta \tag{2.6}$$

$$y = \rho \cos\theta \tag{2.7}$$

Donde θ es la coordenada angular medida con respecto al eje y, y ρ es el radio vector, como se muestra en la Fig. 2.6.

Tabla 2.1 Clasificación de los coeficientes monomiales con respecto a las aberraciones ópticas clásicas.

T_1	Pistón
T_2, T_3	Inclinación (Prismático o distorsión)
T_4, T_5, T_6	Defoco y astigmatismo
T_7, T_8, T_9, T_{10}	Coma
$T_{11}, T_{12}, T_{13}, T_{10}, T_{14}$	Esférica

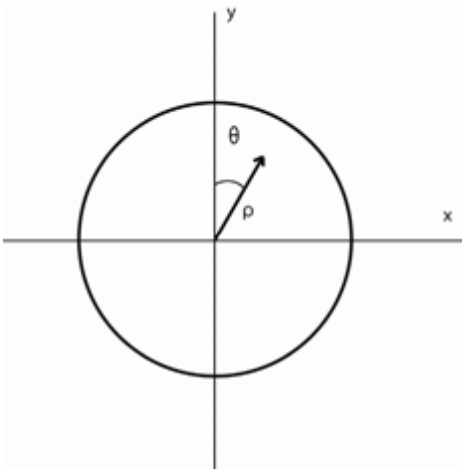

Figura 2.6.- Representación de la forma cartesiana y polar de las coordenadas de la pupila de salida

Como se mencionó anteriormente, algunos sistemas ópticos poseen simetría rotacional, en especial cuando todos los planos meridionales son coplanarios, aunque también hay

asimétricos como aquellos donde los sistemas tienen dos o más planos meridionales denominados no coplanarios. Debido a estas diferencias en los sistemas ópticos, se han definido diversos conjuntos de polinomios (Tabla 2.2) [Malacara y otros, 1992, 2004, 2005; Stephenson, 2009; Gómez y Malacara 2010; Mahajan, 1998] de acuerdo a diversas condiciones y características enunciadas en la Tabla 2.3

Tabla 2.2 Primeros términos de las representaciones del frente de onda en términos polinomiales.

Seidel	Nuestra representación	Zernike (ortogonal)	Stephenson	
1	1	1	1	Pistón
x	x	x	x	Inclinación x
y	y	y	y	Inclinación y
-----	-----	$2xy$	$2xy$	Astigmatismo 45°
x^2+y^2	x^2+y^2	$2\left(x^2+y^2\right)-1$	x^2+y^2	Desenfoque
x^2+3y^2	y^2-x^2	y^2-x^2	y^2-x^2	Astigmatismo
-----	-----	$x\left(3y^2-x^2\right)$	$x\left(3y^2-x^2\right)$	Triangular astigmatismo x
-----	-----	$3x(x^2+y^2)-2x$	$x(x^2+y^2)$	Coma x
$y(x^2+y^2)$	$y(x^2+y^2)$	$3y(x^2+y^2)-2y$	$y(x^2+y^2)$	Coma y
-----	$y(y^2-x^2)$	$y(y^2-3x^2)$	$y(y^2-3x^2)$	Triangular astigmatismo y
-----	-----	$4xy\left(y^2-x^2\right)$	$4xy\left(y^2-x^2\right)$	
-----	-----	$8xy\left(x^2+y^2\right)-6xy$	$2xy\left(x^2+y^2\right)$	2do astigmatismo 45°
$\left(x^2+y^2\right)^2$	$\left(x^2+y^2\right)^2$	$6\left(x^2+y^2\right)^2-6\left(x^2+y^2\right)+1$	$\left(x^2+y^2\right)^2$	Esférica
-----	x^4-y^4	$4\left(x^4-y^4\right)-3\left(y^2-x^2\right)$	x^4-y^4	2do astigmatismo
-----	x^2y^2	$\left(x^2+y^2\right)^2-8x^2y^2$	$\left(x^2+y^2\right)^2-8x^2y^2$	

Sin embargo, dos son las representaciones más empleadas en óptica. En interferometría es común representar a los frentes de onda en polinomios de Zernike, mientras los diseñadores ópticos están más acostumbrados a los polinomios de aberración de Seidel. Y aunque en la práctica se afirma que los primeros coeficientes de Zernike primeros están relacionados con las aberraciones de Seidel. Esto es engañoso, porque no es posible relaciones la base los polinomios de Zernike con el conjunto de términos de Seidel, ni viceversa. Cuando las aberraciones de alto orden están presentes, las aberraciones de Seidel se reparten entre los distintos coeficientes de Zernike de una manera que hace que las aberraciones de Zernike ortogonales. Sólo cuando las aberraciones de alto orden son despreciables, es posible relacionar los coeficientes primarios de Zernike a las aberraciones de Seidel [Goss et al., 2007].

Un análisis del centro de la esfera de referencia de cada una de las representaciones del frente de onda nos lleva a:

Seidel: El centro de curvatura de la esfera de referencia se encuentra en la intersección del rayo principal y la superficie de Petzval.

Zernike (ortogonal): El centro de curvatura de la esfera de referencia se encuentra sobre el rayo principal, en el punto tal que por mínimos cuadrados hallemos la superficie de referencia más cercana al frente de onda considerando el balance de todas las aberraciones presentes en el frente de onda real (mínima varianza).

Nuestra propuesta: El centro de curvatura de la esfera de referencia se encuentra en el cruce del rayo principal con la superficie media. Puede prestar a confusión el término de coma, porque se diría que se encuentra centrada en la superficie de Petzval, pero debe considerarse que cuando el sistema carece de astigmatismo, las superficies tangenciales, sagitales y media, se conjuntan en la superficie de Petzval, por lo que la coma efectivamente se encuentra en la superficie media.

Es importante resaltar, que además de la localización del centro de la esfera de referencia, cada representación de la aberración de frente de onda presenta características diferentes, que son resumidas en la Tabla 2.3.

Como nota histórica, se debe recordar que las aberraciones transversales fueron la base de las investigaciones de Seidel y por esa razón, las aberraciones monocromáticas primarias son llamadas de tercer orden. Debido a que las aberraciones transversales están relacionadas con las aberraciones de frente de onda a través de la Ec. 2.3, se dice que las aberraciones de frente de onda son de cuarto orden. Además, los coeficientes de Zernike son normalmente empleados en un ajuste por mínimos cuadrados a una red de datos de interferométricos o trazo exacto de rayos, mientras que los coeficientes de Seidel se pueden calcular a partir de datos producidos por los rayos paraxiales. La disponibilidad de computadoras de alta velocidad a bajo costo, incremento el interés en el uso de coeficientes de Zernike, principalmente para la representación de las superficies asféricas, y la construcción de funciones de error en el análisis de datos experimentales como simulados.

Una de las principales ventajas de los polinomios de Zernike son su habilidad para describir arbitrariamente los frentes de onda o las aberraciones de los frentes de onda, sin ninguna restricción en sistemas asimétricos, mientras la pupila sea circular unitaria. Aunque no existe ninguna restricción para aplicarlas a cualquier tamaño y forma de pupila, pero pierden su propiedad de ortogonalidad, que es su característica más importante. Muchos autores prefieren usar los polinomios de Zernike ortonormales [Majahan, 1998], donde se conserva todo el análisis presentado hasta el momento.

Los polinomios de Zernike describir las propiedades de un frente de onda aberrado sin tomar en cuenta las propiedades de simetría del sistema que dio lugar a la frente de onda. Además, los polinomios de Zernike tienen algunas propiedades interesantes y útiles: forman un conjunto completo, que son fácilmente separados en funciones radiales y angulares, y los polinomios ortogonales individuales sobre el círculo unitario (todo). Mientras nuestra propuesta representa cualquier frente de onda, sin tomar las propiedades de simetría del sistema. Por otro lado nuestra representación no se encuentra limitada si en tamaño ni forma de pupila.

El lector puede escoger cualquiera de las representaciones analizadas dependiendo de las características del frente de onda y la esfera de referencia pertinente.

Tabla 2.3 Características de las diversas representaciones del frente de onda.

Propiedad	Seidel	Zernike (ortogonal)	Stephenson	Nuestra representación
Centro de la esfera de referencia	Superficie de Petzval	Esfera más cercana		Superficie media
Forma de la pupila	Indiferente	Circular	Indiferente	Indiferente
Simetría	Simétrico	Asimétrico	Asimétrico	Asimétrico
Tamaño de la pupila	Indiferente	Unitario	Indiferente	Indiferente
Ortogonalidad	No	Si	No	No

2.4 REFERENCIAS

Born, M., Wolf, E. (1999), *Principles of Optics*. UK: Cambridge University Press

Mahajan, V.N. (1998), *Optical Imaging and Aberrations: Part I Ray Geometerical Optics.* SPIE Press Monograph Vol PM45. Bellingham, WA:SPIE.

Malacara, D., DeVore, S.L. (1992), en D. Malacara (Ed.), *Optical Shop Testing*. New York: John Wiley.

Malacara, D., M. Servín, Z. Malacara (2005), *Interferogram Análisis for Optical Testing*. New York: Taylor & Francis.

Malacara, D., Z. Malacara (2004), *Handbook of Optical Design*. USA: Marcel Dekker.

Stephenson, P. C. L., "Optical aberrations described by an alternative series expansion," *J. Opt. Soc. Am. A* **26** (2009) 265-273.

Gross, H., Zügge, H., Peschke, M., and Blechinger(2007), *Handbook of Optical Systems* Vol3, Germany: Wiley.

CAPÍTULO 3

Aberraciones geométricas de un espejo esférico fuera de eje.

La mayor parte de los sistemas ópticos se usan centrados y con simetría de rotación, por ejemplo las lentes fotográficas. Sin embargo existen otros tipos de sistemas que no tienen simetría de rotación, ni están centrados y emplean elementos reflectores. En esta clasificación caen algunos resonadores láser, espectrógrafos y cámaras retinianas con óptica adaptativa. Para el diseño de estos instrumentos es necesario conocer el comportamiento de las aberraciones en los espejos esféricos fuera de eje, que son los más empleados en la práctica por su reducido costo. Estos espejos esféricos cóncavos con planos meridionales comunes, presentan una gran curvatura de Petzval, coma, astigmatismo y esférica en la mayoría de los diseños ópticos. En este capítulo, se presenta el comportamiento de las aberraciones para un espejo esférico fuera de eje, respecto a la variación de sus parámetros, lo que ayudará a comprender la mayor parte de los resultados presentados posteriormente. Además, permitirá aplicar estos resultados en el proceso de diseño óptico de sistemas construidos con espejos esféricos fuera de eje.

En el diseño de sistemas fuera de eje, no centrados, con espejos esféricos, es importante entender el comportamiento de las aberraciones de cada elemento, como función de la variación de los parámetros físicos de la configuración. Teniendo esto en cuenta, nos interesa analizar las aberraciones sobre un espejo esférico en configuración fuera de eje.

La Fig. 3.1a muestra un espejo en configuración fuera de eje. Suponiendo que el espejo fuera elipsoidal, con la imagen y el objeto posicionados en los focos del elipsoide, este no presenta aberraciones, por lo que el frente de onda presente en la pupila de salida del sistema será perfectamente esférico. Pero al ser sustituido por un espejo esférico, no se formaría una imagen ideal, es decir, los diversos rayos distribuidos sobre la pupila formarán múltiples imágenes sobre el rayo principal y el frente de onda sobre la pupila presentará desviaciones respecto a cualquier esfera de referencia, en otras palabras, el frente de onda estará aberrado (Fig. 3.1b).

Debido a la necesidad de entender como varían las aberraciones respecto a las diversas variables del sistema (el radio de curvatura del espejo, el ángulo de incidencia oblicua del rayo principal y la distancia del objeto al vértice del espejo medida sobre el rayo principal), desarrollamos las expresiones analíticas de los coeficientes de aberración monocromáticas [Gómez-Vieyra y Malacara-Hernández, 2009] en una representación del frente de onda propuesta por nosotros (V. Sección 2.3), con centro de curvatura de la esfera de referencia en la superficie media, aunque puede emplearse cualquiera de las representaciones discutidas en el capítulo anterior.

En consecuencia estudiaremos la dependencia de los coeficientes de aberración, en función de su evolución con respecto a los parámetros físicos:

- El ángulo de incidencia *(I)*

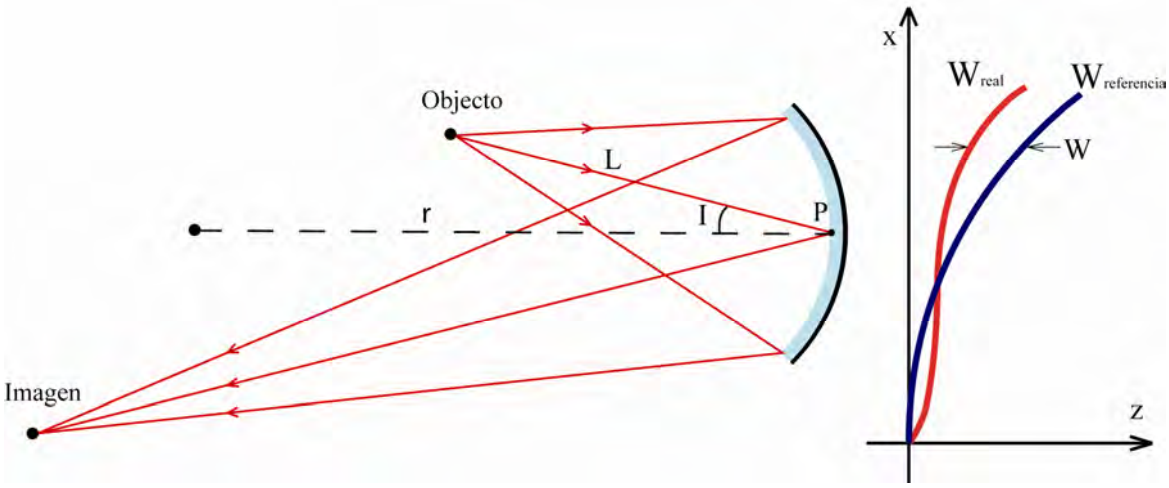

(a) (b)

Figura 3.1.- (a) Representación de la formación de una imagen puntual con un espejo ideal. (b) Representación de la diferencia del frente de onda de un espejo esférico (W_{real}) con respecto al de una superficie de referencia elipsoidal ($W_{referencia}$).

- El radio de curvatura del espejo *(r)*
- La distancia del objeto al vértice del espejo *(L)*.

Lo que nos permitirá entender de una manera adecuada el comportamiento de las aberraciones en el proceso de diseño de sistemas de imaginología retiniana, cavidades laser y espectrógrafos basados en espejos esféricos.

Empleando el principio de Fermat, desarrollamos expresiones analíticas de los coeficientes de aberración. Pero esta no es la única forma de resolver el problema, debido a que la óptica geométrica nos permite relacionar los efectos de las aberraciones, a través la ecuación de haces de rayos marginales [Conrady, 1960] (que está relacionada con la cantidad de astigmatismo presente en el sistema) y la ley del seno (que está relacionada con la cantidad de coma presente en el sistema) [Kingslake, 1974; Malacara y Malacara, 2004]. También es posible

realizar una descripción de las aberraciones mediante el trazo de rayos con programas computacionales. La desventaja del trazo de rayos es que únicamente presenta el comportamiento del frente de onda (o las aberraciones de rayo) para el caso específico en evaluación y el usuario del programa debe tener la experiencia y el conocimiento necesario para interpretar el comportamiento global de los coeficientes de aberración del sistema.

Debido a esta necesidad, de experiencia y de conocimiento en el área de óptica geométrica, los investigadores que tienen la necesidad de diseñar sistemas complejos con espejos esféricos fuera de eje y no son especialistas en el área, han encontrado gran dificultad para obtener los resultados buscados en el diseño óptico de sus instrumentos. Debido a lo cual desarrollamos esta etapa de nuestra investigación. Pretendemos realizar una descripción de las aberraciones del frente de onda basados en la diferencia de caminos ópticos (principio de Fermat). Hasta donde tenemos conocimiento, existen dos desarrollos para este problema para espejos, una descrita por Schroeder[1987], que es un planteamiento similar al presentado por Korsch [1991], basado en diferencia de caminos ópticos de rayos y el desarrollo que fue presentado por nosotros (V. Anexo 1), basado en la diferencia de camino ópticos de frentes de onda.

El planteamiento de Schroeder considera la diferencia de camino óptico entre el rayo principal y el rayo marginal exterior; con un procedimiento muy similar puede ser encontrado en libros clásicos de diseño óptico [Conrady, 1960; Kingslake, 1974; Malacara y Malacara, 2004; Schroeder, 1987; Shannon, 1997; Slyusarev, 1984; Smith, 1992; Welford, 1991], para una superficie refractiva. Schroeder [1987] presenta como resultado general para el caso de un espejo esférico:

$$B = \frac{I^2}{r} \tag{3.1}$$

$$C = \frac{(r - L)I}{L\,r^2} \tag{3.2}$$

$$E = \frac{(r-L)^2}{4L^2 r^3} \tag{3.3}$$

en la configuración de Fig. 3.1a, donde B, C y E son los coeficientes del astigmatismo, la coma y la esfericidad, donde la representación de aberraciones de frente de onda es la de Seidel, donde el centro de curvatura de la esfera de referencia se encuentra en la superficie de Petzval (V. Sección 2.4).

El planteamiento propuesto por nosotros, se basa en que una superficie reflexiva elipsoidal produce un frente de onda perfectamente esférico de un objeto puntual que se localiza en uno de sus focos. Por lo tanto, se puede calcular la diferencia de camino óptico entre el frente de onda producido por un espejo esférico y el frente de onda esférico producido por la superficie de referencia teórica elipsoidal adecuada, obteniendo una representación analítica de la aberración de frente de onda (Fig. 3.2). La descripción del frente de onda puede ser en cualquiera de las notaciones presentadas en el capítulo anterior; aunque preferimos describirla de acuerdo a la notación presentada por nosotros [Gómez-Vieyra y Malacara-Hernández, 2010], debido a las características descritas en el capítulo anterior (V. Sección 2.3, Tabla 2.3). Sin embargo puede emplearse cualquiera de las notaciones para la aberración del frente de onda, con la posibilidad de transformase algebraicamente a cualquier otra notación. Debe recordarse que el cambio de representación del frente de onda nunca es perfecto, como se mencionó en la discusión del capítulo anterior.

Después de una serie de consideraciones geométrico-algebraicas descritas por Gómez-Vieyra y Malacara-Hernández [2010] se pueden encontrar las ecuaciones exactas para la aberración W del frente de onda:

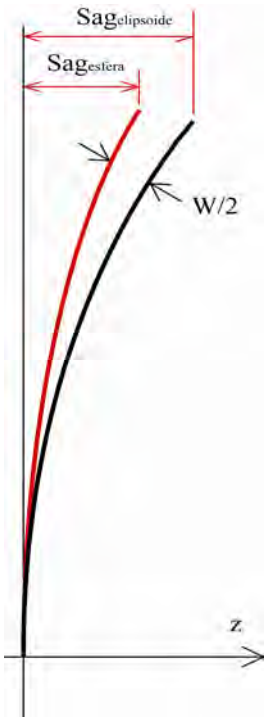

Figura 3.2.- Representación de la diferencia de caminos ópticos respecto a las superficies de reflexión.

$$W = A\left(x^2+y^2\right)+B\left(y^2-x^2\right)+C\,y\left(x^2+y^2\right)+D\,y\left(y^2-x^2\right)+E\left(x^2+y^2\right)^2+F\left(x^4-y^4\right)+Gx^2y^2 \tag{3.4}$$

donde A es el defoco, B el astigmatismo, C la coma, D coma astigmática, E la esférica, F el astigmatismo de 5to orden y G ashtray respectivamente. Con valores:

$$A = 0 \tag{3.5.a}$$

$$B = -\frac{\left(a^2-b^2\right)\sqrt{a^2\cos^2\left(\phi\right)+b^2\sin^2\left(\phi\right)}\,\sin^2\left(\phi\right)}{2a^2b^2} \tag{3.5.b}$$

$$C = -\frac{\left(a^2-b^2\right)\left[a^2\cos^2\left(\phi\right)+b^2\sin^2\left(\phi\right)\right]^2\sin\left(2\phi\right)}{2a^4b^4} \tag{3.5.c}$$

$$D = \frac{\left(a^2-b^2\right)^2\left[a^2\cos^2(\phi)+b^2\sin^2(\phi)\right]\sin^3\left(\phi\right)\cos\left(\phi\right)}{a^4b^4} \tag{3.5.d}$$

$$E=\frac{1}{32768a^6b^6}\left(a^2-b^2\right)$$
$$*\Big(-4\Big[163a^6+191a^4b^2+249a^2b^4+165b^6+4\left(83a^6+32a^4b^2-25a^2b^4-26b^6\right)\cos\left(2\phi\right)$$
$$+4(a-b)(a+b)\left(77a^4+76a^2b^2+47b^4\right)\cos\left(4\phi\right)+12\left(a^2-b^2\right)^2\left(15a^2+14b^2\right)\cos\left(6\phi\right)$$
$$+41\left(a^2-b^2\right)^3\cos\left(8\phi\right)\Big]*\sqrt{a^2\cos^2\left(\phi\right)+b^2\sin^2\left(\phi\right)} \qquad (3.5.e)$$
$$+\Big\{\Big[a^4+6a^2b^2+b^4-\left(a^2-b^2\right)^2\cos\left(4\phi\right)\Big]^3\left(4a^4\cot\left(\phi\right)\left(1-2\csc^2\left(\phi\right)\right)\right.$$
$$\left.+\Big[3a^4+2a^2b^2-b^4+\left(7a^4+4a^2b^2+b^4\right)\sec^2\left(\phi\right)\Big]\tan\left(\phi\right)\Big\}\right)$$
$$/\Big\{\Big[a^2\csc^2\left(\phi\right)+b^2\sec^2\left(\phi\right)\Big]^{3/2}\Big[b^2\cos^2\left(\phi\right)+a^2\sin^2\left(\phi\right)\Big]^3\Big\}$$

$$F=\frac{1}{32768a^6b^6}\left(a^2-b^2\right)$$
$$\Big[4\Big[163a^6+191a^4b^2+249a^2b^4+165b^6+4\left(83a^6+32a^4b^2-25a^2b^4-26b^6\right)\cos\left(2\phi\right)$$
$$4(a-b)(a+b)\left(77a^4+76a^2b^2+47b^4\right)\cos\left(4\phi\right)+12\left(a^2-b^2\right)^2\left(15a^2+14b^2\right)\cos\left(6\phi\right)$$
$$+41\left(a^2-b^2\right)^3\cos\left(8\phi\right)\Big]*\sqrt{a^2\cos^2\left(\phi\right)+b^2\sin^2\left(\phi\right)}+\left(\Big[a^4+6a^2b^2+b^4-\left(a^2-b^2\right)^2\cos\left(4\phi\right)\Big]^3\right. \qquad (3.5.f)$$
$$*\Big\{4\,a^4\cot\left(\phi\right)\Big[1-2\csc^2\left(\phi\right)\Big]+\Big[3a^4+2a^2b^2-b^4+\left(7a^4+4a^2b^2+b^4\right)\sec^2\left(\phi\right)\Big]$$
$$\left.*\tan\left(\phi\right)\Big\}\right)/\Big\{\Big[a^2\csc^2\left(\phi\right)+b^2\sec^2\left(\phi\right)\Big]^{3/2}\Big[b^2\cos^2\left(\phi\right)+a^2\sin^2\left(\phi\right)\Big]^3\Big\}\Big]$$

$$G=\frac{1}{32768a^6b^6}\left(a^2-b^2\right)$$
$$\Big(-8\Big[171a^6+103a^4b^2+17a^2b^4-35b^6+4\left(99a^6+40a^4b^2+39a^2b^4+14b^6\right)\cos\left(2\phi\right)$$
$$+4(a-b)(a+b)\left(85a^4+76a^2b^2+7b^4\right)\cos(4\phi)+4\left(a^2-b^2\right)^2\left(29a^2+2b^2\right)\cos\left(6\phi\right)$$
$$+\left(a^2-b^2\right)^3\cos\left(8\phi\right)\Big]*\sqrt{a^2\cos^2\left(\phi\right)+b^2\sin^2\left(\phi\right)}$$
$$+4\left(163a^6+191a^4b^2+249a^2b^4+165b^6+4\left(83a^6+32a^4b^2-25a^2b^4-26b^6\right)\cos\left(2\phi\right)\right.$$
$$+4(a-b)(a+b)\left(77a^4+76a^2b^2+47b^4\right)\cos\left(4\phi\right)+12\left(a^2-b^2\right)^2\left(15a^2+14b^2\right)\cos\left(6\phi\right)$$
$$*\sqrt{a^2\cos[\phi]^2+b^2\sin[\phi]^2}-\Big\{\Big[a^4+6a^2b^2+b^4-\left(a^2-b^2\right)^2\cos\left(4\phi\right)\Big]^3$$
$$\left.+41\left(a^2-b^2\right)^3\cos\left(8\phi\right)\right\}$$
$$*\Big\{4a^4\cot\left(\phi\right)\Big[1-2\csc^2\left(\phi\right)\Big]+\Big[3a^4+2a^2b^2-b^4+\left(7a^4+4a^2b^2+b^4\right)\sec^2\left(\phi\right)\Big]$$
$$\left.*\tan\left(\phi\right)\Big\}\right)/\Big\{\Big[a^2\csc^2\left(\phi\right)+b^2\sec^2\left(\phi\right)\Big]^{3/2}\Big[b^2\cos^2\left(\phi\right)+a^2\sin^2\left(\phi\right)\Big]^3\Big\}\Big)$$

(3.5.g)

donde a y b son el semieje mayor y menor del elipsoide, ϕ es el ángulo de inclinación (Fig. 3.3).

Estas expresiones (Ecs. 3.5) son complicadas para analizarlas analíticamente. Además de estar relacionadas con parámetros geométricos, no físicos. Debido a lo anterior, se buscaron las relaciones de los parámetros geométricos *(a, b y ø)* y los parámetros físicos *(L,r,I)*, Fig. 3.1. Con ayuda de la Fig. 3.3, es posible relacionar los parámetros geométricos y físicos analíticamente mediante las ecuaciones:

$$a = \frac{L + L'}{2} \tag{3.6.a}$$

$$b = \sqrt{LL'\cos^2(I)} \tag{3.6.b}$$

$$\phi = \arctan\left[\left(\frac{L'+L}{L'-L}\right)\tan(I)\right] \tag{3.6.c}$$

Y empleando las ecuaciones de Coddington, para relacionar L' con el radio de la esfera de referencia, en este caso localizada en la imagen media:

$$L' = \frac{L\,r\left[L - r\cos(I) + L\cos^2(I)\right]}{\left[r - 2L\cos(I)\right]\left[-2L + r\cos(I)\right]} \tag{3.7}$$

Considerando que las Ecs. 3.5 pueden desarrollarse en una serie de MaClaurin de tercer orden sobre ø, obtenemos:

$$A = 0 \tag{3.8.a}$$

$$B \approx \left(\frac{1}{2a} - \frac{a}{2b^2}\right)\phi^2 \tag{3.8.b}$$

$$C \approx \frac{\left(a^2 - b^2\right)\phi\left(-6b^2\phi^2 + a^2\left(-3 + 8\phi^2\right)\right)}{3a^2b^4} \tag{3.8.c}$$

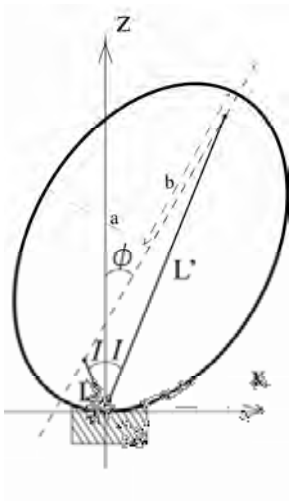

Figura 3.3.- Representación de los parámetros físicos y geométricos del modelo.

$$D \approx \frac{\left(a^2 - b^2\right)^2 \phi^3}{a^2 b^4} \tag{3.8.d}$$

$$E \approx \frac{\left(a^2 - b^2\right)\left(-9b^2\phi^2 + 2a^2\left(-1 + 6\phi^2\right)\right)}{8ab^6} \tag{3.8.e}$$

$$F \approx -\frac{\left(2a^4 - 5a^2b^2 + 3b^4\right)\phi^2}{4ab^6} \tag{3.8.f}$$

$$G \approx 0 \tag{3.8.e}$$

Sustituyendo la Ec. 3.7 en las Ecs. 3.6 y aplicando series de MaClaurin de tercer orden con respecto a I, se obtienen las relaciones directas que relacionan los parámetros físicos y geométricos de nuestro sistema:

$$a = \frac{L^2}{2L - r} \tag{3.9a}$$

$$b \approx \left(1 - \frac{1}{2} I^2\right) L \sqrt{\frac{r}{2L - r}} \tag{3.9b}$$

$$\phi \approx -\frac{L\,I}{L-r}+\frac{\left(2L^2r-Lr^2\right)I^3}{3(L-r)^3} \tag{3.9c}$$

Tomando las Ecs. 3.9 resultantes y sustituyéndolas en las Ecs. 3.8, obtenemos las expresiones de los coeficientes de aberración aproximados en términos de *(L,r,I)*. Considerando únicamente los términos de primer orden, se pueden encontrar las aproximaciones:

$$A = 0 \tag{3.10a}$$

$$B \approx \frac{I^2}{2r} \tag{3.10b}$$

$$C \approx \frac{(r-L)I}{L\,r^2} \tag{3.10c}$$

$$D \approx 0 \tag{3.10d}$$

$$E \approx \frac{(r-L)^2}{4L^2r^3} \tag{3.10e}$$

$$F \approx \frac{\left(2L^2-6Lr+3r^2\right)I^2}{4L^2r^3} \tag{3.10f}$$

$$G \approx 0 \tag{3.10g}$$

Que concuerdan con las reportadas por Schroeder. El factor de diferencia en el coeficiente del astigmatismo *(B)* es debido a la representación empleada de frente de onda, con diferente centro de curvatura de la esfera de referencia. La Fig 3.4 reproducida del artículo de Gómez-Vieyra y Malacara-Hernández [2010], representa el dominio del valor de los coeficientes de aberración dependientes del ángulo de incidencia. Pero como se menciona en el artículo, no se observa claramente cuándo un coeficiente de aberración es mayor que los demás, es decir, en cuál región domina más una aberración. Para ilustrar la dependencia y dominio de los coeficientes de aberración individuales se realizó la Fig. 3.5, que también es una reproducción del artículo mencionado con anterioridad.

En la Fig. 3.5, se observan tres regiones:

- dominio de la esfericidad (paraxial)
- dominio de la coma
- dominio del astigmatismo

A partir de estas regiones se observa que, debido a los ángulos de incidencia empleados, en los sistemas que incluyen telescopios afocales, se emplean campos angulares donde predomina el astigmatismo *(B)*. Donde también es necesario comparar esta región, con la dependencia con respecto a la posición del objeto y la imagen, esto se muestra en la Fig. 3.6.

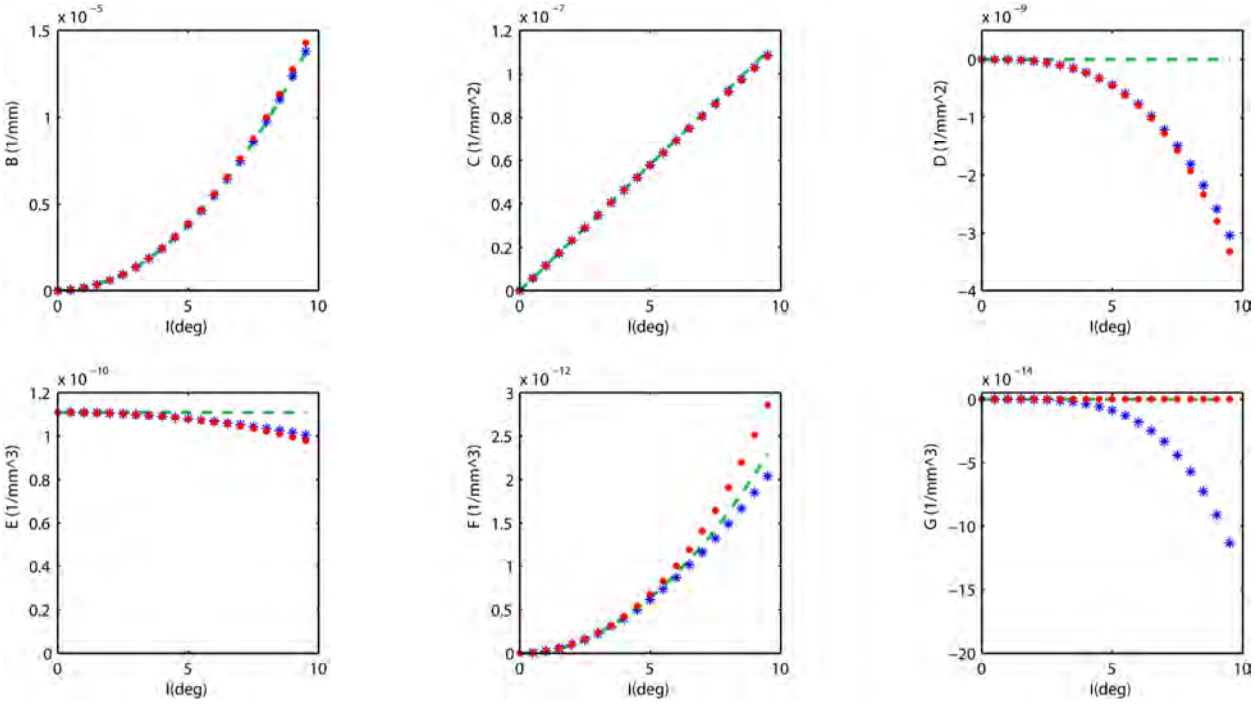

Figura 3.4.- Comportamiento de los coeficientes de aberración exactos Ec. 3.5 (* azules), aproximados Ec. 3.8 (° rojo) y simplificación mínima Ec. 3.10 (-- verde) con respecto al ángulo de incidencia (L=600mm, r=1000mm).

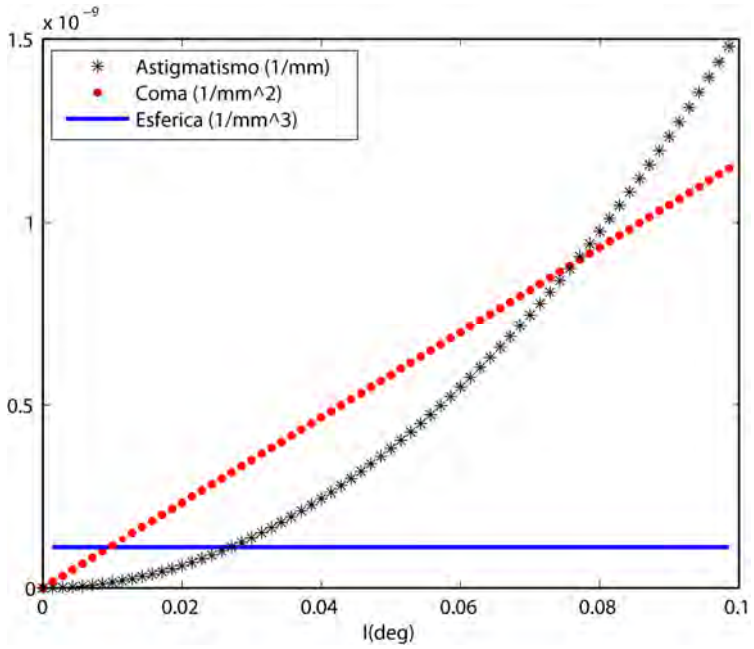

Figura 3.5.- Comportamiento de los coeficientes de aberración para ángulos pequeños (L=600mm, r=1000mm)

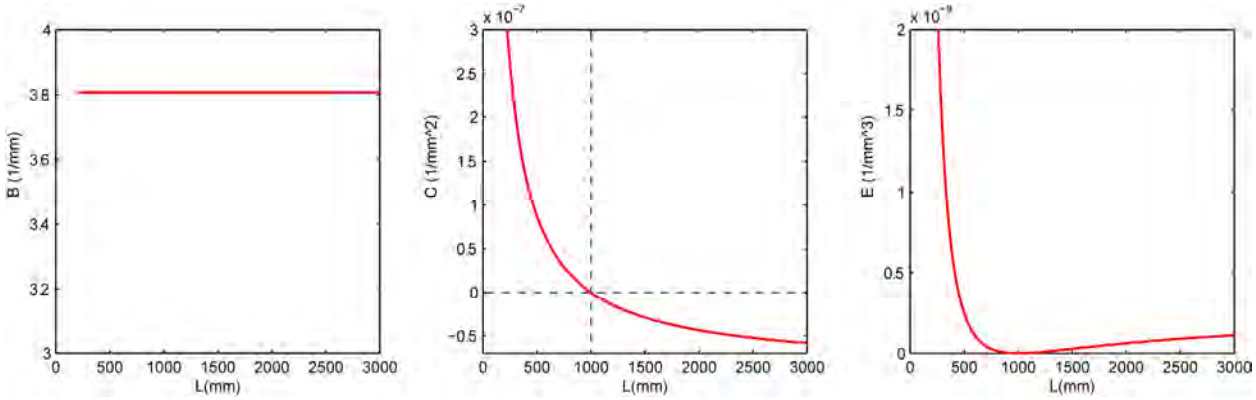

(a) (b) (c)

Figura 3.6.- Comportamiento de los coeficientes de aberración con respecto a la variación de L (I=5 grados, r=1000mm)

En estas gráficas (Fig. 3.6) se observa claramente que para una configuración aplanática de Abbe (L=r), la coma (Fig. 3.6b) y la esfericidad (Fig. 3.6c) tienen un valor igual a cero, mientras que el valor del astigmatismo depende únicamente del ángulo de incidencia (Fig.

3.6a), como puede corroborarse en las Ecs. 3.10. Por otro lado, cuando L=r/2 y L= ∞, es decir, cuando el objeto se encuentra en el foco Gaussiano y cuando el objeto se encuentra en el infinito, los valores de esfericidad (Fig. 3.6c), valores de astigmatismo (Fig. 3.6a) son iguales y valores de coma son iguales pero de signo contrario (Fig. 3.6b), mientras los ángulos de incidencia oblicua sean pequeños. Si el ángulo de incidencia es grande, la pupila se ve elíptica en lugar de circular, entonces lo descrito anteriormente es falso, las igualdades se convierten en valores semejantes y la coma pierde su linealidad. Esto va a ser sumamente importante cuando analicemos las configuraciones con telescopios afocales, en el capitulo siguiente.

Por punto final es conveniente enfatizar que toda la información resultante en este capítulo, nos permite entender la variación de los coeficientes de aberración en el proceso de diseño de los instrumentos que emplean configuraciones de espejos esféricos fuera de eje no centrados, tales como los oftalmológicos, resonadores láser y espectrógrafos.

3.2 REFERENCIAS

Conrady, A. E., *Applied Optics and Optical Design*, (Dover Publications Inc., New York, 1960), parte 1 y 2.

Gómez-Vieyra, A., Malacara-Hernández, D., "Geometrical theory of wavefront aberrations in off-axis spherical mirror " (2010). (Anexo 1)

Kingslake, R., *Lens Design Fundamentals*, (Academic Press, San Diego, 1978).

Malacara, D. y Malacara, Z., *Handbook of Lens Design*, (Marcel Dekker Inc., New York. 2004).

Schroeder, D. J., *Astronomical Optics*, (Academic Press, USA, 1987).

Shannon, R.t R., *The Art and Science of Lens Design*, (Cambridge University Press, USA, 1997).

Slyusarev, G. G., *Aberration and Optical Design Theory*, (Adam Hilger, Great Britain, 1984).

Smith, W. J., *Modern Lens Design*, (McGraw-Hill, USA, 1992).

Welford, W. T., Aberrations of Optical Systems, (Adam Hilger, Great Britain, 1991)

CAPÍTULO 4

Diseño óptico de primer orden con espejos esféricos compensando el astigmatismo de tercer orden.

Los instrumentos actuales de escaneo con óptica adaptativa usan espejos esféricos en arreglos fuera de eje para obtener los planos conjugados de la pupila de ojo y de la imagen de la retina, debido a su bajo costo y su fácil alineación. Las configuraciones típicas empleadas en estos sistemas son los telescopios afocales y los espejos simples en configuraciones aplanáticas de Abbe. La mayoría de estos sistemas presenta un alto grado de astigmatismo al ser diseñados, y aunque Webb sugirió compensar el astigmatismo sacando del plano algún elemento óptico del sistema, no se tenía un tratamiento analítico que permitiera sistematizar el diseño de estos instrumentos. Nosotros hemos demostramos analíticamente lo propuesto por Webb rompiendo la simetría del sistema en telescopios afocales para un plano en específico y así, con la unión de dos telescopios, en dos planos meridionales diferentes es posible compensar dos planos conjugados a la vez. Además, hemos demostrado que es posible compensar astigmatismo en el plano de imagen retiniana, empleando como relevadores únicamente espejos en configuración aplanática de Abbe, pero sin la compensación de astigmatismo en la pupila del ojo. Mostramos que se pueden realizar diseños mixtos, es decir, donde se emplean telescopios afocales y espejos en configuraciones de Abbe para poder obtener diseños limitados por difracción, con ciertas características. Exploramos diversos arreglos que pueden ser implementados dependiendo de las necesidades de los sistemas de resonadores laser, espectroscopia e imaginología retiniana con o sin óptica adaptativa, aunque no exhaustivamente. El lector puede tener la necesidad de emplear sistemas con elementos conexos, los cuales no consideramos en la discusión, y que pueden ayudar a reducir la curvatura de campo.

Los problemas en el diseño óptico en los sistemas de imaginología retiniana con espejos esféricos fuera de eje se pueden resumir en:

- La falta de conocimiento del comportamiento de sistemas no centrados con incidencia oblicua (fuera de eje).
- La presencia de astigmatismo de tercer orden, principalmente, en las configuraciones empleadas comúnmente en estos sistemas.

El primer problema fue discutido en el capítulo anterior, pero parcialmente, debido a que únicamente se estudió un espejo esférico fuera de eje (incidencia oblicua), donde todavía se conserva la simetría del sistema, es decir, tienen un plano meridional único. Se presentaron las expresiones analíticas y un ejemplo que nos permitió entender el comportamiento de los coeficientes de aberración en función de cada uno de los parámetros del sistema. Estas expresiones nos llevan a constricción para el diseño de estos sistemas:

- Los ángulos de incidencia deben ser lo más pequeños que sea posible.
- Los radios de curvatura deben de ser lo más grande que sea posible.

Para ambas configuraciones, con espejo esférico en configuración aplanática de Abbe [Zhong, 2008] y con telescopios afocales [Roorda, 2002], obtenemos aberraciones pequeñas al aplicar estas dos condiciones. Pero, esto no asegura que nuestros sistemas se encuentren limitados por difracción.

Considerando arreglos de espejos esféricos cóncavos, con un sólo plano meridional para todo el sistema, el astigmatismo se incrementará y no podrá ser compensado, como lo demostró Rosendahl [1962], mientras que para casos muy específicos de este tipo es posible compensar la coma. Como se observa en Fig. 3.4, la aberración esférica (E) permanece casi constante con la variación del ángulo de incidencia y únicamente en configuración aplanática de Abbe podemos tener coma y esfericidad igual a cero, Fig. 3.6. Como se ha mencionado anteriormente, la única solución propuesta para compensar el astigmatismo sin emplear componentes adicionales, fue

sugerida por Webb [1981]. Esta solución consiste en romper la simetría del sistema, al sacar uno o varios componentes del plano meridional formando dos o más planos meridionales del sistema óptico. Posteriormente con los sistemas de óptica adaptativa (AO) en visión, muchos grupos emplearon esta sugerencia empíricamente [Burns, 2007], es decir, dejaron que un programa de diseño encontrará los valores adecuados para lograr sistemas bajo el límite de difracción, sacando un telescopio del plano meridional principal. La desventaja es que el programa de diseño puede darnos una solución local basada en la configuración original planteada por nosotros, pero no tenemos la seguridad de que sea la óptima. Antes de continuar con las soluciones analíticas describiremos las dos configuraciones de espejos esféricos empleadas en estos sistemas como relevadores de los planos conjugados.

4.1 TELESCOPIOS AFOCALES

Un sistema en el cual el objeto y la imagen se encuentran a infinito es llamado afocal. La descripción de su magnificación [Gross, 2005] está dada por los ángulos del rayo principal en términos de:

$$\Gamma = \frac{\omega'}{\omega} \tag{4.1}$$

Donde ω y ω’ son los ángulos del rayo principal objeto e imagen respectivamente (Fig. 4.1).

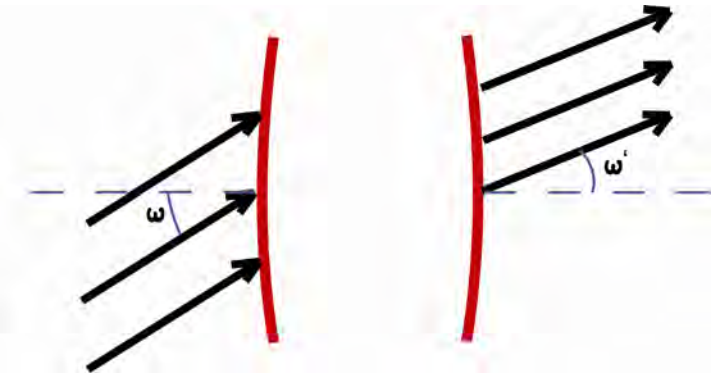

Figura 4.1.- Definición de la amplificación para un telescopio afocal.

Los planos principales para los telescopios afocales están al infinito, y la distancia focal no está definida para estos sistemas. Por otro lado la magnificación angular (Γ) para el caso de sistemas afocales que son de interés (Figs. 4.2 y 4.3), también puede ser definida por [Gross, 2005]:

$$\Gamma = \frac{f_2}{f_1} = \frac{r_2}{r_1} \tag{4.2}$$

Y la condición para que este sistema forme una imagen real es [Gross, 2005]:

$$s_{obj} < \frac{f_1 + f_2}{\Gamma} \tag{4.3}$$

Siendo s_{obj} la distancia del objeto puntual al vértice del primer espejo. Como se observa en las Figs. 4.2 y 4.3 son dos sistemas afocales keplerianos fuera de eje con una imagen real intermedia, y son los más empleados en AO.

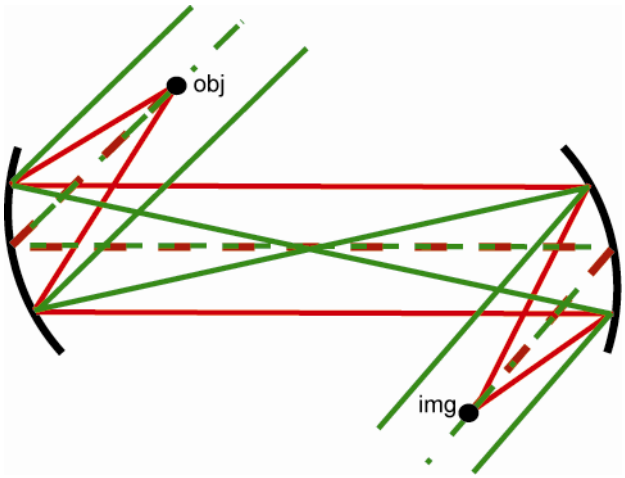

Figura 4.2.- Telescopio afocal antisimétrico fuera de eje

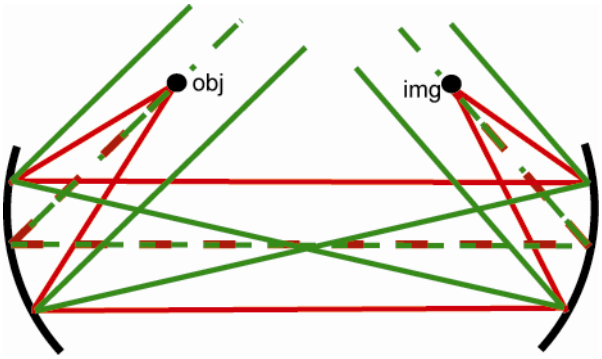

Figura 4.3.- Telescopio afocal simétrico fuera de eje

4.2 ESPEJOS EN CONFIGURACIÓN APLANÁTICA DE ABBE

En los libros clásicos [Welford, 1991; Malacara y Malacara, 2004] se mencionan los puntos aplanáticos de Abbe para una superficie refractora centrada. De esta misma definición, se pueden deducir los puntos aplanáticos de un espejo esférico en eje, que son:

- Objeto sobre el vértice del espejo
- Objeto sobre el centro de curvatura

En configuraciones fuera de eje (Fig. 4.4), se puede observar que se respeta esto, de acuerdo a las Ecs. 3.10c y 3.10e; donde para la configuración $L=r$ se cumple que la coma y esfericidad son cero. Esta configuración es importante cuando los sistemas de escaneo requieren examinar una excentricidad ocular muy grande. La limitante de la configuración es la magnificación unitaria, es decir, no se puede cambiar los tamaños de las imágenes conjugadas (que en este caso son los tamaños de las pupilas).

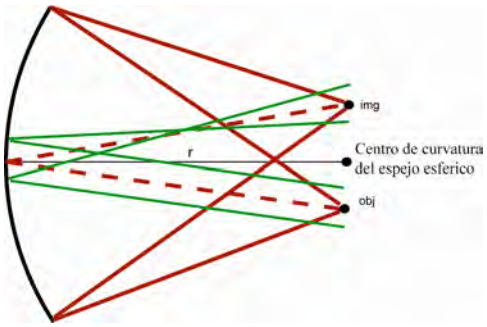

Figura 4.4.- Espejo esférico fuera de eje en configuración aplanática de Abbe.

4.3 EMPLEO DE LAS ECUACIONES DE HACES MARGINALES EN LA COMPENSACIÓN DEL ASTIGMATISMO

En la teoría paraxial de elementos con pupila de simetría rotacional en eje, los rayos viajan de un punto objeto hasta un punto imagen. La imagen de primer orden de tales componentes puede ser descrita por la ecuación de Gauss para lentes delgadas:

$$\frac{1}{s}+\frac{1}{s'}=\frac{1}{f} \tag{4.3}$$

Donde s y s' son las distancias desde el objeto y la imagen hasta la lente delgada, y f es la distancia focal efectiva de la lente delgada. En el caso de objetos fuera de eje, se introducen aberraciones de alto orden, principalmente coma y astigmatismo. Considerando el sistema sin coma de tercer orden, es posible hallar las imágenes marginales a lo largo del rayo principal con ayuda de la ecuación de haces marginales [Conrady, 1966]. La localización de las imágenes marginales depende de la orientación θ del plano marginal, por norma general se emplean los planos transversal (sagital), $\theta=0$, y meridional (tangencial), $\theta=\pi/2$. Para espejos esféricos tiene la forma:

$$\frac{1}{s}+\frac{1}{s_\theta'}=\frac{2\cos I}{r(1-\cos^2\theta\sin^2 I)}, \tag{4.4}$$

siendo I el ángulo de incidencia del rayo principal en el espejo y *r* el radio de curvatura del espejo. Es útil mencionar que para algunos casos, es más adecuado trabajar con su representación en potencias ópticas. Para $\theta=0^\circ$ y $\theta=\pi/2$, se encuentran las ecuaciones de Coddigton:

$$\frac{1}{s_s}+\frac{1}{s_s'}=\frac{2\cos I}{r}, \tag{4.5}$$

$$\frac{1}{s_t}+\frac{1}{s_t'}=\frac{2}{r\cos I}. \tag{4.6}$$

La diferencia entre las posiciones de la imagen sagital y tangencial está directamente relacionada con la magnitud de astigmatismo presente en el sistema. Además, se puede realizar

una secuencia de trazos marginales como se realiza comúnmente con las lentes delgadas, considerando únicamente que si los planos meridionales son comunes, los haces sagitales se propagaran únicamente obedeciendo la Ec. 4.5. Pero si alguno de los planos cambia, por ejemplo perpendicularmente, la imagen sagital anterior al cambio de planos, se convertirá en un objeto tangencial, propagándose empleando la Ec. 4.6. Para un caso de cambio arbitrario de θ, se emplea la Ec 4.4. Si imponemos la condición de que la diferencia Δ_s entre las dos imágenes, sagital y tangencial, del sistema completo sea igual a cero, obtendremos un sistema compensado en astigmatismo de primer orden. A continuación presentamos algunos casos prácticos, que pueden ser expandidos.

4.3.1 Sistema de dos espejos

En el caso general para dos espejos con planos meridionales distintos (Fig. 4.5) obtenemos la relación para la compensación del astigmatismo:

$$I_2 = \frac{s\sqrt{r_1 r_2}\, I_1}{\sqrt{-\cos[2\theta]\left(-2ds + (d+s)r_1\right)^2}} \tag{4.7}$$

Donde claramente se observa que si los dos espejos son cóncavos, ambos r_i positivos, solo existe compensación cuando $|\theta| \in (\pi/4,\ 3\pi/4)$. Si es un espejo cóncavo y uno convexo es posible hallar solución para $|\theta| \in (-\pi/4,\ \pi/4)$, además de depender de los valores de la distancia entre los espejos (d) y la distancia (s) del objeto al vértice del primer espejo (M1).

Para el arreglo de telescopios afocales, presentadas y discutidas en nuestro artículo (Anexo 2), se hallan las expresiones:

$$I_2 \approx \sqrt{-\frac{M}{\cos(2\theta)}}\, I_1 \tag{4.8}$$

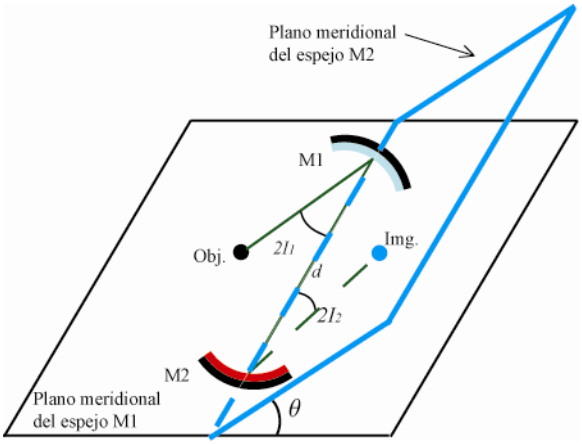

Figura 4.5 Esquema de dos espejos con planos meridionales distintos

para conjugados finitos ($s_o = r_1/2$, cumpliendo la condición de la Ec. 4.3) y

$$I_2 \approx \sqrt{-\frac{1}{M\cos(2\theta)}}I_1 \tag{4.9}$$

para conjugados infinitos ($s_o = \infty$), donde M es la magnificación del telescopio [Gómez-Vieyra, 2010]. Estas configuraciones pueden ser observadas en la Fig. 4.6. Como se ha discutido en el artículo (Anexo 2), el arreglo que presenta la configuración más compacta es la $\theta = \pm\pi/2$, debido a que produce los ángulos más pequeños. Como resultado de esta compensación, se obtendrá una coma con orientación ±π/4, dependiendo de cómo se doble el arreglo óptico. La desventaja de esta compensación es que únicamente se puede compensar un plano a la vez. Debido a que el origen de la investigación es debida a los problemas existentes en el AOSLO de la Universidad de Rochester, donde trabajan con relevadores afocales, lo importante para nosotros es poder medir las aberraciones de la pupila del ojo mientras al mismo tiempo se realiza la imagen de la retina. En otras palabras, ambos planos conjugados, pupila del ojo (plano finito conjugado) e imagen de la retina (plano infinito conjugado), deben estar compensados al mismo tiempo en los sensores de frente de onda y detectores de imágenes. Sin embargo, en los planos de los actuadores (espejos deformables y espejos de escaneo), solamente nos interesa tener perfectamente compensado el plano conjugado de pupila del ojo. Se planteó la solución de unir

dos telescopios compensados a conjugados finitos cada uno y forzando a una co-dependencia para compensar a conjugados infinito, como un sistema global, que discutiremos con mayor detalle un poco más adelante.

4.3.2 Sistema de tres espejos

Para una configuración de tres espejos, Fig. 4.7, obtenemos la expresión:

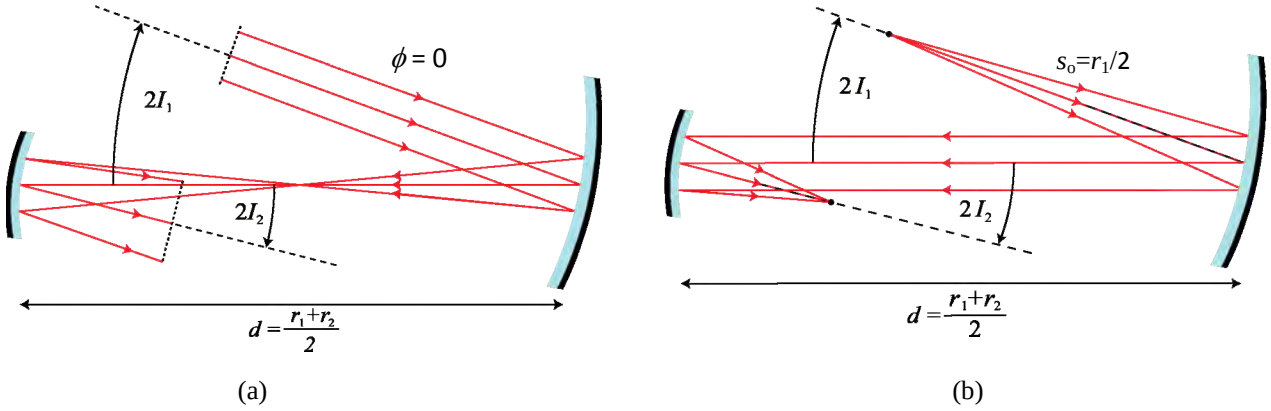

Figura 4.6.- Notación empleada para describir un telescopio afocal formado por un par de superficies fuera de eje en configuraciones (a) finita e (b) infinita.

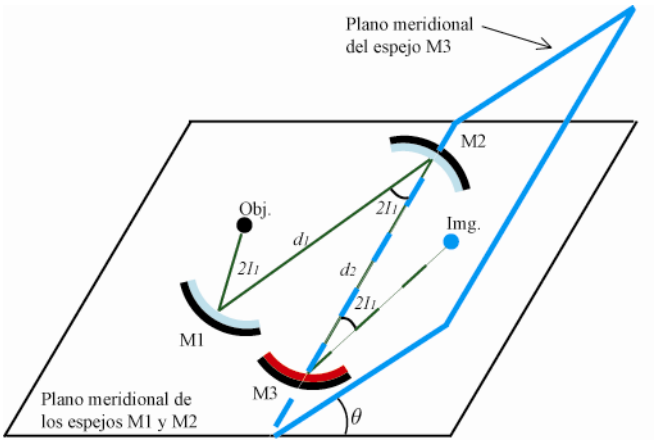

Figura 4.7 Esquema general para un sistema de tres espejos con dos planos meridionales.

$$I_3 = \frac{r_2 r_3 \sqrt{-\sec(2\theta)} \sqrt{s^2 r_1 r_2 I_1^2 + \left[-2sd_1 + (s+d_1) r_1\right]^2 I_2^2}}{d_1 (2s - r_1)(2d_2 - r_2) + s r_1 r_2 + d_2 \left(-2s r_2 + r_1 (-2s + r_2)\right)} \tag{4.10}$$

donde r_i son los radios de los espejos, d_i la distancia entre los vértices de los espejos M_i y M_{i+1}.

Podemos plantear el sistema, que es una idea similar a la planteada por Burns[2007] y Dubra [2010], donde M1 y M2 forman un sistema afocal ($d_1=(r_1+r_2)/2$) y el tercer espejo está en una configuración aplanática de Abbe ($d_2=r_2/2+r_3$), en este caso nuestra condición para compensación del astigmatismo se reduciría a:

$$I_3 = -\frac{\sqrt{-\sec[2\theta]} \sqrt{r_2 \left(r_2 I_1^2 + r_1 I_2^2\right)}}{2\sqrt{r_1 r_3}} \tag{4.11}$$

donde se observa claramente una fórmula simple que nos permite diseñar un sistema acoplado de un telescopio afocal con un espejo simple en configuración aplanática de Abbe. Es claro que la imagen intermedia no se encuentra compensada para el astigmatismo de tercer orden, lo cual es una desventaja, pero no hay que olvidar que puede ser una opción viable si los ángulos de incidencia son pequeños.

Otra opción son tres configuraciones aplanáticas de Abbe, donde $d_1=r_1+r_2$ y $d_2=r_2+r_3$, teniendo tres planos conjugados. Donde nuestra condición para la compensación de astigmatismo se reduce a:

$$I_3 = \frac{\sqrt{-\sec[2\theta]} \sqrt{\left(r_1 I_1^2 + r_2 I_2^2\right)}}{\sqrt{r_3}} \tag{4.12}$$

Este sistema tiene la única desventaja que la magnificación es unitaria, y si empleamos un sólo radio de curvatura para todos los espejos, la compensación estaría únicamente determinada

por los ángulos de incidencia y ángulo del plano desdoblado, que sigue presentando la restricción $|\theta| \varepsilon (\pi/4, 3\pi/4)$.

También se pueden plantear combinaciones para espectrografía y resonadores laser con espejos convexos y expandir la discusión, dependiendo las necesidades del lector.

4.3.3 Sistema de cuatro espejos

Si ahora continuamos con un sistema de cuatro espejos, como el que se esquematiza en Fig. 4.8. Podemos, encontrar con relativa facilidad el valor de I_4 sobre el plano meridional θ para tener compensado el astigmatismo de tercer orden:

$$
\begin{aligned}
I_4 = \sqrt{}\Big(-\Big(\sec[2\theta] r_3 r_4 \Big(4s^2 \Big(d_1^2 r_2 r_3 I_2^2 + \big(-2d_1 d_2 + (d_1 + d_2) r_2\big)^2 I_3^2\Big) + \\
sr_1 \Big(r_2 r_3 \big(s r_2 I_1^2 - 4d_1 (s + d_1) I_2^2\big) - 4\big(2d_1 d_2 - (d_1 + d_2) r_2\big)\big(2(s + d_1) d_2 - (s + d_1 + d_2) r_2\big) I_3^2\Big) + \\
r_1^2 \Big(\big((s + d_1)^2 r_2 r_3 I_2^2 + \big(-2(s + d_1) d_2 + (s + d_1 + d_2) r_2\big)^2 I_3^2\Big)\Big)\Big)\Big) / \\
\big(d_2 \big(r_1 (2s - r_2) + 2s r_2\big)\big(2d_3 - r_3\big) + s r_1 r_2 r_3 - d_1 (2s - r_1)\big(d_2 \big(4d_3 - 2r_3\big) + r_2 r_3 - 2d_3 \big(r_2 + r_3\big)\big) + \\
d_3 \big(-2s r_2 r_3 + r_1 \big(-2s r_3 + r_2 \big(-2s + r_3\big)\big)\big)\big)
\end{aligned}
\qquad (4.13)
$$

que al ser una expresión general y compleja, no permite una evaluación global de la compensación. En las siguientes líneas, profundizaremos en algunos casos específicos para nuestro interés, que nos permitirán apreciar el potencial de la Ec. 4.13.

Primero consideremos el caso de dos telescopios afocales en configuración finita, es decir, $d_1=(r_1+r_2)/2$, $d_2=(r_2+r_3)/2$, $d_3=(r_3+r_4)/2$ y $s=r_1/2$. Por lo que la Ec. 4.13 se reduce a:

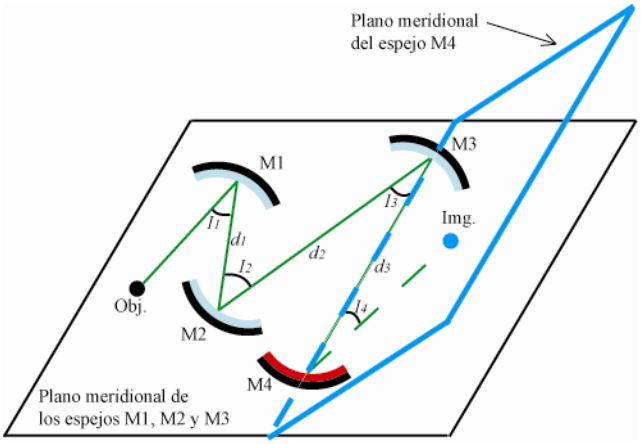

Figura 4.8 Esquema general para un sistema de cuatro espejos con dos planos meridionales.

$$I_4 = -\frac{\sqrt{-\sec[2\theta] r_4 \left(r_2^2 I_1^2 + r_1 r_2 I_2^2 + r_1 r_3 I_3^2\right)}}{r_3 \sqrt{r_1}} \tag{4.14}$$

De esta expresión, se puede deducir que $|\theta| \varepsilon (\pi/4, 3\pi/4)$, para poder lograr la compensación del astigmatismo. También, se observa que la Ec.4.14 depende de los valores de los ángulos de incidencia.

Por otro lado, es posible que al lector le interese un sistema con un telescopio afocal y dos configuraciones aplanáticas de Abbe, por ejemplo con $d_1=(r_1+r_2)/2$, $d_2=r_2/2+r_3$, $d3=r_3+r_4$ y $s=r_1/2$, entonces:

$$I_4 = -\frac{\sqrt{-\sec[2\theta]\left(r_2^2 I_1^2 + r_1 r_2 I_2^2 + r_1 r_3 I_3^2\right)}}{2\sqrt{r_1 r_4}} \tag{4.15}$$

O bien le interese la configuración con $d_1=r_1+r_2/2$, $d_2=(r_2+ r_3)/2$, $d_3=r_3/2+r_4$ y $s=r_1$:

$$I_4 = -\frac{\sqrt{-\sec[2\theta] r_3 \left(r_1 r_3 I_1^2 + r_2 r_3 I_2^2 + r_2^2 I_3^2\right)}}{2 r_2 \sqrt{r_4}} \tag{4.16}$$

Observe que estas expresiones implican diferentes acomodos de sus componentes.

Otro caso sumamente interesante es la combinación de cuatro configuraciones aplanáticas de Abbe ($d_1=r_1+r_2$, $d_2=r_2+r_3$, $d_3=r_3+r_4$ *y* $s=r_1$):

$$I_4 = -\frac{\sqrt{-\sec[2\theta] \quad \left(r_1 I_1^2 + r_2 I_2^2 + r_3 I_3^2\right)}}{\sqrt{r_4}} \tag{4.17}$$

Para todos los casos anteriores podemos también hallar soluciones para valores infinitos de *s*, los cuales también son importantes cuando trabajamos con un sistema que tiene múltiples planos objetos e imágenes como por ejemplo en las cámaras retinianas con óptica adaptativa.

En conclusión es posible seguir extendiendo nuestro análisis para cualquier número de configuraciones y espejos cóncavos o convexos (infinito número de casos) (Anexo 8).

4.4 COMPENSACIÓN DEL ASTIGMATISMO PARA DOS PLANOS IMAGEN CONJUGADOS

El interés inicial en esta investigación, fue poder compensar el astigmatismo para dos planos conjugados al mismo tiempo, uno finito (plano de la pupila del ojo) y otro infinito (plano de la imagen de la retina), para una cámara retiniana con óptica adaptativa. Procederemos a discutir una forma de lograr lo anterior, empleando dos telescopios afocales compensado para el caso finito independientemente y para un par de espejos simples en configuración aplanática de Abbe. Ambas configuraciones tienen sus ventajas y desventajas.

Para lo cual consideramos dos requisitos:

- En cada actuador óptico, ya sea espejo deformable, sensor de frente de onda o espejo resonante debe estar compensado el astigmatismo del plano conjugado de la pupila del ojo.

- En el sistema de imaginología, ya sea un AOSLO o un AOOCT, debe estar compensado el astigmatismo en el plano conjugado de retina.

Con los resultados de la sección anterior podemos compensar el astigmatismo para el plano imagen a distancia finita en los telescopios afocales, pero tenemos como residuo una coma a 45° y el valor de la esfericidad permanece constante con respecto a una configuración no compensada. Como se ha demostrado [Rosendahl, 1962], en una configuración con planos meridionales coplanarios, es posible compensar la coma en una configuración simétrica (Fig 4.3), sin embargo la restricción es una magnificación unitaria, teniendo como residuos un astigmatismo duplicado y la aberración de esfericidad permanece constante respecto a la configuración antisimétrica (Fig. 4.2). Mientras que en configuración de puntos aplanáticos de Abbe, el astigmatismo no es compensado, pero la coma y la aberración de esfericidad son cero como se observa en la Fig. 3.6. Debido a que los ángulos de incidencia pueden ser tan pequeños como las restricciones físicas lo permitan (limitado por el tamaño de las monturas mecanicas), es posible construir sistemas que se encuentren bajo el límite de difracción. La compensación del plano conjugado infinito (planos de la imagen retiniana) es necesaria únicamente en el plano del sistema de detección.

Para telescopios afocales, empleamos dos arreglos, imponiendo la compensación del astigmatismo en planos finitos:

$$I_2 \approx \sqrt{-\frac{M_{12}}{\cos(2\theta_2)}} I_1, \quad I_4 \approx \sqrt{-\frac{M_{34}}{\cos(2\theta_4)}} I_3 \tag{4.18}$$

Y la condición de minimización de astigmatismo para el plano conjugado infinito impone la condición:

$$I_3 = \frac{1}{M_{12}}\sqrt{-\frac{r_3\left(1-M_{12}{}^2\right)\cos(2\theta_4)}{r_1\left\{M_{34}^2\sin\left[2\left(\theta_2+\theta_3\right)\right]\sin\left(2\theta_4\right)+\left(1-M_{34}^2\right)\cos\left[2\left(\theta_2+\theta_3\right)\right]\cos\left(2\theta_4\right)\right\}}}I_1 \qquad (4.19)$$

Donde M_{ij} es la amplificación del espejo, dada por r_j/r_i, θ_k es el ángulo de rotación del plano meridional respecto al plano anterior del sistema. Con esta expresión es posible tener compensados el par de telescopios afocales para ambos planos. Para la configuración más compacta tenemos $|\theta_2| = |\theta_4| = \pi/2$ y $|\theta_3| = 0, \pi/2, \pi$, con lo que se reduce a:

$$I_3 \approx \frac{1}{M_{12}}\sqrt{\pm\frac{r_3}{r_1}\left(\frac{1-M_{12}{}^2}{1-M_{34}{}^2}\right)}I_1 \qquad (4.20)$$

El signo depende de $\theta_3 = 0, \pi$ o $|\theta_3| = \pi/2$, donde tenemos dos familias de soluciones:

- para $|\theta_3| = \pi/2$, $M_{12} > 1$ y $M_{34} < 1$,
- para $\theta_3 = 0, \pi$ $M_{12} < 1$ y $M_{34} < 1$.

Una discusión de los efectos del desenfoque y compensación de Badal (optómetro de Badal), así como un ejemplo numérico, puede ser revisada en nuestro artículo, reproducido en el anexo 2.

En general con este arreglo se puede lograr:

- Compensación de astigmatismo en cada plano conjugado de pupila del ojo, pero residuos de coma inclinada dependiendo de la inclinación del ángulo meridional y la aberración esférica permanecerá constante.
- Compensación de astigmatismo en el plano conjugado de retina final, con residuos de coma, cuyo valor puede variar de acuerdo a los dobleces de los planos meridionales (con posibilidad de ser compensada dependiendo del sistema) y esférica permanecerá constante.

Además debe señalarse, que con estas compensaciones para la compensación del astigmatismo en ambos planos conjugados, Ecs. 4.18 y 4.19, siempre son necesarios arreglos en número par de telescopios afocales.

Por otro lado, para la configuración de dos espejos en configuración aplanática de Abbe, se emplea la Ec. 4.7 con la condición $d=r_1+r_2$ con $s=\infty$.

$$I_2 = \frac{\sqrt{r_1 r_2}\, I_1}{\sqrt{-\cos[2\theta]\left(r_1 + 2r_2\right)^2}} \tag{4.21}$$

Donde claramente se observa que $|\theta| \; \varepsilon \; (\pi/4, \; 3\pi/4)$. En esta configuración, obtenemos:

- Compensación del astigmatismo en el plano de la retina, con coma inclinada proporcional a la inclinación de los planos meridionales y presencia de esférica.
- Compensación de la coma y esférica para el plano de pupila del ojo, pero presencia de astigmatismo (que puede ser muy reducido debido al pequeño ángulo de incidencia)

Donde también es necesario tener un número par de telescopios para poder lograr las compensaciones descritas en ambos planos conjugados.

Estas soluciones son aceptables, y aunque no está totalmente resuelto el problema de la compensación de aberraciones, hemos logrado obtener resultados numéricos y prácticos, que demuestran la mejora en el diseño sistemático de sistemas de escaneo retiniano con óptica adaptativa y la posibilidad de poder emplear estas metodologías en el diseño de resonadores láser y espectrógrafos. Además hemos demostrado que la implementación de arreglos mixtos pueden ser una solución viable en estos sistemas, vea anexo 3 [Dubra, 2010].

4.5 REFERENCIAS

Dubra, A., Gómez-Vieyra, A., Sulai, Y., Díaz-Santana, L., "Optical Design of Clinical Adaptive Optics Instruments for Retinal Imaging," in Frontiers in Optics, OSA Technical Digest (CD) (Optical Society of America, 2010), paper FTuB3, (Anexo C).

Gómez-Vieyra, A., Dubra A., Malacara-Hernández, D., Williams, D.R. "First-order design of off-axis reflective ophthalmic adaptive optics systems using afocal telescopes," Opt. Express **17** (2009) (Anexo B).

Gross, H. (2005), *Handbook of Optical Systems*. Germany: Wiley-VHC

Malacara, D., Z. Malacara (2004), *Handbook of Optical Design*. USA: Marcel Dekker.

Roorda, A., Romero-Borja, F., Donnelly, W.J., et al., "Adaptive Optics Laser Scanning Ophthalmoscopy," *Opt. Express.* **10** (2002).

Rosendahl. G. R., "Contributions to the Optics of Mirror Systems and Gratings with Oblique Incidence. III. Some Applications," J. Opt. Soc. Am. **52** (1962)

Burns, S. A., Tumbar, R., Elsner, A. E. , Ferguson, D. and Hammer, "Large-field-of-view, modular, stabilized, adaptive-optics-based scanning laser ophthalmoscope," J. Opt. Soc. Am. A **24** (2007) 1313-1326.

Webb, R.H., Hughes, G.W., Pomerantzeff, O., "Flying Spot TV Ophthalmoscope," Appl. Opt. **19** (1980).

Welford, W. T. (1991), *Aberrations of Optical Systems*. Great Britain:Adam Hilger.

Zhong, Z., Deng, C. and Burns, S., "Wide-Field Steerable Adaptive Optics SLO with Dual Deformable Mirrors: Optical Design," in Frontiers in Optics, OSA (2008) FThM14.

Conclusiones

Durante el desarrollo de la investigación, hemos derivado expresiones analíticas que describen los coeficientes de las aberraciones de frente de onda en la pupila (V. Capítulo 3), en una representación propuesta aquí, que presenta la propiedad de estar balanceada respecto al astigmatismo, es decir, el centro de curvatura de la esfera de referencia se encuentra sobre la superficie de la imagen media (V. Capítulo 2). Las expresiones de los coeficientes de aberración permiten analizar y entender el comportamiento de aberraciones de espejos esféricos fuera de eje, respecto a su radio de curvatura, la posición de la imagen y el ángulo de incidencia del rayo principal, como se muestra en la Figs. 3.4, 3.5 y 3.6. En especial la Fig. 3.6, es un ejemplo numérico, que permite observar las aberraciones de frente de onda que están presentes en diversas configuraciones como son los telescopios afocales (Figs. 4.2 y 4.3) y de espejos en configuración aplanática de Abbe (Fig. 4.4). La teoría desarrollada, permite evaluar las aberraciones bajo cualquier ángulo de incidencia sobre una pupila pequeña, Ecs. 3.5. También se desarrollaron las expresiones para los coeficientes de aberración con aproximaciones a pupila pequeña y ángulos pequeños, Ecs. 3.8, de manera que el centro de curvatura de la esfera de referencia se encuentre cercano la círculo de mínima confusión. La importancia de las aberraciones ha sido discutida considerando la necesidad de su empleo en el diseño en cavidades láser, espectrógrafos y sistemas de imaginología retiniana con óptica adaptativa.

Al introducir una nueva representación de las aberraciones de frente de onda, cuyos términos tienen interpretaciones físicas de fácil comprensión, se propone una familia de polinomios relacionada con las representaciones tradicionales, Seidel, Zernike y la reciente representación de Stephenson, considerando que el centro de curvatura de la esfera de referencia se

encuentra sobre la superficie de la imagen media, lo que permite la representación del frente de onda de sistemas asimétricos, sobre la pupila de cualquier forma y tamaño.

Además se presentó una metodología para poder compensar el astigmatismo de tercer orden en arreglo de sistemas reflectores fuera de eje derivada del uso de la ecuación de haces de rayos marginales, para configuraciones de dos, tres y cuatro espejos con dos planos meridionales en el sistema. Concentramos nuestra atención en discutir las configuraciones que consideramos interesantes para sistemas de escaneo retiniano, aunque el análisis se puede extender a cualquier sistema reflector con espejos cóncavos y/o convexos. Además nos enfocamos a analizar una forma de compensación del astigmatismo en dos planos conjugados (plano de pupila del ojo y de la imagen retiniana), para telescopios afocales. También discutimos las posibles compensaciones para un arreglo de dos espejos en configuración aplanática de Abbe. En el apéndice se muestra un ejemplo del diseño de dos oftalmoscopios por escaneo láser, empleando los resultados obtenidos en este trabajo. Los anexos, presentan los trabajos publicados en revistas con arbitraje y congresos como resultado de la realización de este trabajo. Todos los resultados presentados pueden ser empleados en el diseño de cavidades láser y espectrógrafos.

En las Fig. C1 y C2, se muestran las imágenes de fondo de ojo, en diversas localizaciones obtenidas con el sistema AOSLO de la Universidad de Rochester, que fue rediseñado a partir de los resultados de este trabajo.

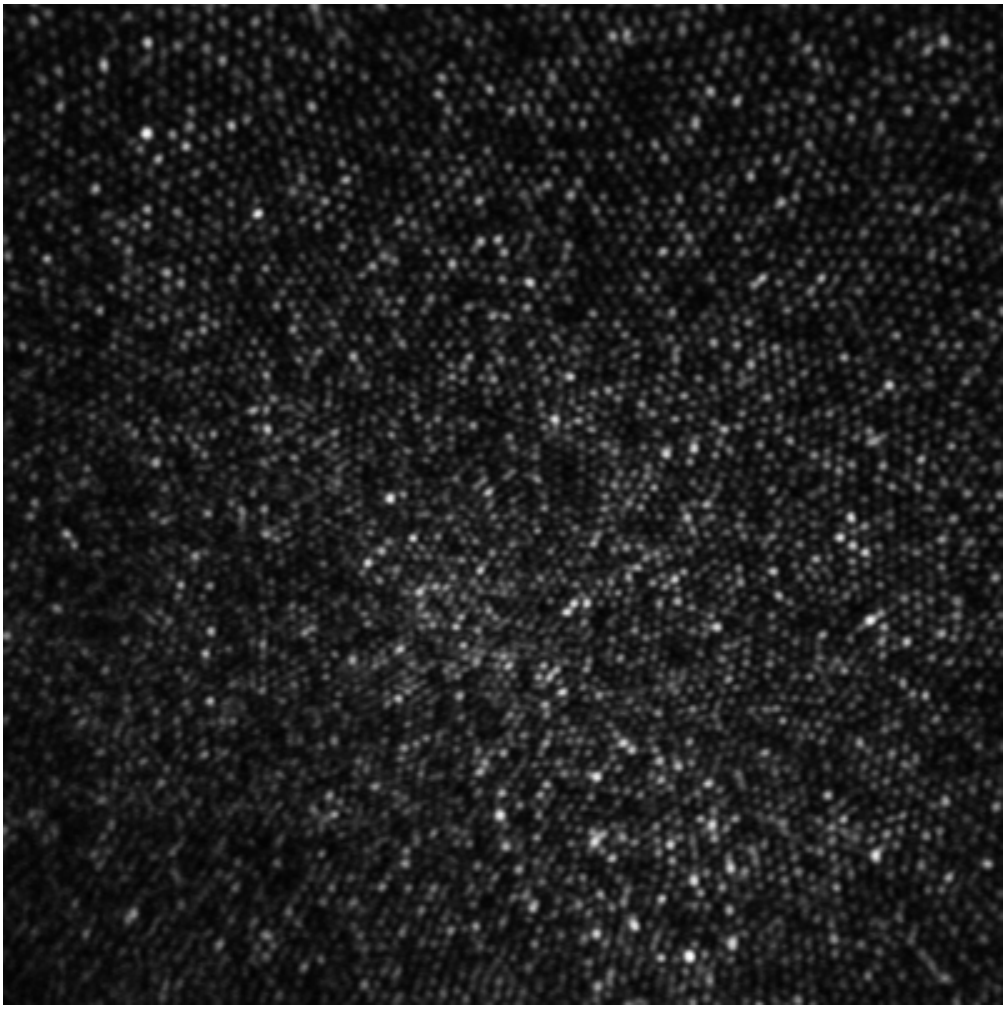

Figura C1.-Imagen de conos por reflexión en el centro de la fóvea. Sujeto: hRY001. Día de la imagen: 21/05/2010. Iluminación por un diodo superluminicente con pico en λ=680nm. Diámetro de la apertura confocal 0.55 de disco de Airy. Cortesía de Alfredo Dubra Suárez y David R. Williams

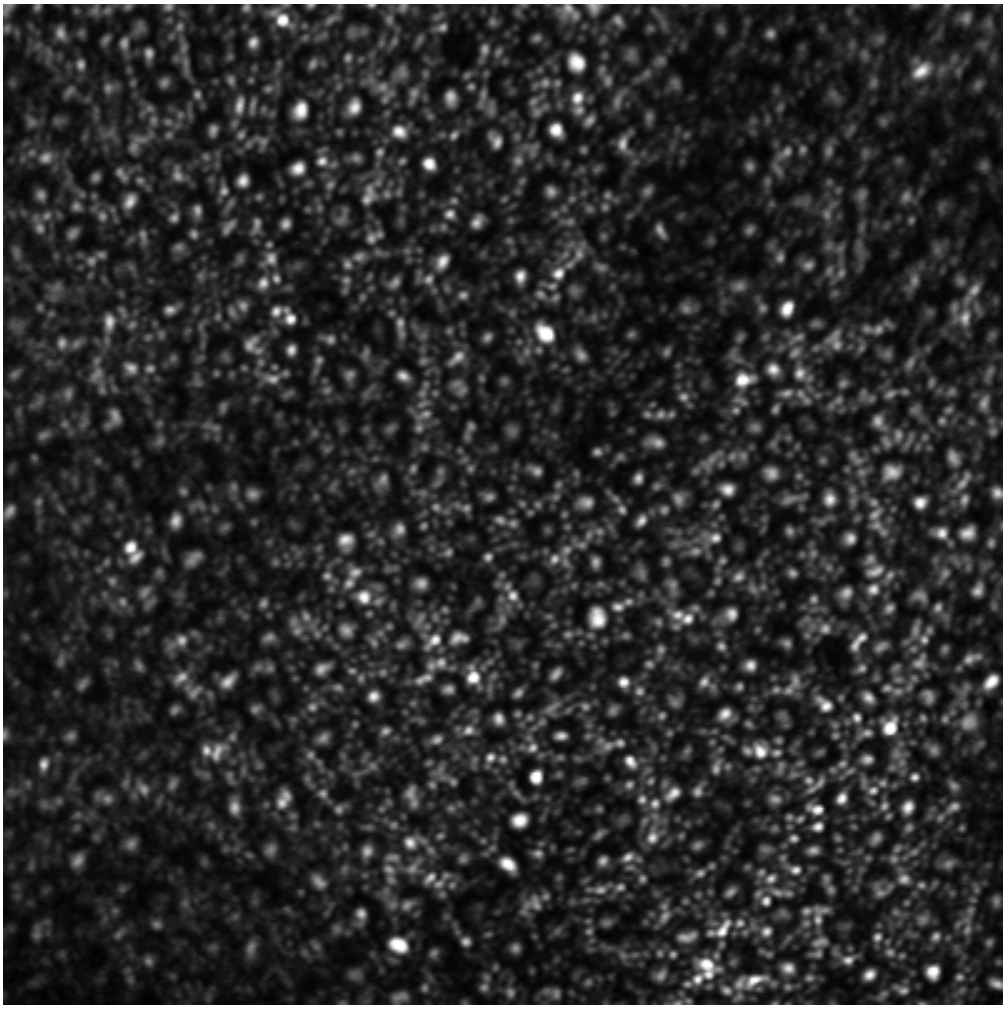

Figura C2.- Imagen de conos y bastones por reflexión en la localización (OS) 10°T, 1°I. Sujeto: hBM001. Día de la imagen: 21/05/2010. Iluminación por un diodo superluminicente con pico en λ=680nm. Diámetro de la apertura confocal 0.55 de disco de Airy. Cortesía de Alfredo Dubra Suárez y David R. Williams

Apéndice

En esta sección se presentan algunos ejemplos simulados con Zemax©, de la aplicación de los resultados obtenidos en el capítulo 4. Además, mostramos los resultados del trazo de rayos en un sistema real, diseñado a partir de los resultados de esta investigación. Donde se muestra que los planos conjugados de pupila del ojo e imagen retiniana se encuentran limitados por difracción, con lo que garantizamos que las aberraciones propias del sistema no afectarán en la medición de aberraciones y por lo tanto, el espejo deformable únicamente compensará las aberraciones propias del sistema ocular.

Debido a los diversos resultados generales y particulares presentados en el capítulo 4, únicamente presentamos algunos ejemplos ilustrativos:

- Dos espejos en configuración aplanática de Abbe con corrección del astigmatismo (Ec. 4.7) para el plano imagen finito (Fig. A1).

- Dos espejos en configuración aplanática de Abbe con compensación del astigmatismo (Ec. 4.7) para el plano imagen infinito (Fig. A2).

- Configuración de tres espejos con radios de curvatura iguales, sin astigmatismo (Ec. 4.10), para el plano conjugado finito (Fig. A3).

- Configuración de tres espejos formadores de imagen con astigmatismo compensado (Ec. 4.10) en el plano imagen finito (Fig. A4).

- Configuración de cuatro espejos formadores de imagen con corrección del astigmatismo (Ec. 4.13) para planos imagen finito (Fig. A5).

Además, las Figs. A7 y A8 muestran los resultados del rediseño de un oftalmoscopio por escaneo láser con óptica adaptativa de la Universidad de Rochester (Fig. A6). En el cual se aplicaron gran parte de los resultados desarrollados durante esta investigación (Ecs. 4.18 y 4.20). Como puede observarse, el sistema es robusto, debido a que soporta hasta ± 2 D de desenfoque (Fig. A7), limitado por difracción para todas las configuraciones. No se observa simetría en los diagramas de manchas de +2 y -2D, debido a que el sistema no es centrado y no presenta simetría de rotación en la pupila. También, se muestra el diagrama de manchas en la pupila (A8), que permanece constante durante el escaneo y el desenfoque; que es ventaja al realizar las mediciones de frente de onda. Lo que beneficiará al subsistema de óptica adaptativa cuando se realice la compensación del frente de onda, es decir, el espejo deformable no compensará de forma aleatoria aberraciones, sino solo compensará las aberraciones estáticas remanentes en el oftalmoscopio y las aberraciones oculares del paciente.

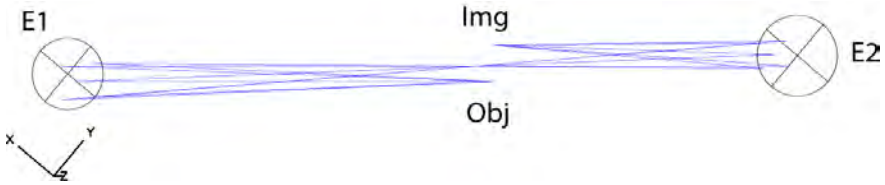

(a)

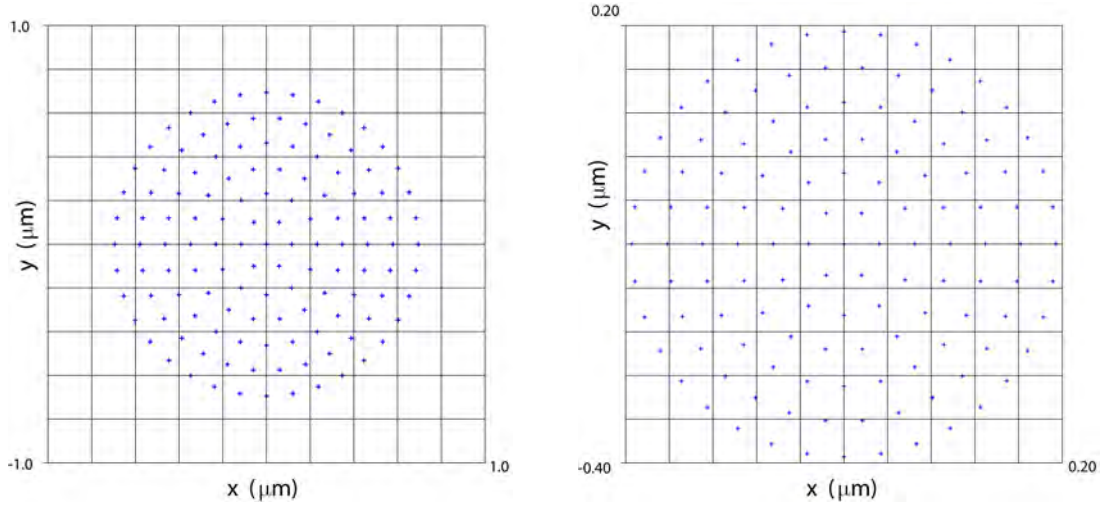

(b) (c)

Figura A1. (a) Diagrama de la configuración de dos espejos
(r_1=1000, r_2=750, s=1000, I_1=5° e I_2=5.7735).
(b) Diagrama de manchas en la imagen sin la compensación (θ=0°).
(c) Diagrama de manchas en la imagen con compensación a θ=90°.

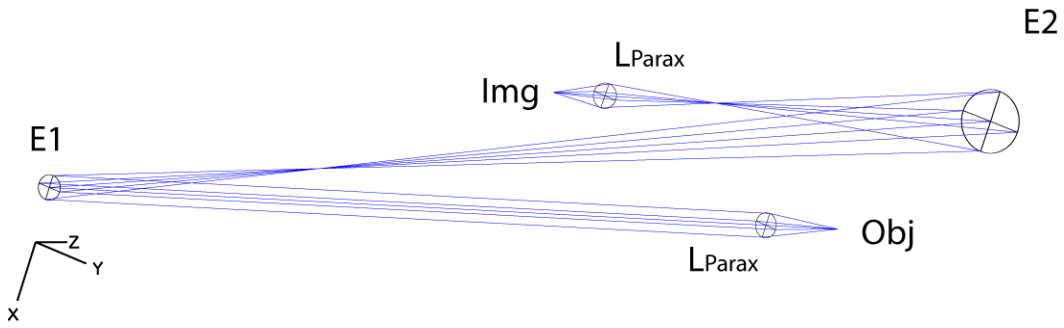

(a)

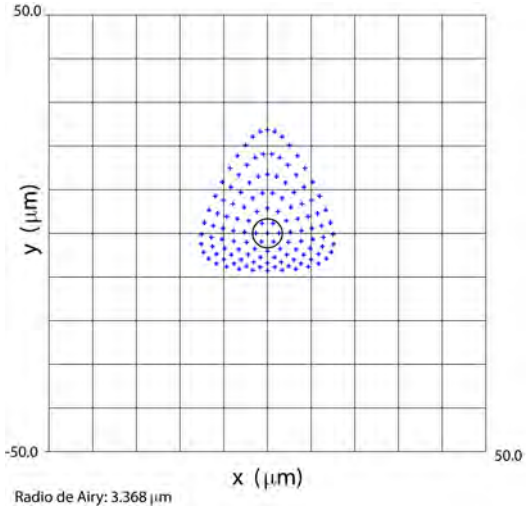

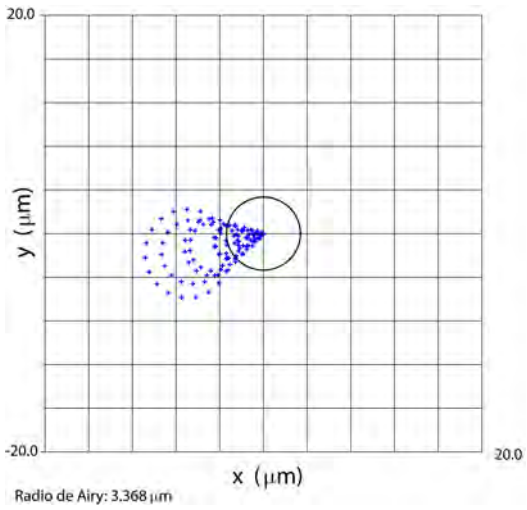

(b) (c)

Figura A2. (a) Diagrama de la configuración de dos espejos
(r_1=1000mm, r_2=750mm, s=∞, I_1=5° e I_2= 1.73205°).
(c) Diagrama de manchas en la imagen sin la compensación (θ=0°).
(b) Diagrama de manchas en la imagen con compensación a θ=90°.

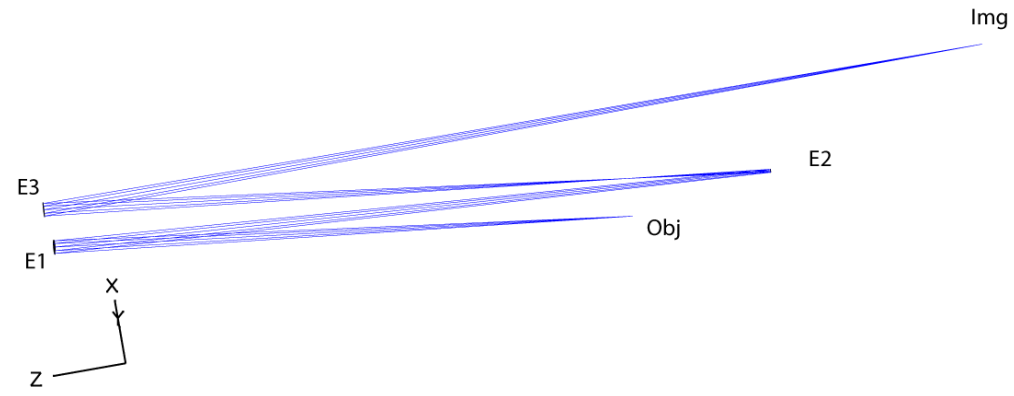

(a)

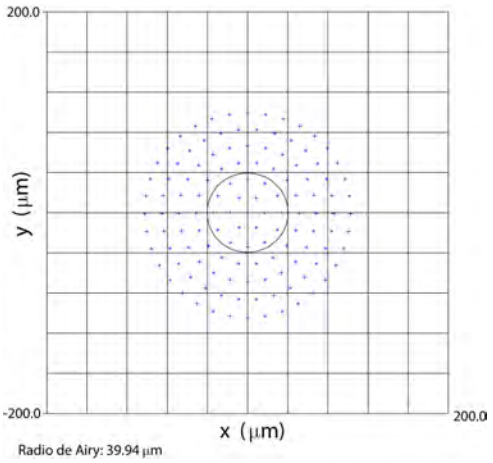

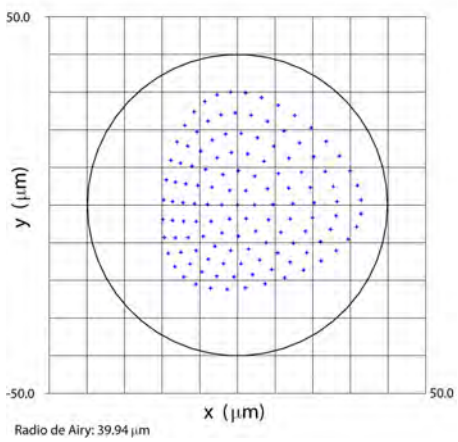

(b) (c)

Figura A3. (a) Diagrama de la configuración de tres espejos (r_1=1000mm, r_2=1000mm, r_3=1000mm, s=800mm, d_1=1000mm, d_2=1000mm, I_1=3°, I_2=3° e I_3=3.99769°).
(b) Diagrama de manchas en la imagen sin la compensación (θ=0°).
(c) Diagrama de manchas en la imagen con compensación a θ=90°.

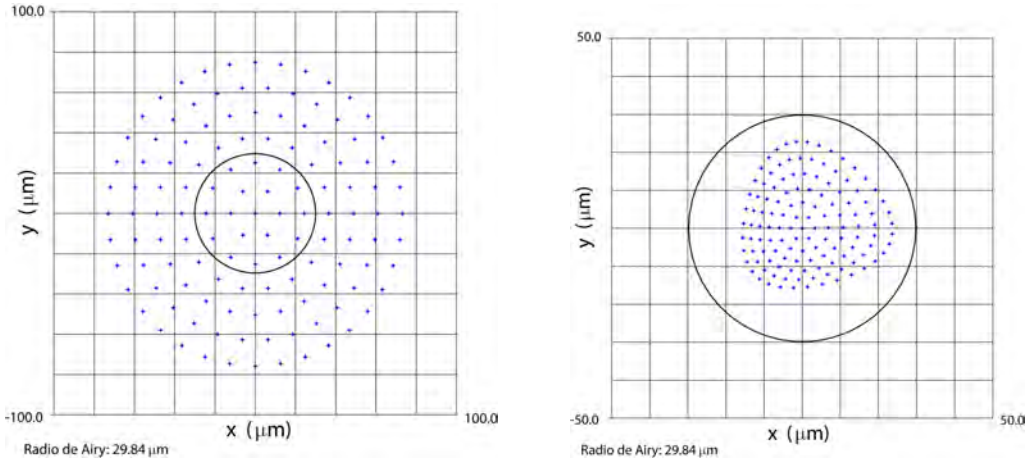

(a) (b)

Figura A4. (a) Diagrama de manchas en la imagen sin la compensación (r_1=1000mm, r_2=2000mm, r_3=1500mm, s=800mm, d_1=1500mm, d_2=1750mm, I_1=3°, I_2=5°, I_3=3.93947° y θ=0°).
(b) Diagrama de manchas en la imagen con la compensación de un sistema tres espejos con plano meridional a θ=90°.

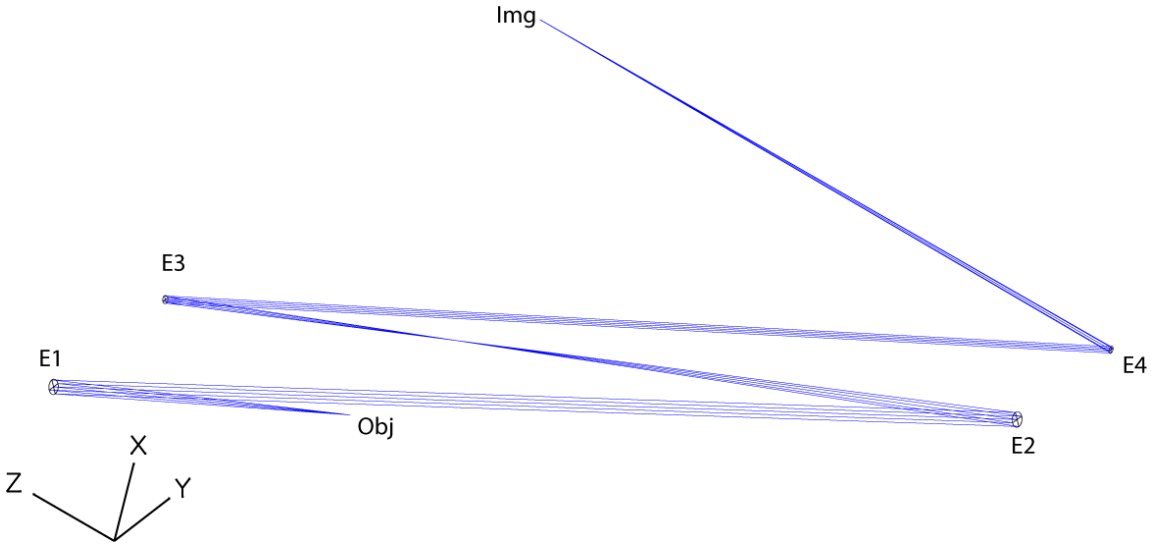

(a)

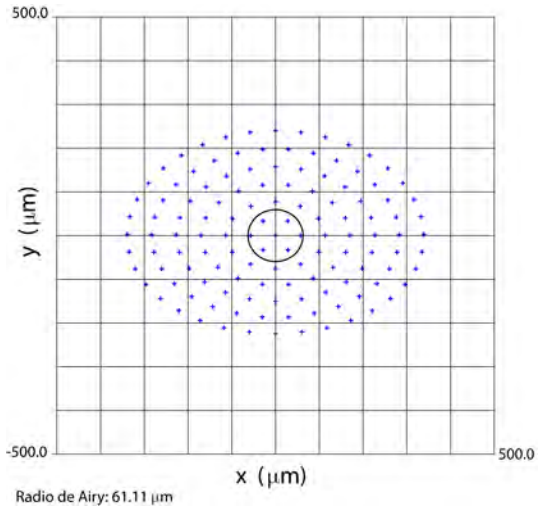

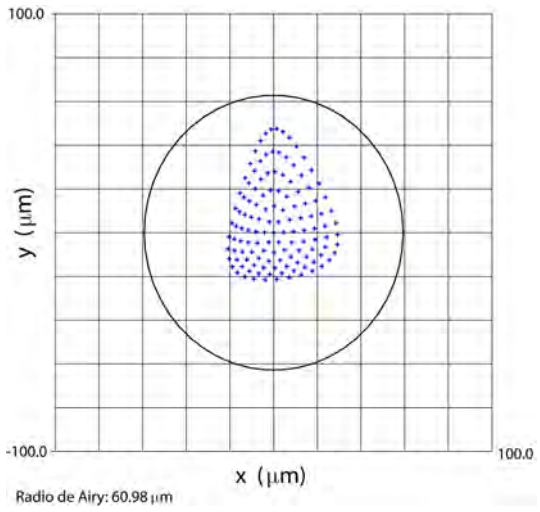

(b) (c)

Figura A5. (a) Diagrama de la configuración de cuatro espejos (*r1=1000mm, r2=2000mm, r3=1000mm, r4=200, s=800mm, d1=1500mm, d2=1500mm, d3=1500mm, I1=3° , I2=5°, I3=4, e I4=14.2842*).
(b) Diagrama de manchas en la imagen sin la compensación (θ=0°).
(c) Diagrama de manchas en la imagen con compensación a θ=90°.

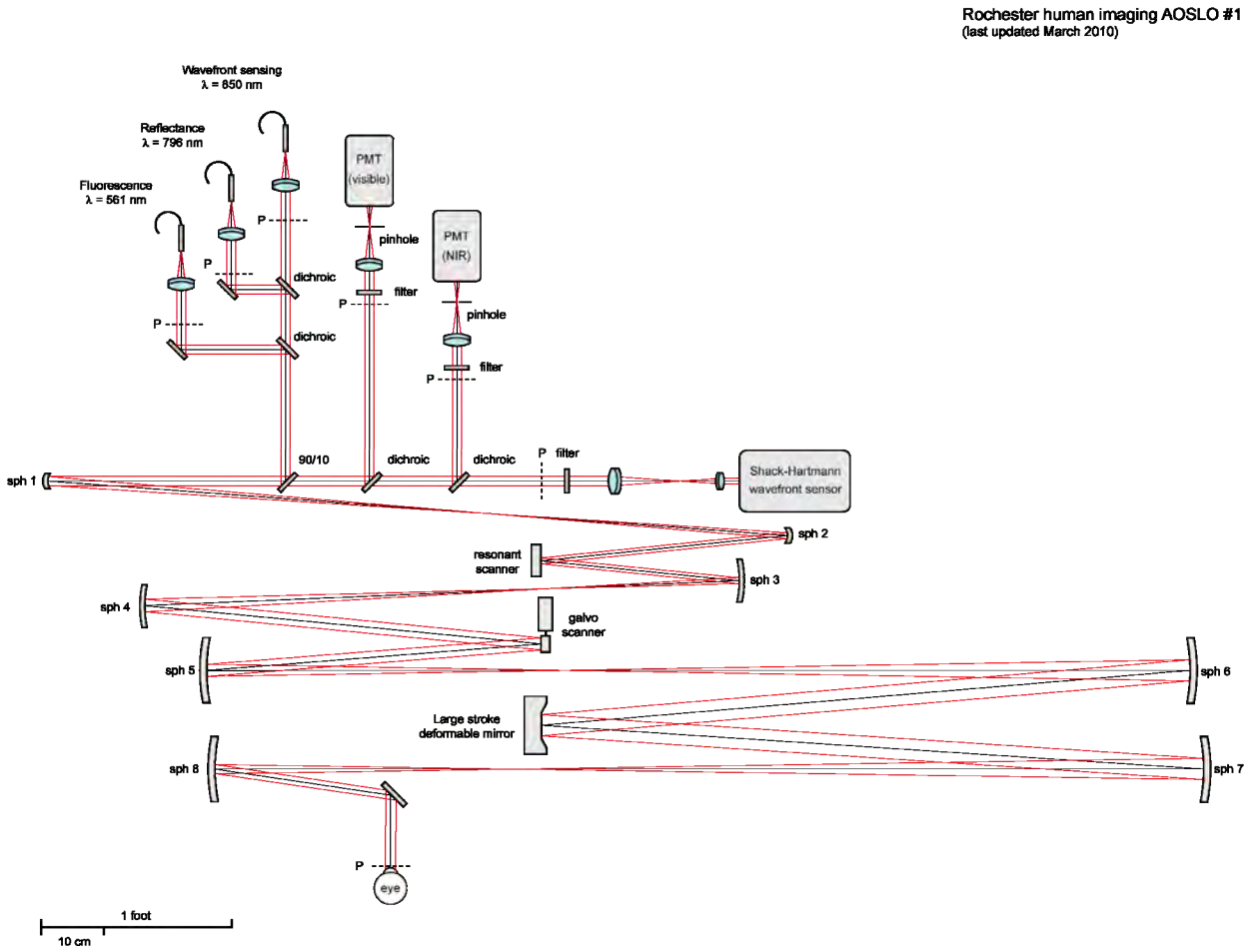

Figura A6. Diagrama general del oftalmoscopio por escaneo láser de la Universidad de Rochester, rediseñado. Compensando el astigmatismo tanto en plano conjugado de la pupila del ojo sobre todos los actuadores y el sensor de frente de onda, y en el plano conjugado de retina sobre el segundo espejo resonante (galvo) y el plano de los fotomultiplicadores (PMTs). Cortesía de Alfredo Dubra.

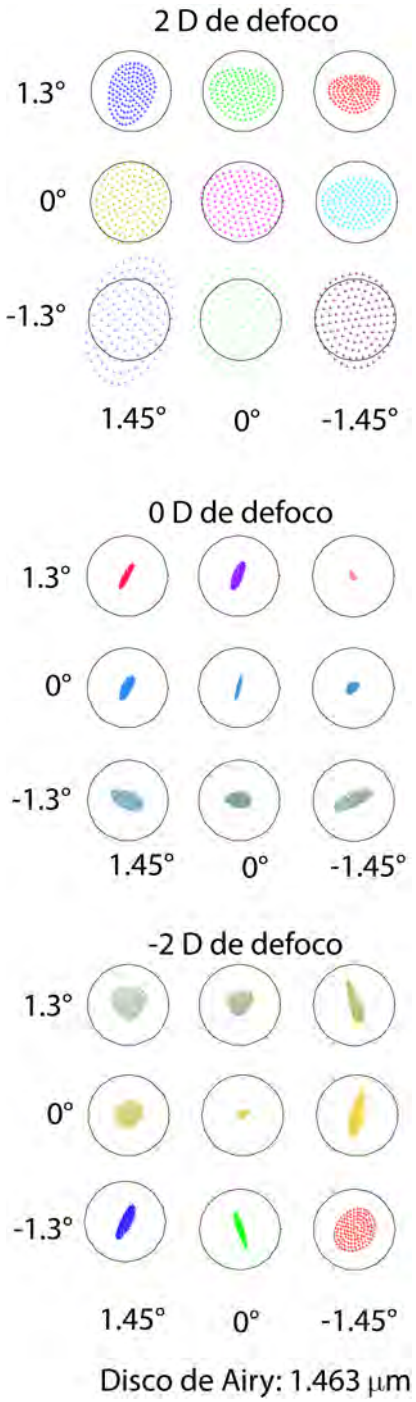

Figura A7. Diagramas de manchas sobre imagen de retina con desenfoque a +2D, 0D y -2D. Los cuales muestran que nuestro diseño óptico se encuentra limitado por difracción para un barrido sobre retina de 1.9° *1.6°.

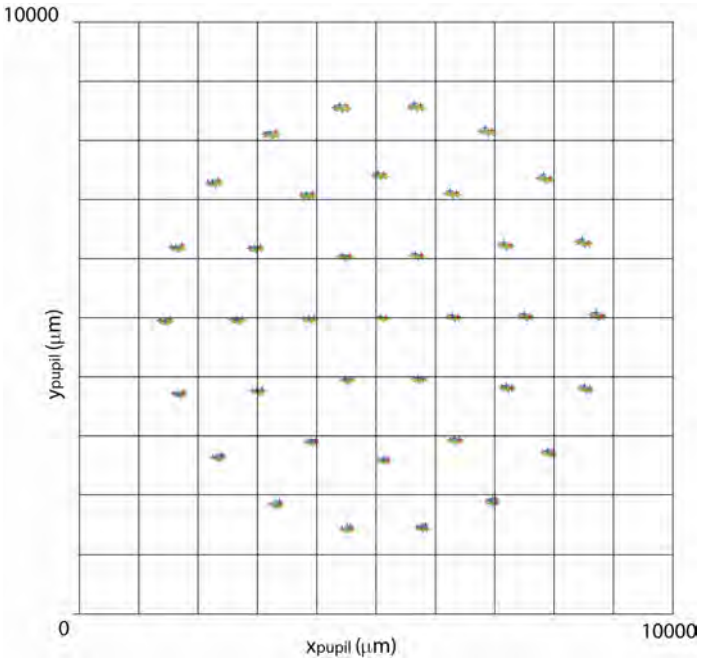

Figura A8. Los rayos sobre pupila mostrados para todas las configuraciones de la Fig.A7, donde se puede observar que coinciden en un solo plano de pupila, lo que indica que el sensor de frente de onda siempre observará la misma imagen de pupila del ojo.

ANEXO 1

Geometrical theory of wavefront aberrations in off-axis spherical mirror

Armando Gomez-Vieyra[1] and Daniel Malacara-Hernández[1,*]

[1] *Centro de Investigaciones en Óptica A.C, Loma del Bosque 115, C.P. 37000, León, Guanajuato, México*

[*] *Corresponding author: dmalacara@cio.mx*

Abstract

Expressions for the wavefront aberrations in an off-axis spherical mirror are presented, analyzed and evaluated. These formulas are derived from the optical path difference between an ellipsoid and a sphere, assuming a relatively small pupil and a small angle of incidence as it will be described with detail. Some well known but also some useful new aberration expressions are obtained. They can be used to design and analyze cavities, spectrographs and retinal adaptive optics imaging systems.

OCIS codes: 080.080, 080.4035, 080.1005, 220.2740.

Introduction

A circular spherical mirror has an axis of rotational symmetry, called optical axis, which is a line passing through the center of curvature and the vertex of the mirror, defined at the center of the clear aperture of the mirror. If the object is laterally displaced from the optical axis we have an off-axis configuration, also known as oblique systems or tilt-decenter systems. Off-axis

mirror configurations are required in some highly specialized systems. The fields that show more fruitful development in off-axis reflective systems are those of adaptive optics ophthalmic instruments, laser resonators and spectrographs. They have some advantages over refractive elements, like the absence of dispersion and chromatic aberration; however, the use of these elements presents different problems, mainly the presence of astigmatism and coma.

Adaptive optics retinal imaging systems use spherical mirrors in an off-axis arrangement to relay the image and pupil planes [1-7]. Most of the designs where the optical axes of all elements are on a common plane (planar configuration) have off-axis aberration problems. Laser resonators with several mirrors are often used in different applications [8], where the design goal is to find off-axis configurations that are free of astigmatism; in other words, the output beam has a regular shape, and the resonator does not have thermal lens effects. Off-axis mirror spectrographs [9,10] present design restrictions mainly in the resolving power and in the off-axis aberrations. In summary, when using off-axis spherical mirrors in a planar arrangement, such as in the previous systems, the resulting instruments are limited by astigmatism in most of the cases. Recently Gómez-Vieyra *et al.*[11], demonstrated that by folding the meridional plane of pairs of spherical mirrors in a prescribed three-dimensional configuration, the astigmatism can be cancelled out at a single off-axis point on the field of view. Spherical aberration and coma are the residual aberrations in third order theory, but the behavior of all aberrations is not yet fully understood.

Here, we will develop a more complete analysis than that given by the third order aberration coefficients, including some important higher order aberrations. Using the principle of the optical path difference principle between the sphere and an ellipsoid surface, we developed the mathematical expressions that describe the third order wavefront aberrations in a single off-

axis spherical mirror (Fig. 1a). We discuss here the implication of the off-axis aberrations and their dependence on the magnitude of the angle of incidence. These approximations are calculated under the assumption that we have a small pupil and a small angle of incidence; however, it is possible to calculate the exact expression for any angle of incidence with the procedure described in this text. The exact expressions are presented in the appendix at the end.

Theory

Methodology

Figure 1a shows a point object at a distance L from the spherical mirror vertex P, with an incidence angle I and spherical mirror radius of curvature r. Some years ago, Malacara [12] developed expressions that describe the wavefront aberration of an off-axis spherical mirror used either to collimate the light from a point source or to concentrate the light from a collimated beam on a point; using the same idea, we present the extended theory for any case. Calculating the optical path difference between the spherical mirror and the closest ellipsoid, it is possible to find the wavefront aberration function (Fig. 1b).

Let us consider the spherical mirror, with its pupil at the same plane as the mirror and with an off-axis point object. The reflected wavefront is aberrated. The aberrations produce an image with tangential, saggital, Petzval and least confusion (medium) foci, assuming a relatively small coma. Then, the spherical mirror is replaced by a reflecting ellipsoid that has one of its foci at the point object and the second focus near the images produced by the spherical mirror, as shown in Fig. 2. The wavefront produced by the reflecting ellipsoid is spherical (no aberration), hence, we can take this wavefront as a reference to measure the aberration for the wavefront produced by the spherical mirror.

The ellipsoid can be chosen so that its second focus is at tangential, saggital, medium or Petzval images. If the image being selected for this ellipsoid second focus is the medium image (Fig. 2a), the astigmatism wavefront aberration will take the typical shape of a saddle.

Under these conditions, the wavefront aberration *W* can now be defined as the separation between the wavefronts produced by the spherical mirror and the reflecting ellipsoid (Fig 1b).

Analytical treatment

The equation for an ellipsoid (Fig. 3a) in the coordinate system *x'*, *y'*, and *z'*, with rotational symmetry about the *z'* axis, is

$$\frac{x'^2}{b^2}+\frac{y'^2}{b^2}+\frac{z'^2}{a^2}=1. \tag{1}$$

Symbols *a* and *b* are the major and minor semiaxes. Then, we rotate the system of coordinates an angle *ø* over the *y* axis, as shown in Fig. 3b (rotation about the x axis if desired). Using the first and second derivatives, it is possible to find the lowest point of the rotated ellipsoid (Fig. 3b). Translating this minimum of the ellipsoid to the origin of coordinates, as in Fig. 3c, we obtain

$$\begin{aligned} 1=\frac{x^2}{b^2}+\cos^4(\phi)+2z\cos(\phi)\sin(\phi)\left[\frac{y}{a^2}-\frac{y}{b^2}-\frac{2}{\sqrt{a^2\csc^2(\phi)+b^2\sec^2(\phi)}}\right]+ \\ \sin^4(\phi)+\cos^2(\phi)\left[\frac{y^2}{b^2}+\frac{z^2}{a^2}-\frac{2z\cot(\phi)}{\sqrt{a^2\csc^2(\phi)+b^2\sec^2(\phi)}}+2\sin^2(\phi)\right]+ \\ \sin^2(\phi)\left[\frac{y^2}{a^2}+\frac{z^2}{b^2}-\frac{2z\tan(\phi)}{\sqrt{a^2\csc^2(\phi)+b^2\sec^2(\phi)}}\right] \end{aligned} \tag{2}$$

Since an expression for the lower part of the ellipsoid is necessary for our development, we can find the expression of this surface by solving Eq. 2 with respect to *z*. We then obtain two expressions; one represents the top region, and the other the lower region of the ellipsoid. Taking only the expression for the lower region, assuming a relatively small aperture, we calculate its Maclaurin series representation. This series is infinite and convergent, but we will consider terms only until the fourth order, corresponding to the third-order aberrations.

$$\begin{aligned} z_{ellipsoid} &= a_0 + a_1 x + b_1 y + a_2 x^2 + b_2 y^2 + c_1 x\, y + a_3 x^3 + b_3 y^3 + c_2 x^2 y + c_3 x\, y^2 \\ &\quad + a_4 x^4 + b_4 y^4 + c_4 x^2 y^2 + \ldots \end{aligned} \tag{3}$$

where a_i, b_i and c_i are coefficients of each term of the series. The aperture is sufficiently small if the spherical aberration is not too large, so that higher order aberrations that have been neglected are even smaller.

The ellipsoid has two principal curvatures, saggital (C_s) and tangential (C_t), which are equal only for a sphere, and they are

$$C_s = 2a_2 \text{ and } \quad C_t = 2b_2 \,. \tag{4}$$

In order to balance the shape of wavefront astigmatism, as it has been mentioned in the previous section, we chose the average of both ellipsoid curvatures, which nearly corresponds to the medium curvature (C_m).

$$C_m = \frac{C_s + C_t}{2} \tag{5}$$

Therefore, the saggita for the sphere is given by

$$z_{sphere} = \frac{C_m}{2}\left(x^2 + y^2\right) + \frac{C_m^3}{8}\left(x^2 + y^2\right)^2 \,. \tag{6}$$

Thus, the wavefront aberration is

$$W\left(x, y\right) = 2\Delta z = 2\left(z_{sphere} - z_{ellipsoid}\right) \,, \tag{7}$$

which is a monomial expression like Eq.3

$$W = \sum \alpha_h x^i y^j \,. \tag{8}$$

This expression in terms of monomials is not convenient in optical design and aberration analysis. The most common representation of the wavefront aberration is in terms of the Seidel aberrations or of the Zernike polynomials, commonly used in optical design and interferometry. They have particular characteristics that make them useful in both areas. The Seidel representation for primary off-axis aberrations is commonly written with reference to the Petzval curvature, because in optical design we know that when astigmatism becomes zero, the saggital and tangential images join at a point on the Petzval surface. On the other hand, in terms of Zernike polynomials, the reference image (center of curvature of the reference sphere) is located at a point between the saggital and the tangential images. The Zernike polynomials are defined in a unit circle pupil. The wavefront aberrations could be written in many different forms, for example as Zernike aberrations, Seidel aberrations as expressed by Kingslake, etc. Including some high order terms, we will use the following:

$$\begin{aligned} W = {} & A\left(x^2+y^2\right)+B\left(y^2-x^2\right)+C\,y\left(x^2+y^2\right)+D\,y\left(y^2-x^2\right) \\ & +E\left(x^2+y^2\right)^2+F\left(x^4-y^4\right)+Gx^2y^2 \end{aligned} \tag{9}$$

where *A*, *B*, *C*, *D*, *E*, *F* and *G* are the defocus, astigmatism, coma, astigmatic coma, spherical, 5th order astigmatism and ashtray aberration respectively. In those expressions, the sphere of reference is placed with its center of curvature at the average focus between the saggital and tangential foci, which is close to the focus of the circle of least confusion, depending on the angle of incidence *I*. If the angle *I* is small, the average and the least confusion foci are quite close each other, but not when angle *I* is larger.

Through the use of algebra, we found the relationship between monomial (Eq. 8) and polynomial (Eq. 9) functions, finding the exact expressions for the wavefront aberration coefficients, where we only assume that the pupil is small and on the mirror plane. Because the exact expressions are complex and unmanageable, mainly the *E*, *F* and *G* coefficients, they are presented in the Appendix. A good approximation for the wavefront aberration coefficients can be found when the incidence angle values are small (see details in Fig. 5). Using an expansion in Maclaurin series, we can find the expressions:

$$A = 0 \tag{10a}$$

$$B = \left(\frac{a}{2b^2} - \frac{1}{2a} \right) \phi^2 \tag{10b}$$

$$C = -\frac{\left(a^2 - b^2\right)\left[-6b^2\phi^2 + a^2\left(-3 + 8\phi^2\right)\right]\phi}{3a^2b^4} \tag{10c}$$

$$D = -\frac{\left(a^2 - b^2\right)^2 \phi^3}{a^2b^4} \tag{10d}$$

$$E = -\frac{\left(a^2 - b^2\right)\left[-9b^2\phi^2 + 2a^2\left(-1 + 6\phi^2\right)\right]}{8ab^6} \tag{10e}$$

$$F = \frac{\left(2a^4 - 5a^2b^2 + 3b^4\right)\phi^2}{4ab^6} \tag{10f}$$

$$G = 0 \tag{10g}$$

These equations are expressed in terms of the geometry of the reference surface. So, we found the relationships between the measurable parameters (*L*, *r*, *I*) and the geometrical

parameters of the reference surface (*a*, *b*, *ø*), aided by Fig. 4. Using simple geometry and trigonometry, it was possible to get the relationships:

$$a = \frac{L + L'}{2} \tag{11}$$

$$b = \sqrt{LL'\cos^2(I)} \tag{12}$$

$$\phi = \arctan\left[\left(\frac{L' + L}{L' - L}\right)\tan(I)\right] \tag{13}$$

The parameter *L'* is the ideal ellipsoid image position (second ellipsoid focus), which corresponds to the medium or least confusion focus, as previously described. This position is found through Coddington's equations, and the parameter *L'*, is given by

$$L' = \frac{L\,r\left[L - r\cos(I) + L\cos^2(I)\right]}{\left[r - 2L\cos(I)\right]\left[-2L + r\cos(I)\right]} \tag{14}$$

Replacing this value of *L'* into Eqs. 11, 12 and 13, and considering small incidence angles (small angles of rotation of the ellipse), we have:

$$a = \frac{L^2}{2L - r} \tag{15}$$

$$b = \left(1 - \frac{1}{2}I^2\right)L\sqrt{\frac{r}{2L - r}} \tag{16}$$

$$\phi = -\frac{L\,I}{L - r} + \frac{\left(2L^2 r - Lr^2\right)I^3}{3(L - r)^3} \tag{17}$$

Going further, we substitute Eqs. 15, 16 and 17 into the third order aberration coefficients (Eqs. 10b, 10c and 10e) and expand them in series, using the incidence angle *I* as a variable.

Then, we retain only up to the second order obtaining the well known expression [13] for the third order aberration coefficients:

$$A = 0 \tag{18a}$$

$$B = \frac{I^2}{2r} \tag{18b}$$

$$C = \frac{(r-L)I}{L r^2} \tag{18c}$$

$$D = 0 \tag{18d}$$

$$E = \frac{(r-L)^2}{4L^2 r^3} \tag{18e}$$

$$F = \frac{\left(2L^2 - 6Lr + 3r^2\right) I^2}{4L^2 r^3} \tag{18f}$$

$$G = 0 \tag{18g}$$

The difference in the astigmatism coefficient with respect to the commonly used Schroeder expression is due to wavefront representation, with the center of curvature of the sphere of reference in the medium image surface while the center of curvature of the sphere of reference in Schroeder's wavefront representation is on the Petzval image surface.

Analysis

Equations 10a through 10g representing the third order aberration coefficients of the off-axis spherical mirror (Fig. 1a) and Eqs. 15, 16 and 17 are the expressions that relate the parameters of the reference ellipsoid with those of the spherical mirror (Fig. 4). Furthermore, if the angle of incidence *I* is zero, all aberration coefficients are zero, with except of the spherical aberration coefficient, which becomes the well known expression:

$$E = \frac{\left(L - r\right)^2}{4L^2 r^3} \tag{19}$$

Equations 10 allow us to obtain the coefficients of aberration for the off-axis mirror when the angle of incidence and the pupils are small. Figure 5 shows the differences between the values obtained with the exact expressions (see the Appendix), which are valid for any angle of incidence of the principal ray, and Eqs. 10a-g, which are valid for relatively small angles. An estimation of how small is the angle can be obtained from this difference. We can safely state from here that an angle smaller than 5° degrees is small enough for most purposes. Figure 5 shows that the spherical coefficient *E* has a decay behavior for large incidence angles. This is mainly due to the changes from circular to elliptical pupil as the angle of incidence increases. The coma coefficient *C* grows linearly, while the astigmatism coefficient *B* grows quadratically with the angle of incidence. Considering this graph, one can observe that our expressions are good enough for first-order aberrations, comparable with the exact wavefront aberration coefficient expressions.

Another important result from this analysis is the comparison between the domain of spherical, coma and astigmatism in function of the incidence angle *I*, shown in Fig 6. This figure allows one to identify that for small incidence angles, spherical aberration is dominant. When angle *I* grows, coma becomes larger, and therefore, dominates the wavefront aberration. But if the angle is large, as in most designs [1-10], the main aberration is astigmatism, as reported in most of the literature [11].

We must point out that when the image and the object are near the center of curvature of the spherical mirror, the reference ellipsoid becomes a sphere. In this case, the orientation of the ellipsoid is ill defined, since in this vicinity, the derived expressions become indeterminate. We have validated these expressions by ray tracing programs (OSLO© and Zemax©) with the

corresponding transformation between the wavefront representations in some cases. We must emphasize that the Eqs. 18 are consistent with those reported by Schroeder.

In conclusion, the optical designer of off-axis reflective systems should consider the behavior of the wavefront aberrations, bearing in mind the shape of the graphs presented in Figs. 5 and 6, and considering the wavefront aberration expression given here (Eq. 9).

Conclusions

The primaries as well as some higher order off-axis mirror wavefront aberration coefficient expressions were derived using the optical difference between the sphere and the ellipsoid. The theory just developed provides results that are valid for off-axis angles and apertures greater that those obtained using third order aberrations analysis. We consider a small pupil and a small angle of incidence, so that the reference sphere center of the wavefront aberration polynomial is close to the mean least confusion focus. This has the advantages over the Zernike and Seidel wavefront aberration representation that the astigmatism wavefront deformation is minimized. The importance of aberrations has been discussed considering the needs of design in laser cavities, spectrographs and retinal adaptive optics imaging systems. The domain region of all third order aberrations has been discussed using a specific case (Fig. 6) and their importance in the design of off-axis spherical mirror system design. For the analysis of a multi-spherical mirror system with multi-meridional planes, it is necessary to extend this theory, propagating the expressions for a system composed of spherical mirrors, in order to understand the full effect of the aberrations and possible compensation.

Appendix. Exact wavefront aberration coefficients.

$$A = 0 \tag{A1}$$

$$B = -\frac{\left(a^2 - b^2\right)\sqrt{a^2\cos^2\left(\phi\right) + b^2\sin^2\left(\phi\right)}\,\sin^2\left(\phi\right)}{2a^2b^2} \tag{A2}$$

$$C = -\frac{\left(a^2 - b^2\right)\left[a^2\cos^2\left(\phi\right) + b^2\sin^2\left(\phi\right)\right]^2\sin\left(2\phi\right)}{2a^4b^4} \tag{A3}$$

$$D = \frac{\left(a^2 - b^2\right)^2\left[a^2\cos^2(\phi) + b^2\sin^2(\phi)\right]\sin^3\left(\phi\right)\cos\left(\phi\right)}{a^4b^4} \tag{A4}$$

$$\begin{aligned}
E = {} & \frac{1}{32768a^6b^6}\left(a^2 - b^2\right) \\
& *\Big(-4\Big[163a^6 + 191a^4b^2 + 249a^2b^4 + 165b^6 + 4\left(83a^6 + 32a^4b^2 - 25a^2b^4 - 26b^6\right)\cos\left(2\phi\right) \\
& + 4(a-b)(a+b)\left(77a^4 + 76a^2b^2 + 47b^4\right)\cos\left(4\phi\right) + 12\left(a^2 - b^2\right)^2\left(15a^2 + 14b^2\right)\cos\left(6\phi\right) \\
& + 41\left(a^2 - b^2\right)^3\cos\left(8\phi\right)\Big] * \sqrt{a^2\cos^2\left(\phi\right) + b^2\sin^2\left(\phi\right)} \\
& + \Big\{\Big[a^4 + 6a^2b^2 + b^4 - \left(a^2 - b^2\right)^2\cos\left(4\phi\right)\Big]^3\left(4a^4\cot\left(\phi\right)\left(1 - 2\csc^2\left(\phi\right)\right)\right. \\
& \left. + \Big[3a^4 + 2a^2b^2 - b^4 + \left(7a^4 + 4a^2b^2 + b^4\right)\sec^2\left(\phi\right)\Big]\tan\left(\phi\right)\Big\}\Big) \\
& / \Big\{\Big[a^2\csc^2\left(\phi\right) + b^2\sec^2\left(\phi\right)\Big]^{3/2}\Big[b^2\cos^2\left(\phi\right) + a^2\sin^2\left(\phi\right)\Big]^3\Big\}
\end{aligned} \tag{A5}$$

$$\begin{aligned}
F = {} & \frac{1}{32768a^6b^6}\left(a^2 - b^2\right) \\
& \Big[4\Big[163a^6 + 191a^4b^2 + 249a^2b^4 + 165b^6 + 4\left(83a^6 + 32a^4b^2 - 25a^2b^4 - 26b^6\right)\cos\left(2\phi\right) \\
& 4(a-b)(a+b)\left(77a^4 + 76a^2b^2 + 47b^4\right)\cos\left(4\phi\right) + 12\left(a^2 - b^2\right)^2\left(15a^2 + 14b^2\right)\cos\left(6\phi\right) \\
& + 41\left(a^2 - b^2\right)^3\cos\left(8\phi\right)\Big] * \sqrt{a^2\cos^2\left(\phi\right) + b^2\sin^2\left(\phi\right)} + \Big(\Big[a^4 + 6a^2b^2 + b^4 - \left(a^2 - b^2\right)^2\cos\left(4\phi\right)\Big]^3 \\
& * \Big\{4\,a^4\cot\left(\phi\right)\Big[1 - 2\csc^2\left(\phi\right)\Big] + \Big[3a^4 + 2a^2b^2 - b^4 + \left(7a^4 + 4a^2b^2 + b^4\right)\sec^2\left(\phi\right)\Big] \\
& *\tan\left(\phi\right)\Big\}\Big) / \Big\{\Big[a^2\csc^2\left(\phi\right) + b^2\sec^2\left(\phi\right)\Big]^{3/2}\Big[b^2\cos^2\left(\phi\right) + a^2\sin^2\left(\phi\right)\Big]^3\Big\}\Big]
\end{aligned} \tag{A6}$$

$$
\begin{aligned}
G = {} & \frac{1}{32768a^6b^6}\left(a^2-b^2\right) \\
& \left(-8\left[171a^6+103a^4b^2+17a^2b^4-35b^6+4\left(99a^6+40a^4b^2+39a^2b^4+14b^6\right)\cos\left(2\phi\right)\right.\right. \\
& +4(a-b)(a+b)\left(85a^4+76a^2b^2+7b^4\right)\cos(4\phi)+4\left(a^2-b^2\right)^2\left(29a^2+2b^2\right)\cos\left(6\phi\right) \\
& \left.+\left(a^2-b^2\right)^3\cos\left(8\phi\right)\right]*\sqrt{a^2\cos^2\left(\phi\right)+b^2\sin^2\left(\phi\right)} \\
& +4\left(163a^6+191a^4b^2+249a^2b^4+165b^6+4\left(83a^6+32a^4b^2-25a^2b^4-26b^6\right)\cos\left(2\phi\right)\right. \\
& +4(a-b)(a+b)\left(77a^4+76a^2b^2+47b^4\right)\cos\left(4\phi\right)+12\left(a^2-b^2\right)^2\left(15a^2+14b^2\right)\cos\left(6\phi\right) \\
& *\sqrt{a^2\cos[\phi]^2+b^2\sin[\phi]^2}-\left\{\left[a^4+6a^2b^2+b^4-\left(a^2-b^2\right)^2\cos\left(4\phi\right)\right]^3\right. \\
& \left.+41\left(a^2-b^2\right)^3\cos\left(8\phi\right)\right\} \\
& *\left\{4a^4\cot\left(\phi\right)\left[1-2\csc^2\left(\phi\right)\right]+\left[3a^4+2a^2b^2-b^4+\left(7a^4+4a^2b^2+b^4\right)\sec^2\left(\phi\right)\right]\right. \\
& \left.\left.*\tan\left(\phi\right)\right\}\right)/\left\{\left[a^2\csc^2\left(\phi\right)+b^2\sec^2\left(\phi\right)\right]^{3/2}\left[b^2\cos^2\left(\phi\right)+a^2\sin^2\left(\phi\right)\right]^3\right\}\Bigg)
\end{aligned}
\tag{A7}
$$

References

1. Y. Zhang, B. Cense, J. Rha, R.S. Jonnal, W. Gao, R.J. Zawadzki, J.S. Werner, S. Jones, S. Olivier, and D. T. Miller, "High-speed volumetric imaging of cone photoreceptors with adaptive optics spectral-domain optical coherence tomography," Opt. Express **14**, 4380-4394 (2006).
2. R. J. Zawadzki, S. M. Jones, S. S. Olivier, M. T. Zhao, B. A. Bower, J. A. Izatt, S. Choi, S. Laut, and J. S. Werner, "Adaptive-optics optical coherence tomography for high-resolution and high-speed 3D retinal in vivo imaging," Opt. Express **13**, 8532-8546 (2005).
3. D. Merino, C. Dainty, A. Bradu, and A. G. Podoleanu, "Adaptive optics enhanced simultaneous en-face optical coherence tomography and scanning laser ophthalmoscopy," Opt. Express **14**, 3345-3353 (2006).

4. A. Roorda, F. Romero-Borja, W. J. Donnelly, H. Queener, T. J. Hebert, and M. C. W. Campbell, "Adaptive optics scanning laser ophthalmoscopy," Opt. Express **10**, 405-412 (2002).
5. D. X. Hammer, R. D. Ferguson, C. E. Bigelow, N. V. Iftimia, T. E. Ustun, and S. Burns, "Adaptive optics scanning laser ophthalmoscope for stabilized retinal imaging," Opt. Express **14**, 3354-3367 (2006).
6. D. C. Gray, W. Merigan, J. I. Wolfing, B. P. Gee, J. Porter, A. Dubra, T. H. Twietmeyer, K. Ahmad, R. Tumbar, F. Reinholz, and D. R. Williams, "In vivo fluorescence imaging of primate retinal ganglion cells and retinal pigment epithelial cells," Opt. Express **14**, 7144-7158 (2006).
7. S.A. Burns, R. Tumbar, A.E. Elsner, D. Ferguson, and D. X. Hammer, "Large-field-of-view, modular, stabilized, adaptive-optics-based scanning laser ophthalmoscope," J. Opt. Soc. Am. A **24**, 1313-1326 (2007).
8. H. Abitan and T. Skettrup, “Laser resonators with several mirrors and lenses with bow-tie laser resonator with compensation for astigmatism and thermal lens effects as an example,” J. Opt. A: Pure Appl. Opt. **7**, 7-20 (2005).
9. Robert J. Melttzer, “Spectrographs and Monocromators,” in *Applied Optics and Optical Engineering* Vol.5, E.D. R. Kingslake (Academic, USA, 1969).
10. H.Gross. F. Blenchinger and B. Achtner, *Handbook of Optival Systems: Survey of Optical Instruments* Vol.4 (Wiley-VCH, 2008), Chap. 45 (45.6).
11. A. Gómez-Vieyra, A. Dubra, D. Malacara-Hernández, and D.R. Williams, "First-order design of off-axis reflective ophthalmic adaptive optics systems using afocal telescopes," Opt. Express **17**, 18906-18919 (2009).

12. D. Malacara-Hernández, “Some parameters and characteristics of an off-axis paraboloid,” Opt. Eng. **35**, 1277-1281 (1991).

13. D. J. Schroeder, *Astronomical Optics*, (Academic Press, 1987)

Acknowledgements

The authors acknowledge the support of the Consejo Nacional de Ciencia y Tecnología de México (CONACYT), through scholar grant No. 170266. The authors are indebted to Alfredo Dubra for suggesting this problem and for discussions that led to its solution; and to Mario Alberto Ruiz Berganza for the invaluable comments that have greatly improved the manuscript.

Figure Captions

Figure 1.- (a) Ideal image formation by an off-axis reflective spherical mirror. (b) Shape of a spherical mirror and a reference ellipsoid

Figure 2.-The off-axis spherical mirror images matched to the ellipsoid image, where m is the medium image (a), *s* is the saggital image (b), *t* is the tangential image (c) and *p* is the Petzval image (d).

Figure 3.- (a) Ellipsoid. (b) Rotated ellipsoid (c)Translated and rotated ellipsoid.

Figure 4.- Off-axis ellipsoid with its geometrical parameters in order to relate with the spherical mirror parameters.

Figure 5.- The behavior of the off-axis spherical coefficients with the variation of the incidence angle for L=600, r=1000. The green dashed lines are Eqs. 18, the red points are Eqs. 10 values and the blue asterisk are the values of the exact expressions (Appendix).

Figure 6.- The behavior of the aberration coefficients for small angles L= 600, r=1000

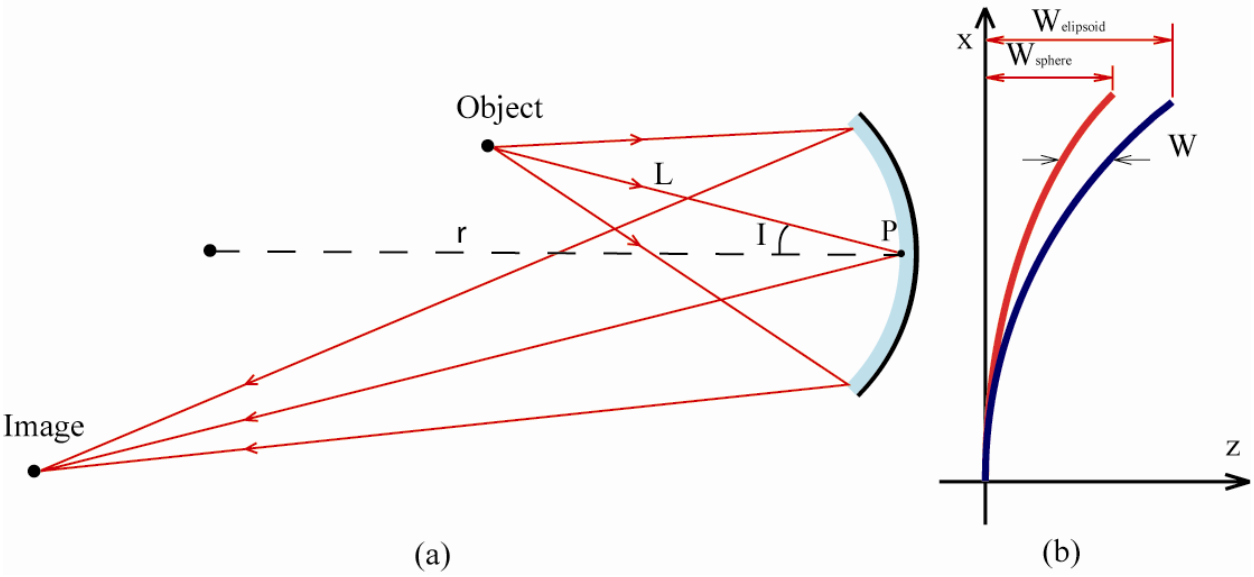

Figure 1

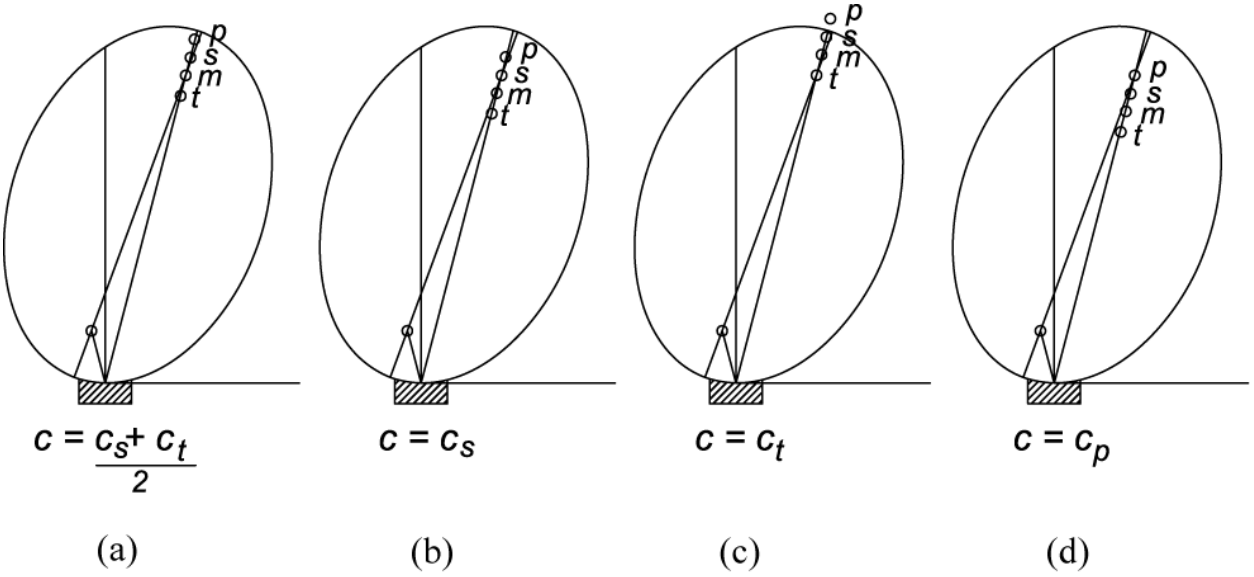

Figure 2

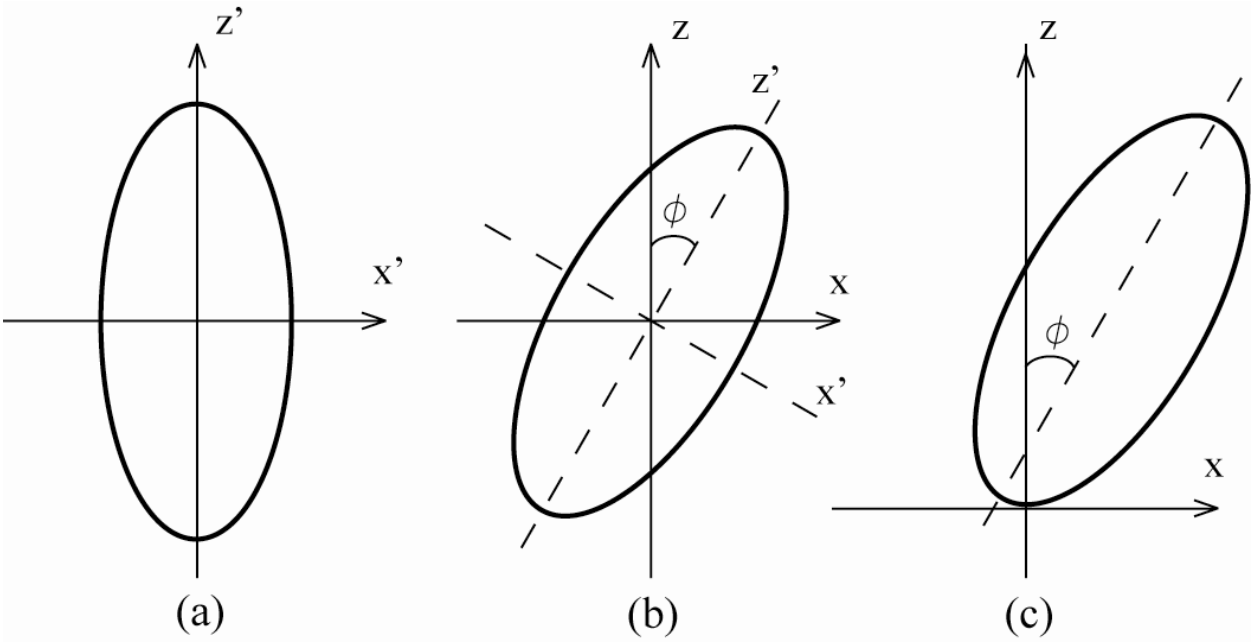

Figure 3

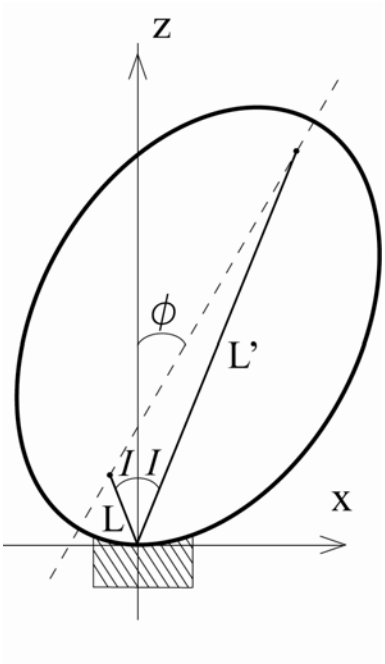

Figure 4

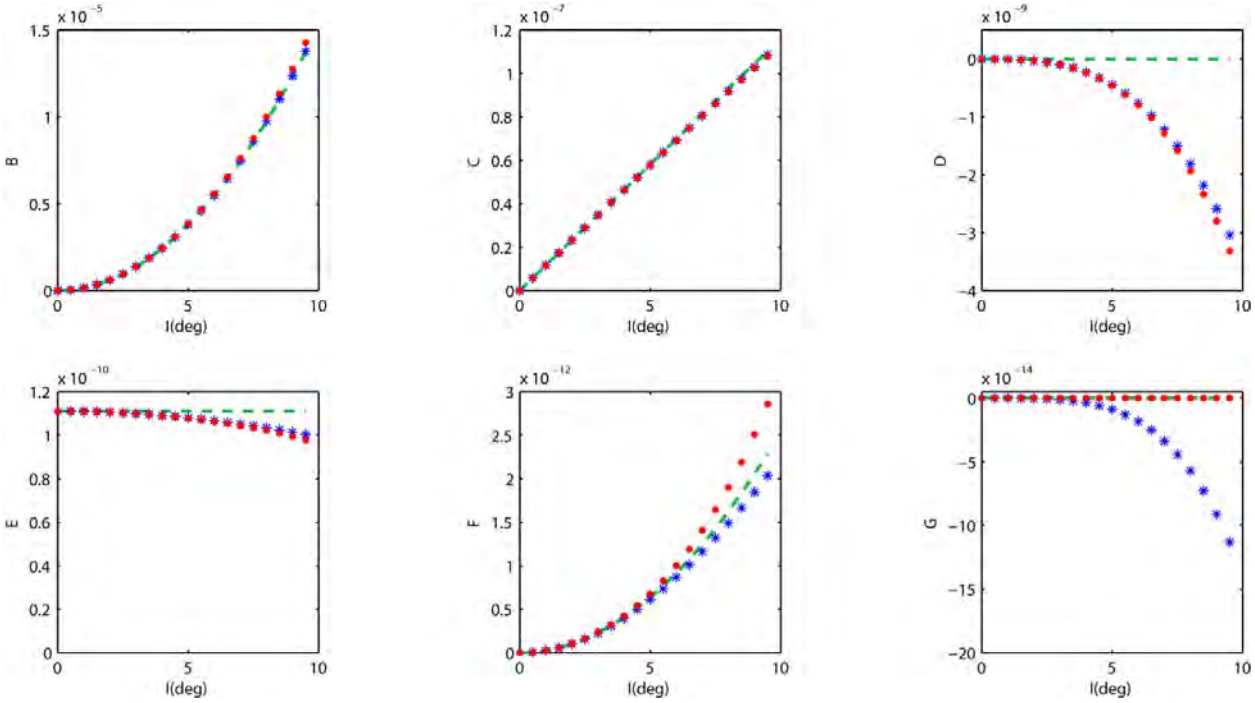

Figure 5

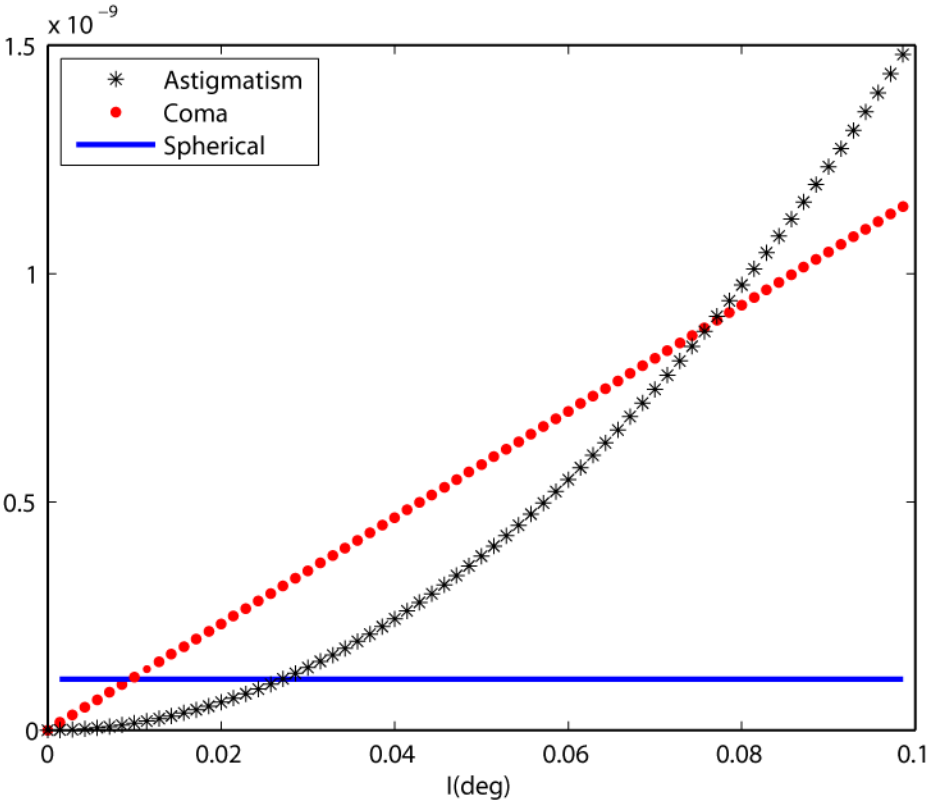

Figure 6

ANEXO 2

First-order design of off-axis reflective ophthalmic adaptive optics systems using afocal telescopes

Armando Gómez-Vieyra,[1] Alfredo Dubra,[2,*], Daniel Malacara-Hernández,[1]and David R. Williams[3]

[1]Centro de Investigaciones en Óptica A.C., Loma del Bosque 115, C.P. 37000, León, Guanajuato, México
[2] University of Rochester Eye Institute, Rochester, NY, 14642-0314, USA
[3]Center for Visual Science, University of Rochester, Rochester, NY, 14627-0270, USA
**adubra@cvs.rochester.edu*

Abstract: Expressions for minimal astigmatism in image and pupil planes in off-axis afocal reflective telescopes formed by pairs of spherical mirrors are presented. These formulae which are derived from the marginal ray fan equation can be used for designing laser cavities, spectrographs and adaptive optics retinal imaging systems. The use, range and validity of these formulae are limited by spherical aberration and coma for small and large angles respectively. This is discussed using examples from adaptive optics retinal imaging systems. The performance of the resulting optical designs are evaluated and compared against the configurations with minimal wavefront RMS, using the defocus-corrected wavefront RMS as a metric.

OCIS codes: (110.1080) Active or adaptive optics, (080.2468) First-order optics, (080.4035) Mirror system design, 220.1000 Aberration compensation, (330.4460) Ophthalmic optics and devices.

References

1. J. Liang, D. R. Williams, and D. T. Miller, "Supernormal vision and high-resolution retinal imaging through adaptive optics," J. Opt. Soc. Am. A **14**(11), 2884–2892 (1997), http://www.opticsinfobase.org/abstract.cfm?URI=josaa-14-11-2884.
2. J. Rha, R. S. Jonnal, K. E. Thorn, J. Qu, Y. Zhang, and D. T. Miller, "Adaptive optics flood-illumination camera for high speed retinal imaging," Opt. Express **14**(10), 4552–4569 (2006), http://www.opticsinfobase.org/abstract.cfm?URI=oe-14-10-4552.
3. B. Hermann, E. J. Fernández, A. Unterhuber, H. Sattmann, A. F. Fercher, W. Drexler, P. M. Prieto, and P. Artal, "Adaptive-optics ultrahigh-resolution optical coherence tomography," Opt. Lett. **29**(18), 2142–2144 (2004), http://www.opticsinfobase.org/ol/abstract.cfm?URI=ol-29-18-2142.
4. R. J. Zawadzki, S. M. Jones, S. S. Olivier, M. T. Zhao, B. A. Bower, J. A. Izatt, S. Choi, S. Laut, and J. S. Werner, "Adaptive-optics optical coherence tomography for high-resolution and high-speed 3D retinal in vivo imaging," Opt. Express **13**(21), 8532–8546 (2005), http://www.opticsinfobase.org/oe/abstract.cfm?URI=oe-13-21-8532.
5. E. J. Fernández, B. Povazay, B. Hermann, A. Unterhuber, H. Sattmann, P. M. Prieto, R. Leitgeb, P. Ahnelt, P. Artal, and W. Drexler, "Three-dimensional adaptive optics ultrahigh-resolution optical coherence tomography using a liquid crystal spatial light modulator," Vision Res. **45**(28), 3432–3444 (2005).
6. Y. Zhang, J. T. Rha, R. S. Jonnal, and D. T. Miller, "Adaptive optics parallel spectral domain optical coherence tomography for imaging the living retina," Opt. Express **13**(12), 4792–4811 (2005), http://www.opticsinfobase.org/oe/abstract.cfm?URI=oe-13-12-4792.
7. D. Merino, C. Dainty, A. Bradu, and A. G. Podoleanu, "Adaptive optics enhanced simultaneous en-face optical coherence tomography and scanning laser ophthalmoscopy," Opt. Express **14**(8), 3345–3353 (2006), http://www.opticsinfobase.org/abstract.cfm?URI=oe-14-8-3345.
8. C. E. Bigelow, N. V. Iftimia, R. D. Ferguson, T. E. Ustun, B. Bloom, and D. X. Hammer, "Compact multimodal adaptive-optics spectral-domain optical coherence tomography instrument for retinal imaging," J. Opt. Soc. Am. A **24**(5), 1327–1336 (2007), http://www.opticsinfobase.org/abstract.cfm?URI=josaa-24-5-1327.
9. A. Roorda, F. Romero-Borja, W. Donnelly Iii, H. Queener, T. J. Hebert, and M. C. W. Campbell, "Adaptive optics scanning laser ophthalmoscopy," Opt. Express **10**(9), 405–412 (2002), http://www.opticsinfobase.org/oe/abstract.cfm?URI=oe-10-9-405.
10. Y. Zhang, S. Poonja, and A. Roorda, "MEMS-based adaptive optics scanning laser ophthalmoscopy," Opt. Lett. **31**(9), 1268–1270 (2006), http://www.opticsinfobase.org/ol/abstract.cfm?URI=ol-31-9-1268.

#112822 - $15.00 USD Received 22 Jun 2009; revised 11 Sep 2009; accepted 12 Sep 2009; published 6 Oct 2009

11. D. X. Hammer, R. D. Ferguson, C. E. Bigelow, N. V. Iftimia, T. E. Ustun, and S. A. Burns, "Adaptive optics scanning laser ophthalmoscope for stabilized retinal imaging," Opt. Express **14**(8), 3354–3367 (2006), http://www.opticsinfobase.org/oe/abstract.cfm?URI=oe-14-8-3354.
12. D. C. Gray, W. Merigan, J. I. Wolfing, B. P. Gee, J. Porter, A. Dubra, T. H. Twietmeyer, K. Ahamd, R. Tumbar, F. Reinholz, and D. R. Williams, "In vivo fluorescence imaging of primate retinal ganglion cells and retinal pigment epithelial cells," Opt. Express **14**(16), 7144–7158 (2006), http://www.opticsinfobase.org/oe/abstract.cfm?URI=oe-14-16-7144.
13. S. A. Burns, R. Tumbar, A. E. Elsner, D. Ferguson, and D. X. Hammer, "Large-field-of-view, modular, stabilized, adaptive-optics-based scanning laser ophthalmoscope," J. Opt. Soc. Am. A **24**(5), 1313–1326 (2007), http://www.opticsinfobase.org/abstract.cfm?URI=josaa-24-5-1313.
14. R. H. Webb, and G. W. Hughes, "Scanning laser ophthalmoscope," IEEE Trans. Biomed. Eng. **BME-28**(7), 488–492 (1981).
15. R. H. Webb, G. W. Hughes, and F. C. Delori, "Confocal scanning laser ophthalmoscope," Appl. Opt. **26**(8), 1492–1499 (1987).
16. H. W. Kogelnik, E. P. Ippen, A. Dienes, and C. V. Shank, "Astigmatically compensated cavities for CW dye lasers," IEEE J. Quantum Electron. **8**(3), 373–379 (1972).
17. W. T. Foreman, "Lens Correction of Astigmatism in a Czerny-Turner Spectrograph," Appl. Opt. **7**(6), 1053–1059 (1968), http://www.opticsinfobase.org/ao/abstract.cfm?URI=ao-7-6-1053.
18. G. R. Rosendahl, "Contributions to the Optics of Mirror Systems and Gratings with Oblique Incidence. III. Some Applications," J. Opt. Soc. Am. **52**(4), 412–415 (1962), http://www.opticsinfobase.org/josa/abstract.cfm?URI=josa-52-4-412.
19. A. E. Conrady, *Applied Optics and Optical Design*, (Dover Publications Inc., New York, 1960), Chap XII, part 2.
20. D. Malacara, and Z. Malacara, *Handbook of Lens Design*, (Marcel Dekker Inc., New York. 2004), Chap. 5.
21. R. Kingslake, *Lens Design Fundamentals*, (Academic Press, San Diego, 1978), Chap 10.
22. D. A. Atchison, A. Bradley, L. N. Thibos, and G. Smith, "Useful variations of the Badal optometer," Optom. Vis. Sci. **72**(4), 279–284 (1995).
23. G. Smith, and D. A. Atchison, *The eye and visual optical instruments*, (Cambridge University Press, Cambridge, U.K., 1997), Chap. 30.

1. Introduction

The introduction of adaptive optics (AO) to ophthalmic imaging in recent years has led to the development of a new generation of high-resolution retinal imaging instruments. These include the AO fundus camera [1,2], the AO optical coherence tomograph (AO-OCT) [3–8] and the AO scanning laser ophthalmoscope (AOSLO) [7,9–13]. Refractive systems are not desirable for these applications given that the back reflections from the optical surfaces can be orders of magnitude brighter than the light scattered or emitted by the retina. For example, the light scattered from human cone photoreceptors in these instruments is 10^{-3}-10^{-4} times lower than the illumination, while the broadband anti-reflection coatings required for the typical broadband sources used in these instruments reflect as much as 10^{-2}. Broadband sources are essential for minimizing speckle and/or increasing axial resolution in all the scattered light imaging modalities. Current low-resolution clinical instruments do not suffer from such back reflection problems because they use different portions of the eye's pupil for illumination and light collection. AO retinal imaging instruments however, need to use the full pupil of the eye for both illumination and imaging in order to achieve maximum lateral and axial resolution. The pupil (aperture stop) of the human eye is defined by the iris, and the planes conjugate to it are referred to as "pupil planes." In order to minimize back reflections, most AO-equipped scanning ophthalmic instruments are at least partially built using off-axis spherical mirrors [1,4,7–13]. Spherical mirrors are preferred over aspheres, given their lower cost and ease of alignment.

Due to the off-axis arrangement, the major optical performance limitation of such systems is astigmatism. This is described by Webb *et al.* [14,15] when reporting the first confocal scanning laser ophthalmoscope, and later by Burns *et al.* [13]. In his work, Webb suggests an off-the-plane perpendicular folding of the optical setup to reduce the astigmatism present in the pupil plane which degrades the image quality in the retinal planes. Since then, the design of AO retinal imaging instruments has been dominated by efforts to improve the retinal image quality, while largely ignoring the aberrations in retinal conjugate planes. Aberrations in retinal planes degrade the image quality at the pupil planes, where the wavefront sensor and corrector(s) are placed. The poor image quality at the pupil planes affects the quality of the AO correction. In the best case scenario, this results in a reduced temporal bandwidth of the

#112822 - $15.00 USD Received 22 Jun 2009; revised 11 Sep 2009; accepted 12 Sep 2009; published 6 Oct 2009

closed-loop AO performance. In the worst case scenario, the higher spatial frequency aberrations will be attenuated to the extent that they cannot be sensed, and therefore, not corrected.

Even though the motivation for this work is improving the performance of AO ophthalmic instruments, other reflective optical systems based on off-axis spherical mirrors, such as spectrographs and laser cavities, can benefit from the astigmatism compensation presented here. In the past, astigmatism compensation in such systems has been performed by adding glass plates [16], lenses [17] or additional convex mirrors [18] among other methods.

In this work, expressions for designing minimal astigmatism optical systems based on pairs of off-axis reflective 4f telescopes using spherical mirrors are derived. In what follows we refer to image planes (retina conjugates) as "infinite conjugates" and the pupil planes as a particular case of "finite conjugates." First, the marginal ray fan equation, the geometry of the off-axis reflective telescope and the astigmatism equations will be introduced. Then the particular cases of small angles of incidence with an object point at the front focal point of the telescope (pupil) and at infinity (retina) will be evaluated. A discussion of the sensitivity of the astigmatism-corrected designs to focus shifts and to Badal shifts (i.e. mirror separation change) will follow. Finally, examples illustrating the range of validity of the derived formulae, and the optical performance of the corresponding designs will be presented.

2. Theory

2.1 General marginal ray fan equation

In the paraxial theory of on-axis rotationally symmetric optical elements in a medium, rays emerging from a point object converge onto an image point. The first-order image formation of such optical components can be described by the Gaussian equation for a thin element that takes the well-known form

$$\frac{1}{s}+\frac{1}{s'}=\frac{1}{f}, \tag{1}$$

where s and s' are object and image distances from the optical element respectively, and f is the focal length of the optical element. For off-axis objects, the marginal rays converge at different points along the principal ray, depending on the orientation θ of the plane defined by the principal ray and the corresponding marginal ray. To first order approximation, the distances along the principal ray between the optical element and the marginal images under the thin lens approximation are given by the general marginal ray fan equation [19], which for spherical mirrors takes the form

$$\frac{1}{s}+\frac{1}{s_\theta'}=\frac{2\cos I}{r\,(1-\cos^2\theta\sin^2 I)}, \tag{2}$$

where I is the angle of incidence of the principal ray onto the mirror, and r is the radius of curvature of the mirror. For the special cases $\theta=\pi/2$ and $\theta=0$, one recovers the more familiar Coddington equations [20,21] that give the position of the sagittal and tangential images respectively,

$$\frac{1}{s_s}+\frac{1}{s_s'}=\frac{2\cos I}{r}, \tag{3}$$

$$\frac{1}{s_t}+\frac{1}{s_t'}=\frac{2}{r\cos I}. \tag{4}$$

As will be shown later, it is sometimes convenient to rewrite the marginal ray fan equation in terms of vergences $\phi=1/s,$ rather than distances,

#112822 - $15.00 USD Received 22 Jun 2009; revised 11 Sep 2009; accepted 12 Sep 2009; published 6 Oct 2009

$$\phi + \phi_\theta' = \frac{2\cos I}{r\,(1-\cos^2\theta \sin^2 I)}. \tag{5}$$

For an off axis spherical mirror and an object point at infinity, the focal length as a function of angle of incidence can be defined as the average of the sagittal and tangential distances along the principal ray,

$$f(I) = \frac{r\left[3+\cos(2I)\right]}{8\cos I}. \tag{6}$$

The position of the average mirror focus defined in this way, corresponds to the circle of least confusion, which for angles of incidence smaller than 30°, can be approximated by its on-axis value (with less than 1% error)

$$f(I) \approx \frac{r}{2}. \tag{7}$$

2.2 Minimization of astigmatism in afocal telescopes

To date, most reflective AO ophthalmic systems consist of a number of off-axis afocal telescopes that relay the pupil of the eye onto the wavefront sensor, wavefront corrector(s) and scanning devices. When these telescopes are formed by pairs of spherical mirrors, they are fully described by the five parameters shown in Fig. 1: the angles of incidence I_1 and I_2 of the principal ray onto the mirrors m_1 and m_2; the mirror radii of curvature r_1 and r_2, and the angle θ between the planes defined by the incident and reflected principal rays. In what follows, unless otherwise stated, it is assumed that the separation between mirrors along the principal ray is the sum of the on-axis mirror focal lengths, which is $d = (r_1 + r_2)/2$, as it is usually implied when referring to afocal telescopes. The dominant aberration in these telescopes is astigmatism. Astigmatism occurs when ray fans passing through different planes containing the principal ray focus at different points along the principal ray. By an appropriate selection of the telescope parameters, astigmatism can be eliminated along the principal ray for one or at most two image points, as is shown next.

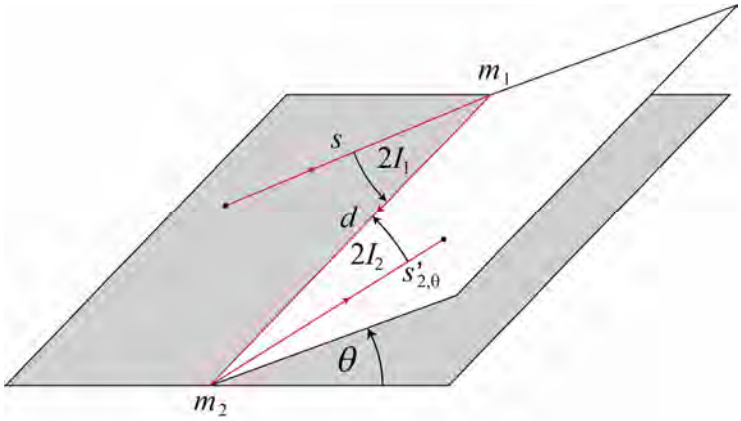

Fig. 1. Geometry of an off-axis reflective afocal telescope: I_1 and I_2 are the angles of incidence of the principal ray (in red) onto the mirrors m_1 and m_2 respectively, and the angle θ between the incidence planes. The object is a distance s from the first mirror, and the image formed by the second mirror is a distance $s'_{2,\theta}$ from it.

Consider the sagittal and tangential images formed by the telescope from a point source a distance s from the first telescope mirror. If these marginal images coincide, then the images

#112822 - $15.00 USD Received 22 Jun 2009; revised 11 Sep 2009; accepted 12 Sep 2009; published 6 Oct 2009

from all other ray fans will also coincide, provided that the only aberration present is astigmatism. Thus, by bringing these images together, the relationship between the telescope parameters that eliminates astigmatism for the particular point can be found. By applying Eq. (2) successively to each mirror, one gets that the separation between the sagittal and tangential images is given by

$$\Delta_s = \frac{r_2\left(\sin^2\theta\sin^2 I_2 - 1\right)\left[\dfrac{s\,r_1}{r_1 - 2s\cos I_1} + d\right]}{r_1\cos I_2\left(d + \dfrac{sr_1}{r_1 - 2s\cos I_1}\right) + r_2\left(\sin^2\theta\sin^2 I_2 - 1\right)} - \frac{r_2\left(\cos^2\theta\sin^2 I_2 - 1\right)\left[\dfrac{s\,r_1\cos I_1}{r_1\cos I_1 - 2s} + d\right]}{2\cos I_2\left(d + \dfrac{s\,r_1\cos I_1}{r_1\cos I_1 - 2s}\right) + r_2\left(\cos^2\theta\sin^2 I_2 - 1\right)}. \quad (8)$$

For small angles of incidence (I_1 and I_2), and $d = (r_1 + r_2)/2$, Eq. (8) can be expressed in terms of the telescope magnification $M = r_2 / r_1$ as

$$\Delta_s \approx -\frac{M\,r_1\cos(2\theta)}{2}\left(1 + M - \frac{2Ms}{r_1}\right)^2 I_2^{\,2} - \frac{2s^2M^2}{r_1} I_1^{\,2}. \quad (9)$$

The corresponding astigmatism equations in terms of vergence rather than object distance are

$$\Delta_\phi = \frac{r_1\phi - 2\cos I_1}{d\left(r_1\phi - 2\cos I_1\right) + r_1} + \frac{2 - \phi\, r_1\cos I_1}{(1 + \phi\, d)\cos I_1 r_1 - 2d} + \frac{2\cos I_2}{r_2(\cos^2\theta\sin^2 I_2 - 1)} + \frac{2\cos I_2}{r_2\left(1 - r_2\sin^2\theta\sin^2 I_2\right)}, \quad (10)$$

and,

$$\Delta_\phi \approx \frac{2\cos(2\theta)}{r_2} I_2^{\,2} + \frac{8}{r_1\left[r_1\phi\left(1 + M\right) - 2M\right]^2} I_1^2. \quad (11)$$

2.2.1 Finite conjugate (s = r_1/2)

Pupil planes in AO scanning ophthalmic instruments are typically placed one focal length in front of the first telescope mirror, (i.e. r_1/2 according to Eq. (7)). The astigmatism in these planes is described by Eqs. (8) and (9) with the geometry depicted in Fig. 2. When substituting s with r_1/2 in Eq. (9), the following condition for astigmatism cancellation is obtained,

$$I_2 \approx \sqrt{-\frac{M}{\cos(2\theta)}}\, I_1. \quad (12)$$

#112822 - $15.00 USD Received 22 Jun 2009; revised 11 Sep 2009; accepted 12 Sep 2009; published 6 Oct 2009

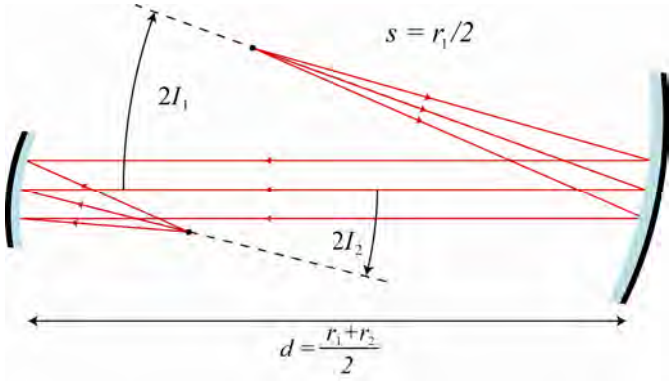

Fig. 2. Notation used to describe an afocal telescope formed by a pair of off-axis spherical mirrors in the finite conjugate case, with s = r1/2. This particular configuration corresponds to θ = 0.

This condition can only be met if $\pi/4 < |\theta| < 3\pi/4$, which is reasonable, given that the second mirror must introduce less astigmatism on the incidence plane of the first mirror than on the perpendicular plane. The particular case $\theta = \pi/2$ produces the most compact optical setup (i.e. the one with the smallest I_2), therefore minimizing other field-dependent aberrations.

Meeting the condition in Eq. (12) cancels the astigmatism for the object point at $s = r_1/2$ along the principal ray, and minimizes the overall astigmatism for other points within a field of view centered on the object point. To illustrate this, consider the astigmatism corresponding to an arbitrary point in the same plane and near the point with null astigmatism. The angles of incidence of the principal ray corresponding to this new point can be expressed as $I_1 + \varepsilon_1$, with $\varepsilon_1 < I_1$, and $I_2 + \varepsilon_2$, with $\varepsilon_2 < I_2$. Substituting in Eq. (9) and imposing the condition in Eq. (12) yields

$$\Delta_s \propto r_1 M^2 I_1 \varepsilon_1 . \tag{13}$$

This result shows that the astigmatism over the field of view is proportional to the angle of incidence I_1, and therefore, whenever possible, small angles of incidence should be used. Similarly, low magnification telescopes and short focal length mirrors will also result in low astigmatism over the field of view. Finally, the linear dependence in ε_1 indicates that the astigmatism will be minimal when the condition in Eq. (12) is met for the point at the center of the field of view.

2.2.2 Infinite conjugates

The second set of relevant optical planes in ophthalmic instruments with AO is the image planes, which are conjugated to the retina. Because the light exiting the relaxed emmetropic eye is nearly collimated, it is more convenient to work with vergences rather than distances. Therefore, with the geometry depicted in Fig. 3 and substituting $\phi = 0$ in Eq. (11), the condition for minimizing astigmatism in image planes becomes

$$I_2 \approx \sqrt{-\frac{1}{M\cos(2\theta)}}\, I_1 . \tag{14}$$

#112822 - $15.00 USD Received 22 Jun 2009; revised 11 Sep 2009; accepted 12 Sep 2009; published 6 Oct 2009

Similar to the finite conjugates case, this condition can only be met if $\pi/4 < |\theta| < 3\pi/4$. Note that while astigmatism is only cancelled for a point at infinity along the principal ray, the overall astigmatism for any point within a symmetric field of view is also minimized as before. Following the same steps that led to relation (13), using Eqs. (11) and (14) yields

$$\Delta_\phi \propto \frac{4I_1}{M}\left(\frac{\varepsilon_2}{r_2}+\frac{\varepsilon_1}{r_1}\right). \tag{15}$$

As in the finite conjugate case studied above, small angles of incidence will result in configurations with lower astigmatism over the field of view. Contrary to the previous case however, high magnification and long focal lengths will reduce the astigmatism across the field of view. This means that in order to have a single telescope with low astigmatism in both pupil and retinal planes, the angles of incidence should be kept to a minimum.

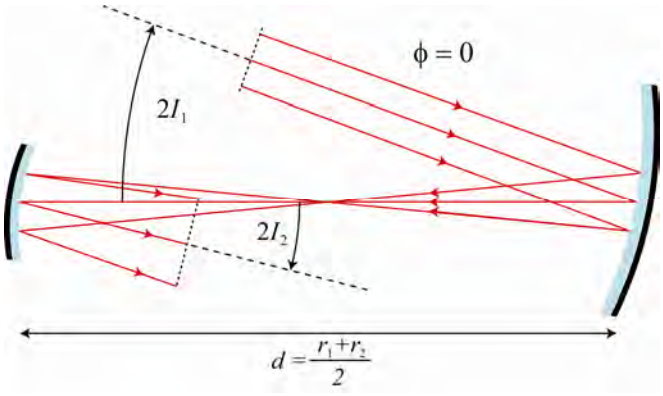

Fig. 3. Notation used to describe an afocal telescope formed by a pair of off-axis spherical mirrors in the infinite conjugates case. This particular arrangement corresponds to the case $\theta = 0$.

2.3 Simultaneous minimization of astigmatism in pupil and image planes in pairs of afocal telescopes

Typically, optical elements such as scanners, wavefront correctors, wavefront sensors and trial lenses are placed in the pupil planes of retinal imaging instruments equipped with AO. As mentioned earlier, in order to take full advantage of the AO correction, astigmatism needs to be corrected so that image quality is good in all pupil planes. The astigmatism affecting retinal planes however, only needs to be corrected at the ends of the optical setup, that is, at the eye and the science detector(s). This dictates that all the telescopes in such systems should meet the condition in Eq. (12) to compensate for astigmatism in the pupil planes. By comparing Eqs. (12) and (14), it is clear that astigmatism can only be minimized simultaneously in both pupil and image planes for telescopes with unit magnification. However, when selecting the second angle of incidence in terms of the first one as prescribed by Eq. (12), a degree of freedom in the selection of the first angle of incidence remains. Thus, by combining a pair of pupil-corrected telescopes, the first angle of each of the telescopes can be selected to minimize astigmatism in the exit image plane, while preserving minimal astigmatism in all the pupil planes.

For example, consider a pair of pupil-corrected (i.e. minimal astigmatism) telescopes in series,

$$I_2 \approx \sqrt{-\frac{M_{12}}{\cos(2\theta_{12})}}\, I_1,\ I_4 \approx \sqrt{-\frac{M_{34}}{\cos(2\theta_{34})}}\, I_3. \tag{16}$$

#112822 - $15.00 USD Received 22 Jun 2009; revised 11 Sep 2009; accepted 12 Sep 2009; published 6 Oct 2009

By calculating the vergence difference between the marginal ray fans from an object at infinity after the reflections on all four mirrors, the condition for minimizing astigmatism in the small angles regime can be obtained,

$$I_3 = \frac{1}{M_{12}} \sqrt{\frac{-r_3\left(1-M_{12}{}^2\right)\cos(2\theta_{34})}{r_1\left\{M_{34}^2 \sin\left[2\left(\theta_{12}+\theta_{23}\right)\right]\sin\left(2\theta_{34}\right)+\left(1-M_{34}^2\right)\cos\left[2\left(\theta_{12}+\theta_{23}\right)\right]\cos\left(2\theta_{34}\right)\right\}}}\, I_1 . \quad (17)$$

As in the previous two sections, this condition cancels the astigmatism for the point along the optical axis and minimizes the average astigmatism over the field of view. By considering the astigmatism-compensated configurations with smaller angles, i.e. $|\theta_{12}| = |\theta_{34}| = \pi/2$, and $|\theta_{23}| = 0, \pi/2, \pi$, other field-dependent aberrations will also be reduced. For these configurations, Eq. (17) becomes

$$I_3 \approx \frac{1}{M_{12}} \sqrt{\pm \frac{r_3}{r_1}\left(\frac{1-M_{12}{}^2}{1-M_{34}{}^2}\right)}\, I_1 . \quad (18)$$

The sign inside the radical depends on whether $|\theta_{23}| = 0, \pi$ or $\pi/2$. This gives rise to two families of telescope configurations with minimal astigmatism: one in which $M_{12} > 1$ and $M_{34} < 1$ ($|\theta_{23}| = \pi/2$), and one in which $M_{12} < 1$ and $M_{34} < 1$ ($|\theta_{23}| = 0, \pi$). An example to illustrate this point will be discussed in the examples section below.

The same steps could be used to obtain an astigmatism cancellation condition for a three-telescope system. With six mirrors instead of four, there would be an infinite number of solutions, instead of just eight as in Eq. (18).

2.4 Impact of focus shift on astigmatism minimization

By calculating the astigmatism introduced by a focus shift in off-axis afocal reflective telescopes, the robustness to beam collimation and to axial alignment can be studied. Indeed, it is sometimes desirable to shift the focus of the retinal planes to image different structures and/or compensate for chromatic aberration when imaging using multiple wavelengths. The expansion of Eqs. (8) and (10) for small angles in the presence of a small defocus, that is $s = r_1/2 + \varepsilon_s$, with $2|\varepsilon_s|/r_1 << 1$, and $\phi = \varepsilon_\phi$, with $r_1|\varepsilon_\phi|/2 << 1$ respectively, give

$$\Delta_s \approx -\frac{r_1 M \cos(2\theta)}{2} I_2{}^2 - \frac{r_1 M^2}{2} I_1{}^2 + \left[2M^2 \cos(2\theta) I_2{}^2 - 2M^2 I_1{}^2\right]\varepsilon_s \quad (19)$$

and

$$\Delta_\phi \approx \frac{2\cos(2\theta)}{r_1 M} I_2{}^2 + \frac{2}{r_1 M^2} I_1^2 + 2\left(\frac{1}{M^3} + \frac{1}{M^2}\right) I_1^2 \varepsilon_\phi . \quad (20)$$

These equations indicate that in the general case, the astigmatism introduced by small focus shifts corresponds to third order terms (i.e. $I_1^2\varepsilon_s$, $I_2^2\varepsilon_s$ and $I_1^2\varepsilon_\phi$) and is therefore negligible compared to the dominant second order terms(I_1^2, I_2^2). However, for pupil or image plane astigmatism-corrected telescopes, the astigmatism introduced by the focus shift is the dominant term,

$$\Delta_s \approx -2M^2\left(1+M\right) I_1^2 \varepsilon_s , \quad (21)$$

$$\Delta_\phi \approx 2\frac{1}{M^2}\left(\frac{1}{M}+1\right) I_1^2 \varepsilon_\phi . \quad (22)$$

#112822 - $15.00 USD Received 22 Jun 2009; revised 11 Sep 2009; accepted 12 Sep 2009; published 6 Oct 2009

It is clear then that reducing the angles of incidence increases the tolerance to focus shifts simultaneously in both sets of planes and independently of the telescopes' magnification.

Applying the same idea to a pair of afocal telescopes that simultaneously meet conditions (16) and (18), yields that the astigmatism in the image plane as a result of a small focus shift is given by

$$\begin{aligned}\Delta_\phi = &\left\{r_3^2\left[r_2 M_{12} + r_3\left(M_{12}-1\right)\right]\cos\left[2\left(\theta_{12}+\theta_{23}\right)\right]\cos\left(2\theta_{34}\right)\right.\\ &\left.- r_3^2 r_4\left(1-M_{12}\right)\cos\left[2\left(\theta_{12}+\theta_{23}+\theta_{34}\right)\right] - r_2 r_4^2 M_{12}\cos\left[2\left(\theta_{12}+\theta_{23}+\theta_{34}\right)\right]\right\} \\ &\times \frac{2\left(1+M_{12}\right)}{r_2 M_{12}^3 M_{34}^2\left\{r_3^2\cos\left[2\left(\theta_{12}+\theta_{23}\right)\right]\cos\left(2\theta_{34}\right) - r_4^2\cos\left[2\left(\theta_{12}+\theta_{23}+\theta_{34}\right)\right]\right\}} I_1^2\ \varepsilon_\phi ,\end{aligned} \tag{23}$$

with the defocus term being a third order term, as before. As in the case of a single telescope, the impact of the defocus shift can be reduced by selecting small angles of incidence.

2.5 The off-axis Badal optometer

Many ophthalmic imaging instruments use the Badal optometer [22,23], to either partially or completely compensate for the refractive error of the eye. In these instruments, a positive lens (the Badal lens) is kept a focal length away from the eye, while its distance to the instrument is adjusted until the retinal image is in focus (Badal shift). This can also be achieved using a concave mirror. In the off-axis afocal telescopes discussed in this work, a Badal shift would introduce an undesired astigmatism component in the retinal plane. This astigmatism would be negligible in comparison to the defocus being compensated for, provided the angles of incidence on the telescope mirrors are small, as it is shown next.

In an off axis pupil-corrected afocal telescope, changing the mirror separation $d = (r_1 + r_2)/2$ by a small amount ($|\varepsilon_d| << (r_1 + r_2)/2$) introduces astigmatism in the pupil plane. This astigmatism can be calculated by substituting in Eq. (8) and performing a polynomial expansion retaining only the lower order terms,

$$\Delta_d \approx \frac{1-M}{3r_1} I_1^4 + \frac{\left(1+M\right)\left(211+59M\right)}{180 r_1} I_1^6 + \frac{3+2M}{r_1^2} I_1^6 \varepsilon_d . \tag{24}$$

This expression indicates that for small angles of incidence and to 6th order, the pupil astigmatism is independent of the Badal adjustment.

3. Examples

In this section we evaluate the performance of three systems. The first and second are single telescopes corrected for astigmatism in the pupil and image planes respectively. The third is a pair of telescopes with astigmatism corrected in the entrance and exit image planes, as well as all three pupil planes. For comparison, the angles predicted by the marginal ray fan Eqs. (8) and (10), their linear approximations, that is Eqs. (12), (14) and (18) and, the optimal angles determined by minimizing the wavefront RMS are presented. In all examples, the wavefront RMS was calculated using the ray tracing software from Zemax Development Corporation (Bellevue, Washington, USA) after correcting for defocus. Optimization in Zemax was performed by allowing the program to vary only the second angle of incidence when considering a single telescope. When considering two telescopes in sequence, only the third angle of incidence was varied, with the second and fourth angles calculated using Eqs. (16).

3.1 Single off-axis afocal telescope finite conjugate corrected ($s = r_1/2$)

In order to illustrate the dependence on telescope magnification and folding angle θ, three telescopes are evaluated. The first is a 2:1 telescope with a 90° folding angle. The second and

#112822 - $15.00 USD Received 22 Jun 2009; revised 11 Sep 2009; accepted 12 Sep 2009; published 6 Oct 2009

third are 3:1 and 2:1 telescopes with 90° and 80° folding angles respectively. The results are presented in Fig. 4.

The plots on the top row compare the results of solving Eq. (8) exactly with its linear approximation given by Eq. (12). These results are also compared to the optimal angle which minimizes the wavefront RMS as calculated by Zemax. The plots show that for θ = 90°, the angles predicted by the marginal ray fan equation (Coddington) and its linear approximation minimize the wavefront RMS for angles of incidence ≥ 1°. The prediction of the optimal angle is not as good for the θ = 80° configuration due to the presence of coma. The plots on the second row show how the axial separation of the image point from the second mirror decreases with increasing angles of incidence. This is also the case for magnifications greater than one. The plots on the bottom row show the corresponding wavefront RMS values for all the configurations, including the planar case ($\theta = 0^{\circ}$) for reference. The most outstanding feature in all three plots is that by folding the telescope off the plane, the wavefront RMS decreases by an order of magnitude. Also, the Coddington solution and its linear approximation are virtually identical to that of the optimal configuration. This means that the linear approximation model in Eq. (12) is acceptable for all practical purposes in the 1 to 15° range. For angles less than 1°, the predicted angles are far from optimal because of the presence of spherical aberration. Finally, it should be noted that the 90° configuration produces the smallest second angle of incidence, hence minimizing other aberrations. This is illustrated by comparing the first and third plots of the bottom row.

3.2 Single off-axis afocal telescope infinite conjugate corrected

The performance of the three previously described telescopes is evaluated with an object point placed at infinity. The results are displayed in Fig. 5.

The plots on the top row compare the results of solving Eq. (10) exactly, with its linear approximation given by Eq. (14). These results are also compared to the optimal angle which minimizes the wavefront RMS. For the θ = 90° configurations, the angles predicted by the Coddington equation and its linear approximation minimize the wavefront RMS over a range of 1 to 5°. This is significantly limited compared to the results of the previous section. The estimation of the second angle of incidence is poorer for the θ = 80° configuration due to the presence of coma. The plots on the second row show that the vergence of the beam reflected off the second mirror becomes more negative with increasing angles of incidence. The same effect is observed for magnifications greater than one. The plots on the bottom row show the corresponding wavefront RMS values for all the configurations, including the planar case for reference. The exact Coddington solution and its linear approximation perform better than the planar configuration, but the optimal configuration results in a more significant improvement for angles larger than 5°. This indicates that the linear approximation to the Coddington solution can be used as a starting point for the optimization software, which has to vary only two parameters to find the best solution. These parameters are the angle of incidence of the principal ray onto the second mirror and the vergence of the beam reflected by the second mirror. As in the previous section, spherical aberration dominates when angles of incidence are less than 1°. When angles of incidence are greater than 1°, the limiting aberration after astigmatism correction is coma. Coma is also the aberration that limits the range of validity of the linear approximation in Eq. (14). It should also be noted that the 90° configuration performs better than the 80° which is consistent with the results from the previous section.

3.3 Off-axis afocal telescopes pair finite and infinite conjugate corrected

The following example illustrates how to simultaneously correct astigmatism in both pupil and exit image planes by taking advantage of Eq. (18). The same reasoning could be applied to the more general Eq. (17), but for simplicity only the most compact designs (which also have the lowest wavefront RMS) will be discussed. The optical setup evaluated consists of a pair of reflective off-axis afocal telescopes in series, with the following spherical mirror radii of curvature in order: 1000, 500, 333 and 1000mm. Each of the two telescopes is pupil-

#112822 - $15.00 USD Received 22 Jun 2009; revised 11 Sep 2009; accepted 12 Sep 2009; published 6 Oct 2009

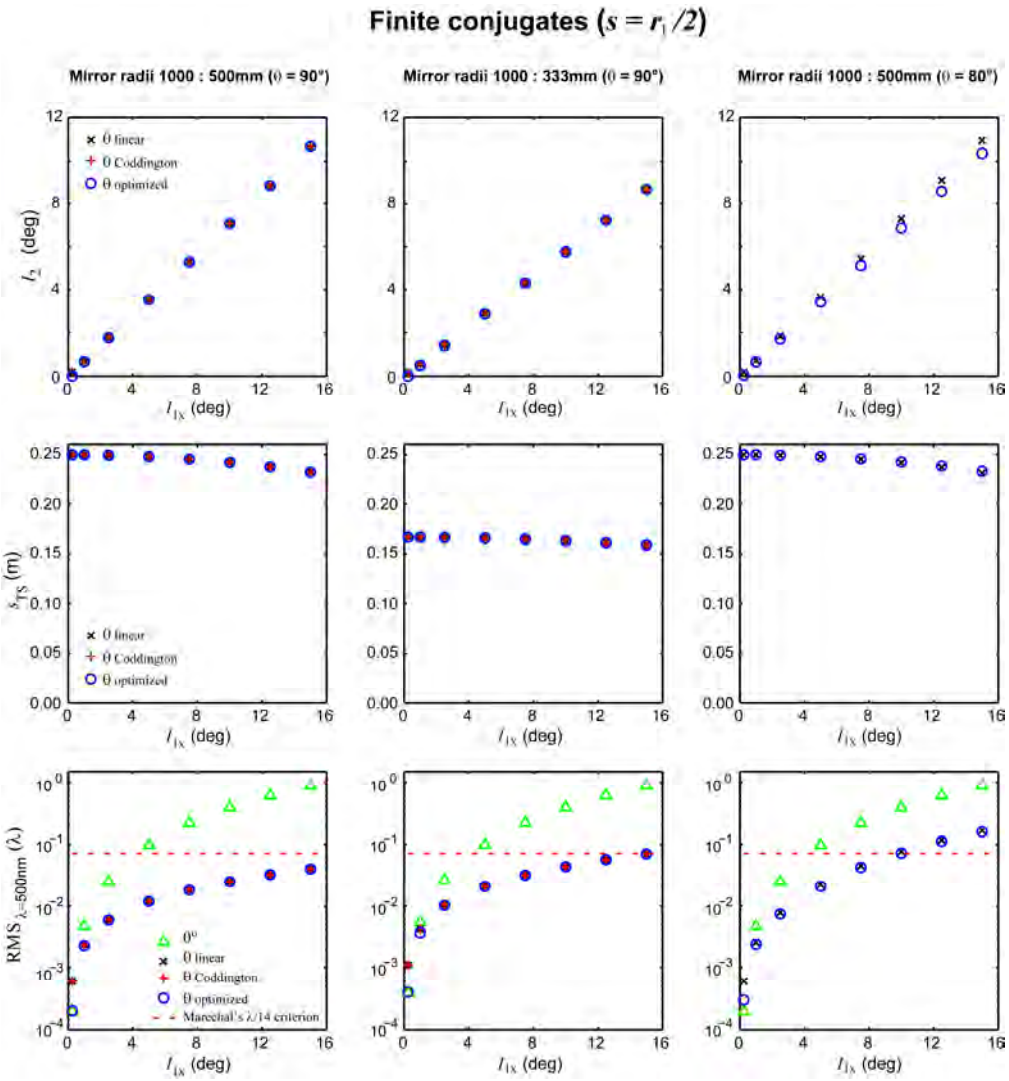

Fig. 4. Each column describes a different off-axis reflective afocal (4f) telescope, with the parameters indicated at the top. The object point is at the front focal point of the first mirror (Fig. 2). The top row shows the angle of incidence of the principal ray onto the second mirror as a function of the angle of incidence onto the first mirror. The second row shows the distance between the second mirror and the image point as a function of the first angle of incidence for the same configurations. The bottom row shows the wavefront RMS values for the (defocus-corrected) corresponding configurations. The RMS of the planar (θ = 0°) configuration is also plotted for comparison. The red dashed lines indicate Marechal's diffraction limit.

corrected using Eq. (16). Retinal astigmatism is corrected by either using the linear approximation in Eq. (16), or by optimization with the absolute values of θ_{12}, θ_{23} and θ_{34} being 90°. The separation between the two telescopes accounted for the focus shift shown in the middle row of Fig. 6.

As mentioned earlier, Eq. (18) has two families of solutions depending on the sign within the radical. The magnifications dictate which of the two families of solutions should be used. Each solution family is formed by four different configurations, given by the signs of θ_{23} and θ_{34}. The geometries of all 8 folding solutions are sketched in Table 1 below, and only the family of solutions that correspond to $|\theta_{23}| = \pi/2$ are plotted in Fig. 6.

#112822 - $15.00 USD Received 22 Jun 2009; revised 11 Sep 2009; accepted 12 Sep 2009; published 6 Oct 2009

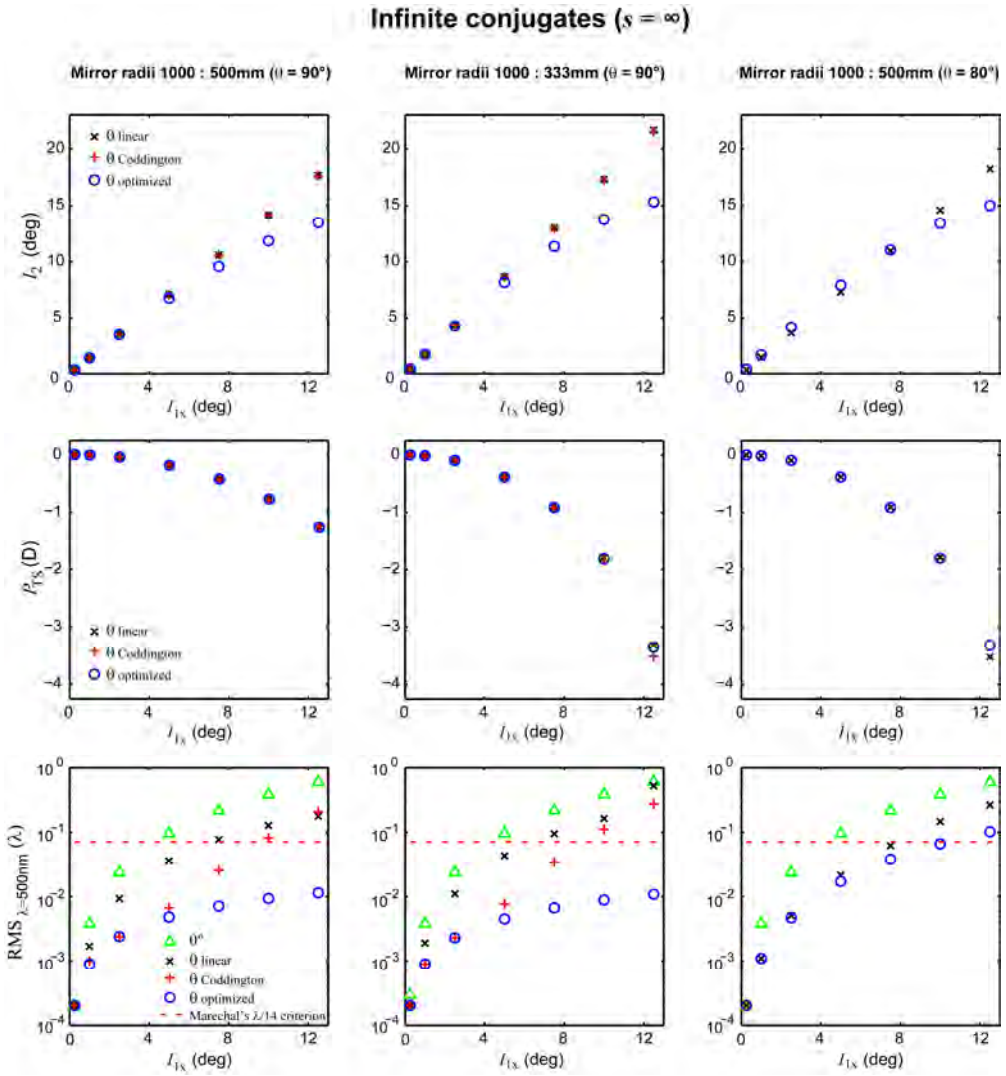

Fig. 5. Each column describes a different off-axis reflective afocal (4f) telescope, with the parameters indicated at the top. The object point is at the front focal point of the first mirror (see Fig. 3). The top row shows the angle of incidence of the principal ray onto the second mirror as a function of the angle of incidence onto the first mirror. The second row shows the power (vergence) between the second mirror and the image point in diopters (D) as a function of the first angle of incidence for the same configurations. The bottom row shows the wavefront RMS values for the (defocus-corrected) corresponding configurations. The RMS of the planar (θ = 0°) configuration is also plotted for comparison. The red dashed lines indicate Marechal's diffraction limit.

Astigmatism is minimized in all four configurations evaluated, but the impact of other aberrations (mostly coma) is different for each. This is shown by the four RMS values on the left side of the table. The plots in Fig. 6 show all four optimal configurations but only one solution of the linear approximation. This was done in order to maintain the readability of the plots. The first plot in Fig. 6 shows the angles calculated using Eq. (18) and the optimal angles for each of the four configurations sketched on the left side of Table 1. The linear approximation correctly predicts the optimal angles in the 1° to 5° range. The second plot shows the vergence of the beam reflected off the fourth mirror for all configurations. Similar to the single telescope case, the vergence becomes more negative with increasing angles of incidence. The third plot shows the corresponding wavefront RMS values for all the

#112822 - $15.00 USD Received 22 Jun 2009; revised 11 Sep 2009; accepted 12 Sep 2009; published 6 Oct 2009

Table 1. Wavefront RMS of the most compact configurations of two different pairs of off-axis telescopes with minimal aberrations, for I_1 = 5°. The numbers on the top row are the mirror radii of curvature in mm. The entrance beam diameter considered was 8mm and λ = 500nm.

	cos ($2\theta_3$) = –1 1000: 500: 333: 1000				cos ($2\theta_3$) = 1 500: 1000: 333: 1000			
θ_3, θ_4 Folding geometry	π/2, π/2	-π/2, π/2	π/2, -π/2	-π/2, -π/2	π, -π/2	0, -π/2	π, π/2	0, π/2
RMS (λ)	0.0064	0.0078	0.0089	0.0099	0.1502	0.1531	0.1638	0.1693

configurations at the image planes. The planar case is provided as a reference. The RMS for all non-planar configurations is significantly lower than for the planar design. The optical performance of the linear approximation is close to optimal in the 1° to 5° range. As in the previous cases, for angles less than 1°, the predicted angles are not optimal, due to spherical aberration.

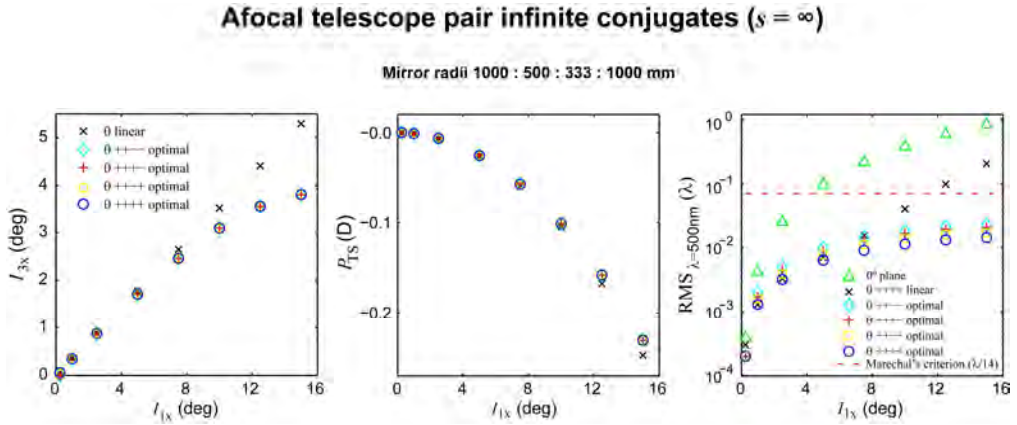

Fig. 6. Data from a pair of off-axis reflective afocal (4f) telescopes, with astigmatism simultaneously corrected in pupil and image planes. The left plot shows the angle of incidence of the principal ray onto the second mirror as a function of the angle of incidence onto the first mirror, for the linear approximation, and the four different optimal configurations sketched on the left side of Table 1. The middle plot shows the distance between the second mirror and the image point as a function of the angle of incidence. The plot on the right shows the wavefront RMS values for the (defocus-corrected) corresponding configurations. The RMS of the planar (θ = 0°) configuration is also plotted for comparison. The red dashed line in the last plot indicates Marechal's diffraction limit.

4. Conclusion

Expressions for minimal astigmatism in pupil and image planes applicable to off-axis reflective afocal telescopes were derived using the marginal ray fan equation. Three simple formulae, Eqs. (12), (14) and (18) for the small angle approximation were obtained and evaluated in different examples. The first two examples illustrate that by adequate off-plane folding, astigmatism can be corrected in the pupil or image planes of these telescopes. The third example shows that for a pair of reflective afocal telescopes, one could correct for astigmatism simultaneously in all the pupil planes and in the exit image plane. The formulae for a telescope pair could be directly applied to a system formed by any number of telescope pairs. The extension to a system with an odd number of telescopes has been discussed.

#112822 - $15.00 USD Received 22 Jun 2009; revised 11 Sep 2009; accepted 12 Sep 2009; published 6 Oct 2009

The obtained wavefront RMS plots show that the off-plane telescope configurations based on the conditions in Eqs. (12), (14) and (18), can perform an order of magnitude better than the corresponding planar configurations. It was also found that the 90° folding configuration always results in the lowest wavefront RMS, and in the particular cases presented here, below the diffraction limit.

It was also shown that reducing the angles of incidence on the studied reflective telescopes has multiple benefits. First, the astigmatism over the whole field of view is minimized. Second, other angle-dependent aberrations are also reduced. Finally, the system is more tolerant to axial misalignment and less sensitive (in terms of astigmatism) to Badal optometer-like shifts.

Even though the formulae presented were derived with AO ophthalmoscopy in mind, astigmatism minimization is desirable in other off-axis optical systems, such as spectrographs and laser cavities. To obtain these conditions, one simply has to calculate the difference between the sagittal and tangential images for the desired conjugate and number of mirrors, and solve for $\Delta_s = 0$.

Acknowledgements

The authors want to acknowledge the support of the Consejo Nacional de Ciencia y Tecnología de México (CONACyT), project No. 78812 and the scholar grant No. 170266. Alfredo Dubra-Suarez, Ph.D., holds a Career Award at the Scientific Interface from the Burroughs Welcome Fund. This research was also supported by the National Institute for Health, Bethesda, Maryland (NIH EY014375, NIH EY01319), Bausch and Lomb, Research to Prevent Blindness, the National Science Foundation, through the Center for Adaptive Optics, managed by the University of California at Santa Cruz (cooperative agreement no.: AST-9876783). We would like to thanks the reviewers and Yusufu Sulai for invaluable comments that have greatly improved the manuscript.

#112822 - $15.00 USD Received 22 Jun 2009; revised 11 Sep 2009; accepted 12 Sep 2009; published 6 Oct 2009

ANEXO 3

Optical Design of Clinical Adaptive Optics Instruments for Retinal Imaging

A. Dubra,[1,2*] A. Gómez-Vieyra[3], Y. Sulai[4] and Luis Díaz-Santana[5]

[1] *Flaum Eye Institute University of Rochester, Rochester, NY, 14642, USA*
[2] *Center for Visual Science, University of Rochester, Rochester, NY, 14627, USA*
[3] *Centro de Investigaciones en Óptica A.C, Loma del Bosque 115, C.P. 37000, León, Guanajuato, México*
[4] *The Institute of Optics, University of Rochester, Rochester, NY, 14627, USA*
[5] *The Henry Wellcome Laboratories for Vision Sciences, Department of Optometry and Visual Science, City University, London, EC1V 0HB, UK.*

[*] *adubra@cvs.rochester.edu*

Abstract: Simple design rules can be used to reduce astigmatism in off-axis reflective ophthalmic adaptive optics instruments. These rules will be illustrated by presenting the design of such devices with footprints smaller than a square foot.

OCIS codes: (110.1080) Active or adaptive optics, (080.2468) First-order optics.

1. Introduction

Ophthalmic adaptive optics (AO) instruments allow for non-invasive imaging of the retina with great lateral and axial resolution [1-7]. Within this family of instruments, the AO scanning laser ophthalmoscope (AO-SLO) and the AO optical coherence tomograph (AO-OCT) provide the greatest axial sectioning. These scanning instruments are typically based on reflective optics to avoid undesired back-reflections that would be comparable to the light reflected or scattered by the retina. Current clinical instruments avoid this problem by using different portions of the pupil of the eye for illumination and imaging. This is not possible in AO instruments, because the full pupil of the eye is needed for both illumination and imaging, in order to achieve maximum lateral and axial resolution. Current AO scanning instruments use spherical mirrors in an off-axis arrangement to relay the planes conjugate to the pupil of the eye, mainly because of their low cost and ease of alignment [2-7]. These mirrors are used either individually, with the object and image planes two focal lengths away from the mirror surface (2f-2f), or in pairs, creating an afocal telescope. When using spherical mirrors in an off-axis planar arrangement, the resulting instruments are limited by astigmatism. Recently Gómez-Vieyra *et al.* [8], demonstrated that by folding the afocal telescopes in a prescribed three-dimensional configuration, astigmatism can be cancelled at a single point in the field of view. The work presented here builds on that of Gómez-Vieyra *et al.*, exploring whether ophthalmic AO scanning instruments can be built with dimensions comparable to those of existing clinical instruments. Three different instruments where designed based on the method used to relay the planes conjugate to the pupil of the eye: 3 afocal telescopes (configuration #1, left panel of figure 1); 1 afocal telescope and 2 single mirrors (configuration #2) and 3 single mirrors (configuration #3, right panel of figure 1). The spherical mirrors in all three configurations are either 125 or 250 mm in focal length. All pupil relays have unit magnification, to keep the instrument dimensions and optical aberrations to a minimum. The diameter assumed at the pupil of the eye was 6.5 mm, and the assumed illumination wavelength was 800 nm. The instruments were designed with a 2.5×2.5° field of view. A realistic mechanical mounting of the pupil elements was assumed, by considering their radius larger than those of the optics by 5 mm. The angles of incidence at the spherical mirrors were kept to the minimum required by the mechanical mounts of the elements in the pupil plane.

2. Results and Conclusions

Table 1 below summarizes the optical performance of the evaluated instruments, as estimated using the ray tracing program Zemax (Zemax Development Corporation, Bellevue, Washington, USA). The wavefront root-mean-squared (RMS) error at the pupil and retinal (image) planes were evaluated as the generalized quadratic mean of all the 9 points evaluated across the field of view, in both retinal and pupil conjugate planes. All evaluated configurations are diffraction-limited according to Marechal's criterion simultaneously at the retinal planes, and at the pupil planes with only one exception (# 2). The smaller instruments (f = 125 mm) can only tolerate a small prescription correction range at the deformable mirror plane, thus requiring an additional system, such as a phoropter, or trial lenses for correcting prescription in front of the eye. The larger systems (f = 250 mm) provide diffraction-limited performance over a much larger prescription range. In the configuration #1, the defocus range can be further extended by varying the distance between the two spherical mirrors closest to the eye (Badal optometer), without degrading the optical performance at the pupil plane of the eye.

Depending on the focal length of the spherical mirrors which determines the angles required to clear the mechanical mounts, one configuration performs better than the other two. Finally, all performance parameters being comparable, configuration #3 would be the preferred one for a clinical instrument. The smaller number of optical elements in configuration #3 would result in the highest light throughput, which in turn, could be translated in either better light safety conditions and/or images with higher signal-to-noise ratio, as well as simpler alignment.

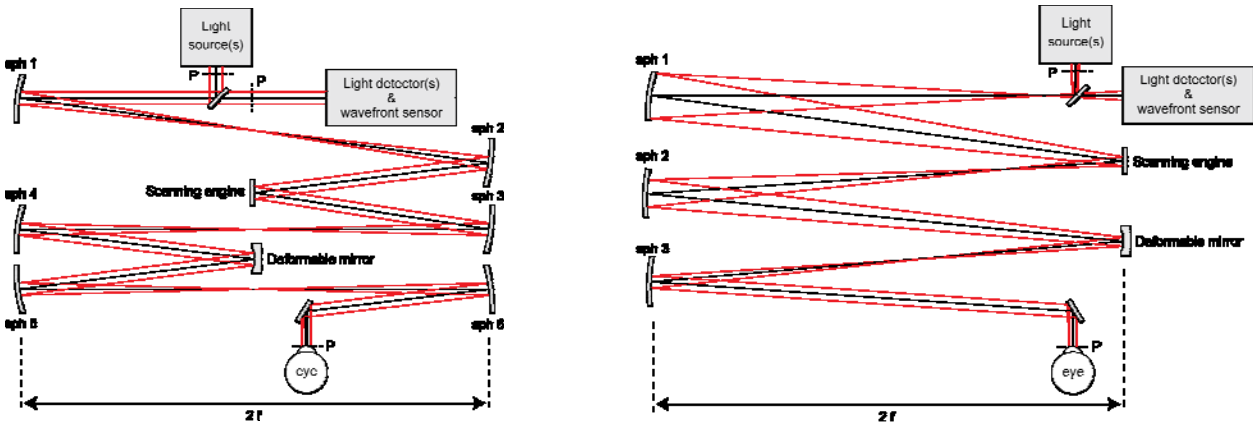

Figure 1: Schematic of evaluated ophthalmic AO instruments using configuration #1 (left) and configuration #3 (right). For clarity, the systems have been drawn in a plane arrangement. All the spherical mirrors (sph) have the same focal length. The scanning engines and deformable mirrors are in planes conjugate to the pupil of the eye (P).

Table 1: optical performance of evaluated AOSLO configurations.

Configuration	Pupil relays	f (mm)	RMS_{retina}	RMS_{pupil}	DM prescription range (D)
# 1	3 afocal telescopes	125	λ/28	λ/26	-1.5, +1.5
# 2	1 afocal telescope, 2 single mirrors	125	λ/27	λ/3	-2.0, +1.5
# 3	3 single mirrors	125	λ/19	λ/13	-1.0, +1.0
# 1	3 afocal telescopes	250	λ/120	λ/110	-6.0, +6.0
# 2	1 afocal telescope, 2 single mirrors	250	λ/200	λ/22	-8.0, +4.0
# 3	3 single mirrors	250	λ/130	λ/130	-8.0, +4.0

Acknowledgements

The authors acknowledge the support of the Consejo Nacional de Ciencia y Tecnología de México (CONACYT), the scholar grant No. 170266. Alfredo Dubra-Suarez, Ph.D., holds a Career Award at the Scientific Interface from the Burroughs Welcome Fund. This research was also supported by NIH (EY014375, EY01319), Bausch and Lomb, Research to Prevent Blindness.

References

1. J. Liang, D.R. Williams, and D.T. Miller, "Supernormal vision and high-resolution retinal imaging through adaptive optics," J. Opt. Soc. Am. A 14, 2884-2892 (1997).
2. Y. Zhang, B. Cense, J. Rha, R.S. Jonnal, W. Gao, R.J. Zawadzki, J.S. Werner, S. Jones, S. Olivier, and D. T. Miller, "High-speed volumetric imaging of cone photoreceptors with adaptive optics spectral-domain optical coherence tomography," Opt. Express **14**, 4380-4394 (2006),.
3. R. J. Zawadzki, S. M. Jones, S. S. Olivier, M. T. Zhao, B. A. Bower, J. A. Izatt, S. Choi, S. Laut, and J. S. Werner, "Adaptive-optics optical coherence tomography for high-resolution and high-speed 3D retinal in vivo imaging," Opt. Express **13**, 8532-8546 (2005).
4. D. Merino, C. Dainty, A. Bradu, and A. Gh. Podoleanu, "Adaptive optics enhanced simultaneous en-face optical coherence tomography and scanning laser ophthalmoscopy," Opt. Express **14**, 3345-3353 (2006).
5. A. Roorda, F. Romero-Borja, W. J. Donnelly, H. Queener, T. J. Hebert, and M. C. W. Campbell, "Adaptive optics scanning laser ophthalmoscopy," Opt. Express **10**, 405-412 (2002),.
6. D. X. Hammer, R. D. Ferguson, C. E. Bigelow, N. V. Iftimia, T. E. Ustun, and S. Burns, "Adaptive optics scanning laser ophthalmoscope for stabilized retinal imaging," Opt. Express **14**, 3354-3367 (2006).
7. D. C. Gray, W. Merigan, J. I. Wolfing, B. P. Gee, J. Porter, A. Dubra, T. H. Twietmeyer, K. Ahmad, R. Tumbar, F. Reinholz, and D. R. Williams, "In vivo fluorescence imaging of primate retinal ganglion cells and retinal pigment epithelial cells," Opt. Express **14**, 7144-7158 (2006).
8. A. Gómez-Vieyra, A. Dubra, D. Malacara-Hernández, and D.R. Williams, "First-order design of off-axis reflective ophthalmic adaptive optics systems using afocal telescopes," Opt. Express 17, 18906-18919 (2009).

ANEXO 4

First-order design of off-axis reflective ophthalmic adaptive optics systems using afocal telescopes

Armando Gómez-Vieyra,[1] Alfredo Dubra,[2] David R. Williams,[3]
and Daniel Malacara-Hernández[1]

[1]Centro de Investigaciones en Óptica A.C., Loma del Bosque 115, C.P. 37000, León, Guanajuato, México
[2] University of Rochester Eye Institute, Rochester, NY, 14642-0314, USA
[3]Center for Visual Science, University of Rochester, Rochester, NY, 14627-0270, USA

ABSTRACT

Scanning laser ophthalmoscopes (SLOs) and optical coherence tomographs are the state-of-the-art retinal imaging instruments, and are essential for early and reliable diagnosis of eye disease. Recently, with the incorporation of adaptive optics (AO), these instruments have started to deliver near diffraction-limited performance in both humans and animal models, enabling the resolution of the retinal ganglion cell bodies, their processes, the cone photoreceptor and the retinal pigment epithelial cells mosaics. Unfortunately, these novel instruments have not delivered consistent performance across human subjects and animal models. One of the limitations of current instruments is the astigmatism in the pupil and imaging planes, which degrades image quality, by preventing the wavefront sensor from measuring aberrations with high spatial content. This astigmatism is introduced by the sequence of off-axis reflective elements, typically spherical mirrors, used for relaying pupil and imaging planes. Expressions for minimal astigmatism on the image and pupil planes in off-axis reflective afocal telescopes formed by pairs of spherical mirrors are presented. The formulas, derived from the marginal ray fans equation, are valid for small angles of incidence (≤15º), and can be used to design laser cavities, spectrographs and vision adaptive optics systems. An example related to this last application is discussed.

Keywords: Aberrations, astigmatism, marginal rays, adaptive optics, off-axis reflective telescopes.

1. INTRODUCTION

The introduction of adaptive optics (AO) to ophthalmic imaging in recent years has led to the development of a new generation of high-resolution retinal imaging instruments, such as the AO fundus camera [1,2], the AO optical coherence tomograph (AO-OCT) [3,4] and the AO scanning laser ophthalmoscope (AOSLO) [4-8]. In order to maximize the resolution of the AO scanning instruments (i.e. AO-SLOs and AO-OCTs), the full entrance and exit pupils should be used. In this system, the use of refractive elements is not desirable, given that the back reflections from the optical surfaces can be orders of magnitude brighter than the light collected from the retina. Low-resolution clinical instruments do not suffer from such problem because they use different portions of the pupil for illumination and light collection. To avoid the problem of back reflections, most AO-equipped scanning ophthalmic instruments are at least partially built using off-axis spherical mirrors, given their low-cost and ease of alignment [2-8]. The major optical performance limitation of such systems is the astigmatism introduced by the off-axis arrangement, as it has been reported by Webb *et al*. [9,10] when reporting the first confocal laser scanning ophthalmoscope, and later by Burns *et al.* [8]. In his work, Webb suggested an off-the-plane perpendicular folding of the optical setup to reduce the astigmatism on the retinal planes. Since then, the focus of AO retinal imaging instruments design has been to minimize aberrations on the retinal conjugate planes, largely ignoring the aberrations on pupil conjugate planes. However, reducing aberrations on these planes however, is critical to the quality of the AO correction. Poorly corrected pupil aberrations will result at best in a reduced temporal bandwidth of the system, with the aberrations with higher spatial frequencies being more attenuated than the lower ones. In the worst case, the higher spatial frequency aberrations will not be sensed, and therefore, not corrected. In this work, we present the expressions that allow the design of optical systems based on pairs of off-axis reflective 4f telescopes using spherical mirrors, with minimal astigmatism on both image and pupil planes, along with a preliminary design as an example.

2. GENERAL MARGINAL RAY FAN EQUATION

In paraxial theory of on-axis rotationally symmetric optical elements, rays emanating from a point object converge onto an image point. The first-order image formation of such optical components can be described by the Gaussian equation, that takes the well-known form,

$$\frac{1}{s}+\frac{1}{s'}=\frac{1}{f}, \tag{1}$$

where s and s' are object and image distances from the optical element, respectively, and f is the effective focal length of the optical element. For off-axis objects, the marginal rays converge at different points along the principal ray, depending on the orientation θ of the plane defined by the principal ray and the corresponding marginal ray. To a first approximation, the distances along the principal ray between the optical element and the marginal images under the thin lens approximation are given by the general marginal ray fan equation [11], which for spherical mirrors takes the form

$$\frac{1}{s}+\frac{1}{s_\theta'}=\frac{2\cos I}{r(1-\cos^2\theta\sin^2 I)}, \tag{2}$$

with I being the angle of incidence of the principal ray onto the mirror, and r the mirror radius of curvature. For $\theta = 0^\circ$ and $\theta = \pi/2$, one recovers the more familiar Coddigton equations [11].

3. MINIMIZATION OF ASTIGMATISM IN AFOCAL TELESCOPES

To date, most reflective AO ophthalmic systems consist of a number of off-axis afocal telescopes that relay the pupil of the eye onto a set of planes commonly referred to as "pupil planes". These pupil planes are where the wavefront sensor, wavefront corrector(s) and scanning devices are typically placed. When these telescopes are formed by pairs of spherical mirrors, they are fully described by the five parameters shown in Fig. 1: the angles of incidence I_1 and I_2 of the principal ray or optical axis onto the mirrors, the mirror's radii of curvature r_1 and r_2, and the angle θ between the planes defined by the incident and reflected principal rays. In what follows, unless otherwise stated, it is assumed that the separation between mirrors along the principal ray is the sum of the on-axis mirror focal lengths, that is $d = (r_1 + r_2)/2$, as it is usually implied when referring to afocal telescopes. The dominant aberration in these telescopes is astigmatism. This astigmatism manifests as ray fans passing through different planes that contain the principal ray, focus at different points on it. Through an appropriate selection of the telescope parameters, astigmatism can be eliminated along the principal ray.

The marginal distance $s'_{2,\theta}$ of the image of a point a distance s_o from the first mirror, formed by the ray fan that after reflection from the second mirror is contained in a plane defined by the principal ray and the angle $\theta \in (-\pi/2, \pi/2]$, with respect to the plane of incidence. In the Fig, 1, the former plane is indicated in white, and the latter in gray in Fig. 1. If any two of such marginal image distances for different θ values coincide, then all the images will coincide, provided that the only aberration present is astigmatism. Thus, by nullifying the distance Δ_s between any two of these images, the relation between the telescope parameters that eliminates astigmatism for the particular object point can be found. In particular, this will be valid for the most extreme of the images formed by the first mirror, namely, the sagittal ($\theta_1 = 0$) and tangential ($\theta_1 = \pi/2$) images. The intermediate images are $s_{2,\theta} = d - s'_0$ and $s_{2,\theta+\pi/2} = d - s'_{\pi/2}$ with s'_0 and $s'_{\pi/2}$ calculated using Eq. (2). For small angles of incidence, we can express, in terms of telescope magnification $M = r_2/r_1$ and vergence $\phi = 1/s_0$, the relation between the angles of incidence for minimal astigmatism.

$$I_2 = \sqrt{-\frac{8M}{2\cos(2\theta)\left[r_1\phi(1+M)-2M\right]^2}}\,I_1 \tag{3}$$

We have two particular cases of interesting in ophthalmic instruments with adaptive optics:

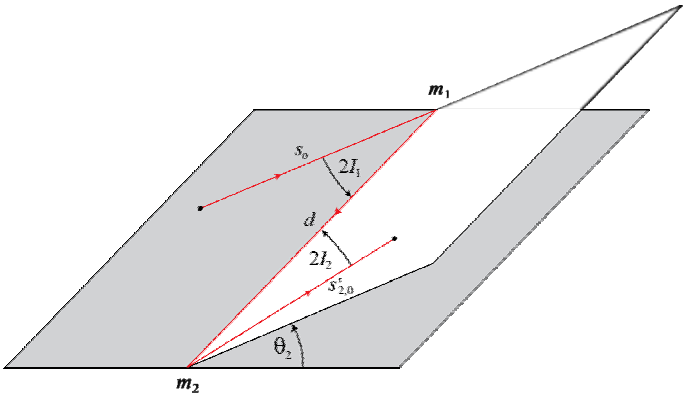

Fig. 1. Geometry of an off-axis reflective afocal telescope: I1 and I2 are the angles of incidence of the principal ray (in red) onto the corresponding mirrors (m1 and m2), and the angle θ between the incidence planes.

a) The finite conjugate ($\phi = 2/r_1$).- The pupil planes, which to a first approximation are also the aperture stop planes, are placed a focal length in front of the first telescope mirror and a focal length after the second mirror. The condition for cancelling astigmatism in pupil planes is given by

$$I_2 \approx \sqrt{-\frac{M}{\cos(2\theta)}} I_1 \tag{4}$$

b) The infinite conjugate ($\phi = 0$).- The second set of relevant optical planes is the set of planes conjugated to the retina, or image planes, with the stop aperture being on the pupil plane, which again is a focal length away from the mirror surface. The condition for minimizing astigmatism on image planes becomes

$$I_2 \approx \sqrt{-\frac{1}{M\cos(2\theta)}} I_1 \tag{5}$$

It should be noted that even though meeting this condition only cancels the astigmatism for the object point at $\phi = 2/r_1$ or $\phi = 0$ along the principal ray, the overall astigmatism for object points over a centered field of view around this point will be minimized. As it is clear from Eqs. (4,5), these conditions can only be met if $\pi/4 < |\theta| < 3\pi/4$, which is reasonable, given that the second mirror must introduce less astigmatism on the incidence plane of the first mirror than on the perpendicular one. The particular case $\theta = \pi/2$ produces the most compact optical setup and also minimizes other aberrations.

4. SIMULTANEOUS MINIMIZATION OF ASTIGMATISM IN PUPIL AND IMAGE PLANES IN PAIRS OF AFOCAL TELESCOPES

As mentioned earlier, in order to take full advantage of the AO correction, astigmatism needs to be well corrected in all pupil planes, while the image planes only need to be corrected at the ends of the optical setup, that is, at the eye and the science detector(s). By comparing Eqs. (4) and (5), it is clear that astigmatism can only be minimized simultaneously for both pupil and image planes for telescopes with unit magnification. However, when selecting the second angle of incidence in terms of the first one, as prescribed by Eq. (4), a degree of freedom in the selection of the first angle of incidence remains. Thus, by combining a pair of telescopes, each of them pupil-corrected, the first angle of each of the telescopes pair can be selected to minimize astigmatism on the exit image planes, while preserving minimal astigmatism on all the pupil planes. Let us then consider each pair of pupil-corrected telescopes for minimal astigmatism. The vergence difference between the marginal ray fan from an object at infinity after the reflections on all four mirrors can now be calculated, and the condition for minimizing the astigmatism in the small angles regime ($|I_i| << 1$) can be derived as

$$I_3 = \frac{1}{M_{12}}\sqrt{-\frac{r_3\left(1-{M_{12}}^2\right)\cos(2\theta_4)}{r_1\left\{M_{34}^2\sin\left[2\left(\theta_2+\theta_3\right)\right]\sin\left(2\theta_4\right)+\left(1-M_{34}^2\right)\cos\left[2\left(\theta_2+\theta_3\right)\right]\cos\left(2\theta_4\right)\right\}}}I_1 . \quad (6)$$

By considering the most compact configurations, i.e. $|\theta_2| = |\theta_4| = \pi/2$, and $|\theta_3| = 0, \pi/2, \pi$, other aberrations will also be reduced, and Eq. (6) becomes

$$I_3 \approx \frac{1}{M_{12}}\sqrt{\pm\frac{r_3}{r_1}\left(\frac{1-{M_{12}}^2}{1-{M_{34}}^2}\right)}I_1 . \quad (7)$$

The sign inside the radical depends on whether $\theta_3 = 0, \pi$ or $|\theta_3| = \pi/2$. This leads to two families of solutions: one in which provided $M_{12} > 1$ and $M_{34} < 1$, $|\theta_3| = \pi/2$, and one in which provided $M_{12} < 1$ and $M_{34} < 1$, $\theta_3 = 0, \pi$. An example to illustrate this point will be discussed in the next section.

5. EXAMPLE

In order to illustrate the application of the minimal astigmatism expressions, we present the design of an adaptive optics scanning laser ophthalmoscope for human subjects. The mirror radii of curvature and the angles of incidence obtained with Eqs. (4) and (7) at perpendicular configuration ($\theta = 90^\circ$) are show in Table 1. The optical angle of scanning in the eye is 2.5 degrees in both directions (x,y), and the wavelength of the Zemax simulation is 550nm. Fig. 2 shows a diagram of the system, that for the sake of clarity only display the optical axis. The spot diagrams at retina and pupil planes and the corresponding modulation transfer function (MTF) are display in Figs. 3 and 4. These figures illustrate that the system's astigmatism is corrected for and also because of the small angles of incidence and scanning the impact of the other aberrations is small as well.

The spot diagrams on the retinal plane were calculated for three different focii (-2D, 0D and 2D) and nine different points over the scanned field of view. Minimizing aberrations for the selected focusing range guarantees that the system will perform well in multi-wavelength experiments despite the chromatic aberration of the eye. The scanning field of view at the eye covers a 2.5º angle, which is comparable to the isoplanatic angle of the eye. The pupil spot diagrams show 5 different points over the aperture evaluated in all configurations of the scanning mirrors

Figure 4 shows the MTFs of the most extreme cases in the retinal and pupil planes, that is, the largest departure from the optical axis and maximum defocus. In both these cases the optical performance of the system is good. It is worth noting that the maximum spatial frequency that a deformable mirror with 10 actuators across the pupil can generate is approximately 1 cycle/mm, and the system performs close to the diffraction limit at that frequency. In Fig. 4, the retinal MTF plots, first configuration (-2D,-2.5º,-1.5º) in blue and fourteenth configuration (0D, 0, -0º) in red, and the pupil MTF plots show that our system out of the principal ray configuration has low aberrations, and as we expected it has a good shape in the others with low aberrations.

6. CONCLUSIONS

Expressions for minimal astigmatism on pupil and image planes applicable to off-axis reflective afocal telescopes were presented from the marginal ray fans equation. Three simple formulas (Eqs. 4, 5 and 7) for the small angle approximation were obtained and evaluated in an example. From varying the telescope folding angle θ, it is possible to find that the 90º configuration always results in the lowest wavefront RMS, and in the particular case presented here, below Marechal's diffraction limit. The range of validity of the condition in Eq. (4) for pupil plane astigmatism correction is larger than the equivalent condition for image plane minimization. Astigmatism minimization can be applied to the design of other off-axis optical systems, such as spectrographs or laser cavities.

Table 1. Data of the system simulated in Zemax using the expressions of Eqs. (4) and (7). All length values are expressed in mm and angles in degrees

Element	Radius	Thickness	I_x	I_y	Pupil	Magnification
Entrance Pupil	Infinity		0	0	8	
Mirror_1	1500	750	2.15	0		
Mirror_2	750	1125	0	1.52027958		
Resonant scanner	Infinity	375	0	0	4	0.5
Mirror_3	500	250	1.241303079	0		
Mirror_4	1000	750	0	1.755467649		
Galvo Mirror	Infinity	500	0	0	8	2
Mirror_5	1100	550	2	0		
Mirror_6	2000	1550	0	2.69679945		
DM	Infinity	1000	0	0	14.545	1.818181818
Mirror_7	2000	1000	2.69679945	0		
Mirror_8	1100	1550	0	2		
EYE	Infinity	550	0	0	8	0.55

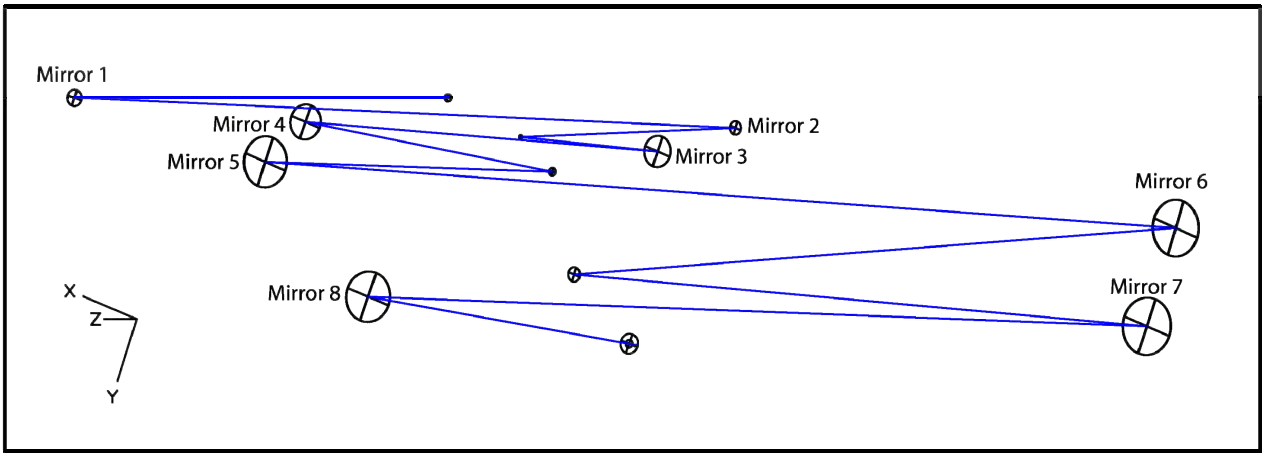

Fig. 2 Diagram of the system, with the trace in blue indicating the configuration (0D, 0, -0º) , the data are reported in Table 1.

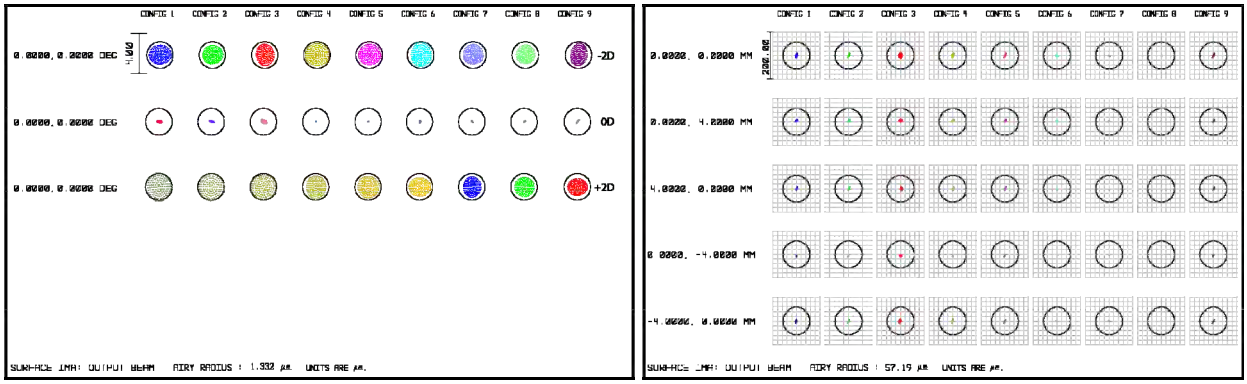

Fig. 3 Spot diagrams of the example design at the retinal (left) and the pupil (right) planes.

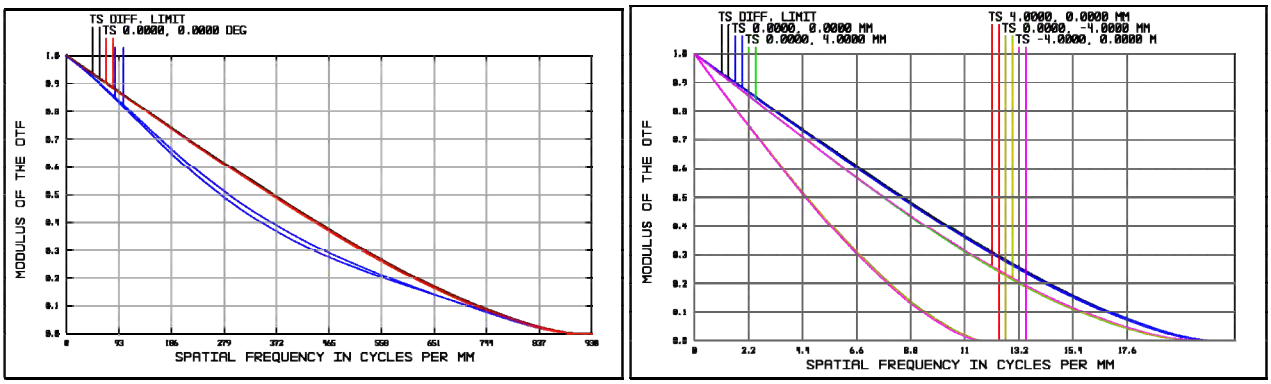

Fig. 4 The MTF plot of the example design at the retinal (left) and the pupil (right) planes.

REFERENCES

[1] J. Liang, D.R. Williams, and D.T. Miller, "Supernormal vision and high-resolution retinal imaging through adaptive optics," J. Opt. Soc. Am. A **14**, 2884-2892 (1997).

[2] Y. Zhang, B. Cense, J. Rha, R.S. Jonnal, W. Gao, R.J. Zawadzki, J.S. Werner, S. Jones, S. Olivier, and D. T. Miller, "High-speed volumetric imaging of cone photoreceptors with adaptive optics spectral-domain optical coherence tomography," Opt. Express **14**, 4380-4394 (2006),.

[3] R. J. Zawadzki, S. M. Jones, S. S. Olivier, M. T. Zhao, B. A. Bower, J. A. Izatt, S. Choi, S. Laut, and J. S. Werner, "Adaptive-optics optical coherence tomography for high-resolution and high-speed 3D retinal in vivo imaging," Opt. Express **13**, 8532-8546 (2005).

[4] D. Merino, C. Dainty, A. Bradu, and A. Gh. Podoleanu, "Adaptive optics enhanced simultaneous en-face optical coherence tomography and scanning laser ophthalmoscopy," Opt. Express **14**, 3345-3353 (2006).

[5] A. Roorda, F. Romero-Borja, W. J. Donnelly, H. Queener, T. J. Hebert, and M. C. W. Campbell, "Adaptive optics scanning laser ophthalmoscopy," Opt. Express **10**, 405-412 (2002),.

[6] D. X. Hammer, R. D. Ferguson, C. E. Bigelow, N. V. Iftimia, T. E. Ustun, and S. Burns, "Adaptive optics scanning laser ophthalmoscope for stabilized retinal imaging," Opt. Express **14**, 3354-3367 (2006).

[7] D. C. Gray, W. Merigan, J. I. Wolfing, B. P. Gee, J. Porter, A. Dubra, T. H. Twietmeyer, K. Ahmad, R. Tumbar, F. Reinholz, and D. R. Williams, "In vivo fluorescence imaging of primate retinal ganglion cells and retinal pigment epithelial cells," Opt. Express **14**, 7144-7158 (2006).

[8] S.A. Burns, R. Tumbar, A.E. Elsner, D. Ferguson, and D. X. Hammer, "Large-field-of-view, modular, stabilized, adaptive-optics-based scanning laser ophthalmoscope," J. Opt. Soc. Am. A **24**, 1313-1326 (2007).

[9] R. H. Webb and G. W. Hughes, "Scanning laser ophthalmoscope," IEEE Transactions on Biomedical Engineering **28**, 488-492 (1981).

[10] R. H. Webb, G.W. Hughes, and F.C. Delori, "Confocal scanning laser ophthalmoscope," Appl. Opt. **26**, 1492-1499 (1987).

[11] A. E. Conrady, *Applied optics and optical design*, part 2 (Dover Publications Inc., New York, 1960), Chap XII.

Acknowledgments

The authors want to acknowledge the support of the Consejo Nacional de Ciencia y Tecnología de México (CONACYT), project No. 78812 and the scholar grant No. 170266. Alfredo Dubra-Suarez, Ph.D., holds a Career Award at the Scientific Interface from the Burroughs Welcome Fund. This research was also supported by the National Institute for Health, Bethesda, Maryland (NIH EY014375, NIH EY01319), Bausch and Lomb, Research to Prevent Blindness, the National Science Foundation Science and Technology, through the Center for Adaptive Optics, managed by the University of California at Santa Cruz (cooperative agreement no.: AST-9876783).

ANEXO 5

First-order design of off-axis reflective ophthalmic adaptive optics systems using afocal telescopes

A. Dubra,[1,2*] A. Gómez-Vieyra[3], D. Malacara-Hernández,[3] and D.R. Williams[2]

[1] *University of Rochester Eye Institute, Rochester, NY, 14642.20036, USA*
[2] *Center for Visual Science, University of Rochester, Rochester, NY, 14627, USA 115, C.P. 37000, León, Guanajuato, México*
[3] *Centro de Investigaciones en Óptica A.C., Loma del Bosque*
[*] *adubra@cvs.rochester.edu*

Abstract: Expressions for minimal astigmatism in image and pupil planes in off-axis reflective afocal telescopes formed by pairs of spherical mirrors are presented and evaluated for small angles of incidence.

OCIS codes: (110.1080) Active or adaptive optics, (080.2468) First-order optics, (080.4035) Mirror system design, 220.1000 Aberration compensation, (330.4460) Ophthalmic optics and devices.

1. Introduction

The introduction of adaptive optics (AO) to ophthalmic imaging in recent years has lead to the development of a new generation of high-resolution retinal imaging instruments, such as, the AO fundus camera [1,2], the AO optical coherence tomograph (AO-OCT) [3,4] and the AO scanning laser ophthalmoscope (AOSLO) [4-8]. In order to maximize the resolution of the AO scanning instruments, the full entrance and exit pupils should be used. Hence, a system with refractive elements is not desirable, given that the back reflections from the optical surfaces can be orders of magnitude brighter than the light collected from the retina. Low-resolution clinical instruments do not suffer of such problem because they use different portions of the pupil for illumination and light collection. Currently, most AO-equipped scanning ophthalmic instruments are at least partially built using off-axis spherical mirrors, given their low-cost and ease of alignment [2-8]. The major optical performance limitation of such systems is the astigmatism introduced by the off-axis arrangement, as it has been reported by Webb *et al*. [9,10] when reporting the first confocal laser scanning ophthalmoscope, and later by Burns *et al.* [8]. In his work, Webb suggested an off-the-plane perpendicular folding of the optical setup to reduce the astigmatism in the retinal planes. Since then, the focus of AO retinal imaging instruments design has been minimizing aberrations at the retinal conjugate planes, largely ignoring the aberrations in pupil conjugate planes. Reducing aberrations in these planes however, is critical to the quality of the AO correction. Poorly corrected pupil aberrations will result at best in a reduced temporal bandwidth of the system, with the aberrations with higher spatial frequencies being more attenuated than the lower ones. In the worst case, the higher spatial frequency aberrations will not be sensed, and therefore, not corrected. In this work, we present the expressions for simultaneously minimizing astigmatism, in pupil and image planes.

2. Theory

In paraxial theory of on-axis rotationally symmetric optical elements, rays emanating from a point object converge onto an image point. For off-axis objects however, the marginal rays converge at different points along the principal ray, depending on the orientation θ of the plane defined by the principal ray and the corresponding marginal fan. To first approximation, the distances along the principal ray between the optical element and the marginal images under the thin lens approximation are given by the general marginal fan of rays' equation [11], that for spherical mirrors takes the form

$$\frac{1}{s}+\frac{1}{s_\theta'}=\frac{2\cos I}{r(1-\cos^2\theta\sin^2 I)}, \qquad (1)$$

where s and s_θ' are object and image distances from the optical element, respectively, I is the principal ray the angle of incidence onto the mirror, and r the mirror radius of curvature.

To date, most reflective adaptive optics ophthalmic systems consist of a number of off-axis afocal telescopes that relay the pupil of the eye onto a set of planes commonly referred to as "pupil planes". These pupil planes are where the wavefront sensor, wavefront corrector(s) and scanning devices are typically placed. When these telescopes are formed by pairs of spherical mirrors, they are fully described by five parameters: the angles of incidence I_1 and I_2 of the principal ray or optical axis onto the mirrors; the mirror radii of curvature r_1 and r_2, and the angle θ between the planes defined by the incident and reflected principal rays. The dominant aberrations in these telescopes is

astigmatism, and it manifests as ray fans passing through different planes containing the principal ray focusing at different points on it. By an appropriate selection of the telescope parameters, the astigmatism can be eliminated along the principal ray. When using the marginal ray fans equation, one gets that for pupil planes (i.e. $s_o = r_1/2$), and for small angles, the minimal astigmatism configuration is achieved when

$$I_2 \approx \sqrt{-\frac{M}{\cos(2\theta)}} I_1 . \tag{3}$$

Even though meeting this condition only cancels the astigmatism for a single point along the principal ray, the overall astigmatism for points over a centered field of view around this point will be minimized. It should be noted that this conditions can only be met if $\pi/4 < |\theta| < 3\pi/4$. In particular, the case $\theta = \pi/2$ produces the most compact optical setup and the one with lowest wavefront RMS. By combining a pair of telescopes, each of them pupil-corrected, the first angle of each of the telescopes pair can be selected to minimize astigmatism in the exit image plane, while preserving the pupil plane astigmatism correction. The resulting condition, valid for small angles, and for the particular case where each telescope is folded such that $|\theta_2| = |\theta_4| = \pi/2$, and $|\theta_3| = 0, \pi/2, \pi$ is

$$I_3 \approx \frac{1}{M_{12}} \sqrt{\pm \frac{r_3}{r_1} \frac{\left(1 - M_{12}^{\ 2}\right)}{\left(1 - M_{34}^{\ 2}\right)}} I_1 . \tag{4}$$

The sign inside the radical depends on whether $\theta_3 = 0, \pi$ or $|\theta_3| = \pi/2$, leading to two family of solutions; one in which if $M_{12} > 1$ and $M_{34} < 1$ with $|\theta_3| = \pi/2$, and one in which if $M_{12} < 1$ and $M_{34} < 1$ with $\theta = 0, \pi$. Even though astigmatism minimization can be achieved for large angles of incidence, it can be shown, that small angles lead to optical systems robust to focus shifts and Badal optometer-like shifts. A sketch of all the possible folding solution is shown in table 1.

3. Example

In this section we evaluate the performance of a telescope pair with pupil planes and exit image plane astigmatism correction. The angles predicted by the linear approximation solution to the marginal ray fans are compared against the optimal values determined by minimizing the wavefront RMS. The wavefront RMS was calculated after correcting for defocus, using the ray tracing software from Zemax Development Corporation, Bellevue, Washington, USA. The optical setup evaluated consists of a pair of reflective off-axis afocal telescopes in series, with the following spherical mirror radii of curvature in order: 1000, 500, 333 and 1000mm. Each of the two telescopes is pupil-corrected, using Eqs. (3). The retinal astigmatism is corrected either by using the linear approximation in Eq. (4), or by optimization, with the absolute values of θ_2, θ_3 and θ_4 being 90º. The telescope magnifications dictate that only one of the two family solutions can be used to compensate for the image plane astigmatism. Each of the folding solutions corresponds to a different combination of θ_3 and θ_4 signs. The geometry of the four configurations with minimal astigmatism are sketched on the left side of in table 1.

Table 1. wavefront RMS of the 8 most compact configurations of two different pairs of off-axis telescopes with minimal aberrations, for I_1 = 5º. The numbers on the top row are the mirror radii of curvature in mm. The entrance beam diameter considered was 8mm and λ = 500nm.

	cos (2θ_3) = -1 1000 : 500 : 333 : 1000				cos (2θ_3) = 1 500 : 1000 : 333 : 1000			
θ_3, θ_4	π/2, π/2	-π/2, π/2	π/2, -π/2	-π/2, -π/2	π, -π/2	0, -π/2	π, π/2	0, π/2
RMS (λ)	0.0064	0.0078	0.0089	0.0099	0.1502	0.1531	0.1638	0.1693

Note that astigmatism is minimized in all four configurations, but the impact of other aberrations (mostly coma) is different on each of them as shown on table 1. Therefore, depending on the mechanical dimensions of the components of the optical setup, the designer, can select the sign of the folding angles that produce the lowest wavefront RMS. The plots in Fig. 6 show all four optimal configurations, but only one of the linear approximation, in order to keep the plots readable. The left plot in the figure shows the angles calculated using Eq. (4), and the angles optimal angles, for each of the four configurations sketched on the left of table 1. The center plot shows the vergence of the beam reflected off the fourth mirror for all configurations, which becomes more negative with

increasing angles of incidence. The rightmost plot shows the corresponding wavefront RMS values for all the configurations, and the planar case for comparison. The RMS for all non-planar configurations is significantly lower than for the planar design. The optical performance of the linear approximation is close to optimal in the 1º to 5º range. For angles smaller than 1º, the predicted angles are not optimal, due to spherical aberrations, while for angles greater than 1º, the dominant aberration after astigmatism correction is coma.

Fig. 1. Data from pair of off-axis reflective afocal telescopes, with astigmatism simultaneously corrected in pupil and image planes.

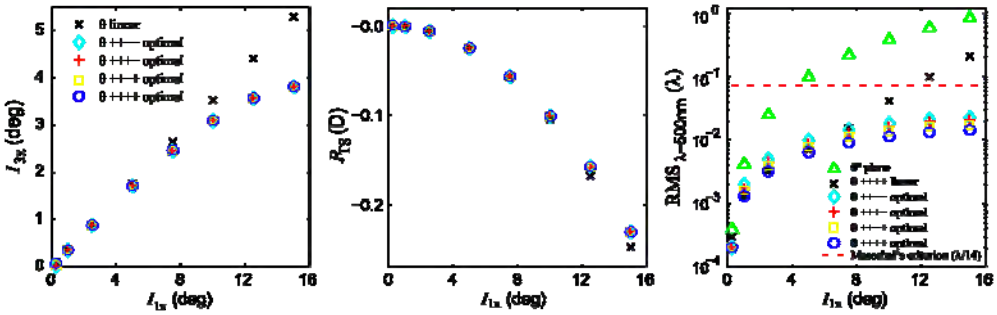

4. Conclusions

Expressions for minimal astigmatism in pupil and image planes applicable to off-axis reflective afocal telescopes were derived from the marginal ray fans equation. Simple formulas for the small angle approximation were obtained and evaluated. Even though astigmatism minimization can be achieved for large angles of incidence, it has been shown, that small angles lead to optical systems robust to focus shifts and Badal optometer-like shifts. Even though these conditions were studied with adaptive optics ophthalmoscopy in mind, the astigmatism minimization conditions can be applied to the design of other off-axis optical systems, such as spectrographs or laser cavities.

The example discussed in this work, illustrate that the configurations based on the small angle approximations that lead to the conditions in Eqs. (1) and (2), perform as well as the configuration optimized based on RMS minimization. From varying the telescope folding angles θ_i, it was found that the 90º configuration always results in the lowest wavefront RMS.

Acknowledgements

The authors acknowledge the support of the Consejo Nacional de Ciencia y Tecnología de México (CONACYT), project No. 78812 and the scholar grant No. 170266. Alfredo Dubra-Suarez, Ph.D., holds a Career Award at the Scientific Interface from the Burroughs Welcome Fund. This research was also supported by NIH (EY014375, EY01319), Bausch and Lomb, Research to Prevent Blindness and NSF through the CfAO (AST-9876783).

References

1. J. Liang, D.R. Williams, and D.T. Miller, "Supernormal vision and high-resolution retinal imaging through adaptive optics," J. Opt. Soc. Am. A **14**, 2884-2892 (1997).
2. Y. Zhang, B. Cense, J. Rha, R.S. Jonnal, W. Gao, R.J. Zawadzki, J.S. Werner, S. Jones, S. Olivier, and D. T. Miller, "High-speed volumetric imaging of cone photoreceptors with adaptive optics spectral-domain optical coherence tomography," Opt. Express **14**, 4380-4394 (2006),.
3. R. J. Zawadzki, S. M. Jones, S. S. Olivier, M. T. Zhao, B. A. Bower, J. A. Izatt, S. Choi, S. Laut, and J. S. Werner, "Adaptive-optics optical coherence tomography for high-resolution and high-speed 3D retinal in vivo imaging," Opt. Express **13**, 8532-8546 (2005).
4. D. Merino, C. Dainty, A. Bradu, and A. Gh. Podoleanu, "Adaptive optics enhanced simultaneous en-face optical coherence tomography and scanning laser ophthalmoscopy," Opt. Express **14**, 3345-3353 (2006).
5. A. Roorda, F. Romero-Borja, W. J. Donnelly, H. Queener, T. J. Hebert, and M. C. W. Campbell, "Adaptive optics scanning laser ophthalmoscopy," Opt. Express **10**, 405-412 (2002),.
6. D. X. Hammer, R. D. Ferguson, C. E. Bigelow, N. V. Iftimia, T. E. Ustun, and S. Burns, "Adaptive optics scanning laser ophthalmoscope for stabilized retinal imaging," Opt. Express **14**, 3354-3367 (2006).
7. D. C. Gray, W. Merigan, J. I. Wolfing, B. P. Gee, J. Porter, A. Dubra, T. H. Twietmeyer, K. Ahmad, R. Tumbar, F. Reinholz, and D. R. Williams, "In vivo fluorescence imaging of primate retinal ganglion cells and retinal pigment epithelial cells," Opt. Express **14**, 7144-7158 (2006).
8. S.A. Burns, R. Tumbar, A.E. Elsner, D. Ferguson, and D. X. Hammer, "Large-field-of-view, modular, stabilized, adaptive-optics-based scanning laser ophthalmoscope," J. Opt. Soc. Am. A **24**, 1313-1326 (2007).
9. R. H. Webb and G. W. Hughes, "Scanning laser ophthalmoscope," IEEE Transactions on Biomedical Engineering **28**, 488-492 (1981).
10. R. H. Webb, G.W. Hughes, and F.C. Delori, "Confocal scanning laser ophthalmoscope," Appl. Opt. **26**, 1492-1499 (1987).
11. A. E. Conrady, *Applied optics and optical design*, part 2 (Dover Publications Inc., New York, 1960), Chap XII.

ANEXO 6

Primary wavefront aberrations calculation from a defocused image or a Hartmanngram

Daniel Malacara-Doblado,* Zacarias Malacara-Hernández, and Armando Gómez-Vieyra

Centro de Investigaciones en Optica, A. C., Loma del Bosque 115, León Gto. México 37150

*Corresponding author: dmalacdo@cio.mx

Received 15 January 2010; revised 11 March 2010; accepted 18 March 2010; posted 19 March 2010 (Doc. ID 122684); published 13 April 2010

A wavefront aberration can be retrieved from a defocused image or a Hartmanngram by several different methods using diffraction theory and Fourier transforms. In this manuscript, we describe an alternate method for wavefront aberration determination from a defocused image or a Hartmanngram using a geometric l approximation. The main assumption is that the image is defocused, with the observation plane outside the caustic limits. The result will be applied to the retrieval of a wavefront with primary aberrations from a Hartmanngram or defocused image without the need for any transversal aberration integration.

OCIS codes: 080.1010, 220.4840.

1. Introduction

In principle, wavefront aberration determination from a defocused image can be performed by a Fourier transform, provided that both the irradiance and the phase at the image are known at all points on the image. Through the use special techniques, the wavefront aberration has been obtained from the image, mathematically known as the point spread function, even when the phase is not known, as has been described by many researchers. Gonsalves [1] was apparently the first to solve a one-dimensional problem, by using two methods, the space frequency iterative technique of Gerchberg and Saxton [2] and a parametric search technique. Artal *et al.* [3] applied a bi-dimensional Gerchberg–Saxton phase retrieval algorithm to measure the wave aberration of human eyes from the point spread function. Nakajima [4] and later some other researchers, for example Brady and Fienup [5], proposed retrieving the wavefront from two or more intensity measurements. Roddier *et al.* [6] used a single defocused image with iterative Fourier transforms. In these methods, the local curvatures in the wavefront are sensed and the irradiance transport equation is used to retrieve the wavefront shape. Barakat and Sandler [7] used a similar technique to analyze the Hubble telescope.

If the image is outside the caustic [8], either inside or outside of focus, the problem becomes simpler. A geometric optics calculation can be performed to obtain the wavefront primary aberrations. A typical procedure in this is to sample the entrance pupil wavefront to produce a defocused image similar to the spot diagram used in lens design. This test is the well-known Hartmann test [9] with an antecedent in the Tscherning test [10] used to measure refractive defects in the human eye. To obtain the wavefront aberrations, the standard method is to integrate the transverse aberrations, as described in many publications [11]. This method requires a complete identification of each image spot to determinate from which point of the entrance pupil it comes in order to perform the integration. When the spherical aberration is relative large as in the case of aspherical wavefronts, the association to the entrance pupil

0003-6935/10/122302-07$15.00/0

coordinate is simple for a visual human examination but difficult to implement in the automatic procedure.

In this paper, we describe a geometrical method that retrieved the primary aberrations without the need for this spot association. It can be carried out even if the wavefront is not sampled with holes in the entrance pupil, a simple defocused image can be measured. In conclusion the results will be obtained from the analysis of defocused images or Hartmanngrams with primary aberrations.

2. Mathematical Procedure

The standard Hartmann test is typically performed as in Fig. 1, with a Hartmann screen with an array of holes at the entrance pupil of the system under test. As illustrated in Fig. 2, a plane wavefront illuminates an optical system with a refracted aberrated, but nearly spherical, wavefront, convergent to the point C. It is convenient to normalize the entrance pupil semidiameter to unity, as is frequently done. If the wavefront is perfectly spherical, the radius of curvature at the exit pupil is r, and L is the defocused distance, as measured from the paraxial center of curvature of the wavefront to the observation plane, we may see that

$$\rho' = \frac{L}{r}\rho, \tag{1}$$

where ρ is the ray radial distance from the optical axis at the entrance pupil, and ρ' is the ray radial distance from the optical axis at the observation plane. Now, let us assume that the refracted wavefront is not spherical, but has some primary aberrations. The light rays will have a radial transverse aberration $\mathrm{TA}_\rho(\rho,\theta)$ and $\mathrm{TA}_\theta(\rho,\theta)$ in the radial and tangential directions, respectively, given by

$$\mathrm{TA}_\rho = -r\frac{\partial W(\rho,\theta)}{\partial \rho}, \tag{2}$$

$$\mathrm{TA}_\theta = -\frac{r}{\rho}\frac{\partial W(\rho,\theta)}{\partial \theta}, \tag{3}$$

where $W(\rho,\theta)$ is the wavefront deformation with respect to the ideal spherical wavefront.

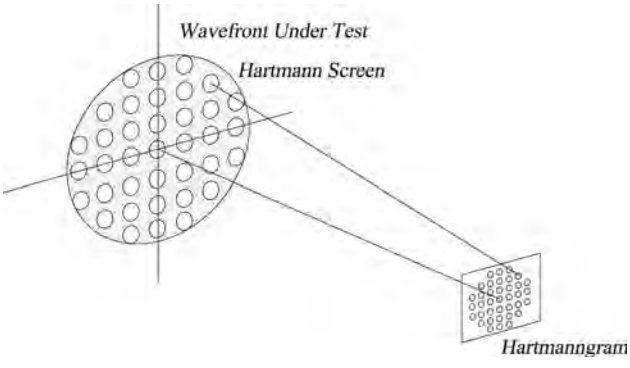

Fig. 1. Hartmann test of a convergent wavefront.

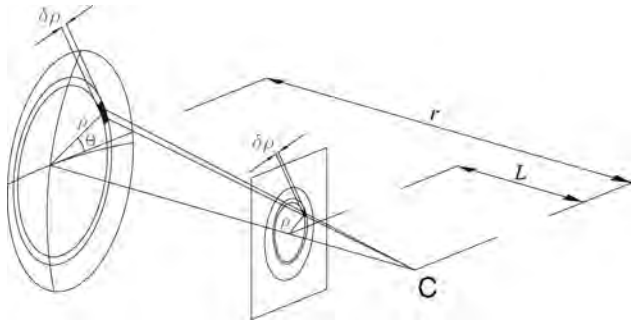

Fig. 2. Hartmann screen and Hartmann plate in the classical test.

Considering only primary aberrations, the wavefront aberration $W(\rho,\theta)$ can be written as

$$W = A\rho^2 + B\rho^2\cos[2(\theta-\varphi_a)] + C\rho^3\sin(\theta-\varphi_c) + D\rho^4, \tag{4}$$

where A, B, C, and D are the aberration coefficients for defocusing, astigmatism, coma, and spherical aberration, respectively. The angles φ_a and φ_c are the angle orientations with respect to the x axis for the astigmatism and the coma aberrations. The angle θ is also measured with respect to the x axis. The defocusing coefficient A is related to the actual shift L of the observation plane from the focus by

$$A = -\frac{L}{2r^2}. \tag{5}$$

Now, substituting the value of the derivative of $W(\rho,\theta)$ with respect to ρ in Eq. (5), we obtain

$$\mathrm{TA}_\rho = \frac{L}{r}\rho - 2Br\rho\cos[2(\theta-\varphi_a)] - 3Cr\rho^2\sin(\theta-\varphi_c) - 4Dr\rho^3. \tag{6}$$

Let us now consider a centered thin ring at the incident wavefront on the entrance pupil plane with semidiameter ρ and thickness $\delta\rho$, which is projected to a small region at the observation plane, with the shape of a distorted ring, with radius ρ' and thickness $\delta\rho'$ in the direction θ. Let us assume that the defocusing is large enough that the transverse aberration in the tangential direction is small compared with the transverse aberration in the radial direction. Then a small ring sector in the direction θ has corresponding radius ρ' equal to

$$\rho' = \frac{L}{r}\rho - 2Br\rho\cos[2(\theta-\varphi_a)] - 3Cr\rho^2\sin(\theta-\varphi_c) - 4Dr\rho^3. \tag{7}$$

We will see later that what we need is an expression for ρ as a function of ρ' and θ. So, we need to solve a cubic expression, which, in principle, has three solutions. However, in our geometry, the defocusing

is made large so that the function $\rho(\rho',\theta)$ is nearly a linear function with small high-order deviations due to the presence of the relatively small primary aberrations. In other words, we assume that the image has a large defocusing with some astigmatism and some spherical aberration and even a smaller coma. So, we may assume that there is only one ray at the pupil at the point (ρ,θ), for each ray intersection (ρ',θ'), at the image plane. Hence, a centered circular thin ring on the pupil corresponds to a distorted, not necessarily circular, thin ring at the observation plane. We need to consider a centered circular thin ring at the observation plane and then to determine the corresponding distorted thin ring on the pupil. This function $\rho'(\rho,\theta)$ has to be inverted to obtain the function $\rho(\rho',\theta)$. This is a third-degree equation that is not simple to solve using standard procedures. However, taking advantage of the fact that a large defocus makes the solution for ρ single valued, this function $\rho'(\rho,\theta)$ can be inverted with the following iterative procedure. First, let us write the value ρ from the first term in the right-hand expression in Eq. (7) as follows:

$$\rho = \frac{r}{L}\{\rho' + 2Br\cos[2(\theta-\varphi_a)]\rho + 3Cr\sin(\theta-\varphi_c)\rho^2 + 4Dr\rho^3\}. \tag{8}$$

Now we can use an iterative procedure, substituting the whole value of Eq. (8) into the values of ρ in the same expression. Neglecting terms above the third power and also terms that contain the product of any two aberration coefficients, we obtain

$$\rho = \frac{r\rho'}{L}\left\{1 + \frac{2Br^2\cos[2(\theta-\varphi_a)]}{L} + \frac{3Cr^3\sin(\theta-\varphi_c)}{L^2}\rho' + \frac{4Dr^4}{L^3}\rho'^2\right\}, \tag{9}$$

and, differentiating the last equation,

$$\delta\rho = \frac{r}{L}\left\{1 + \frac{2Br^2\cos[2(\theta-\varphi_a)]}{L} + \frac{6Cr^3\sin(\theta-\varphi_c)}{L^2}\rho' + \frac{12Dr^4}{L^3}\rho'^2\right\}\delta\rho'. \tag{10}$$

3. Energy Density on the Image

Let us assume that the energy density (irradiance) in the pupil of the optical system producing the wavefront $W(\rho,\theta)$ is a constant E for all points in the pupil. Thus, the energy $\delta\phi$ in the ring with radius ρ and thickness $\delta\rho$ at the entrance pupil is given by

$$\delta\phi = E\rho\delta\rho\delta\theta. \tag{11}$$

There is a corresponding ring at the image plane with radius ρ' and thickness $\delta\rho'$ where all of this energy arrives. Thus,

$$\delta\phi = E'\rho'\delta\rho'\delta\theta. \tag{12}$$

Hence, we can write

$$\frac{E'}{E} = \frac{\rho\delta\rho}{\rho'\delta\rho'}. \tag{13}$$

The energy density E is a constant, but E' is not, because it is a function of ρ'. Hence, substituting Eqs. (9) and (10) into Eq. (13) yields

$$\frac{E'}{E} = \frac{r^2}{L^2}\left\{1 + \frac{2Br^2\cos[2(\theta-\varphi_a)]}{L} + \frac{3Br^3\sin(\theta-\varphi_c)}{L^2}\rho' + \frac{4Dr^4}{L^3}\rho'^2\right\} \times \left\{1 + \frac{2Br^2\cos[2(\theta-\varphi_a)]}{L} + \frac{6Br^3\sin(\theta-\varphi_c)}{L^2}\rho' + \frac{12Dr^4}{L^3}\rho'^2\right\}. \tag{14}$$

In a first-order approximation, we neglect terms that contain the product of any two aberrations, because the aberrations are assumed to be small, including the defocus term, and also neglect terms with a power of ρ' higher than ρ'^2. This expression can be written as

$$\frac{E'}{E} = \frac{r^2}{L^2} + \frac{4Br^4\cos[2(\theta-\varphi_a)]}{L^3} + \frac{9Br^5\sin(\theta-\varphi_c)}{L^4}\rho' + \frac{16Dr^6}{L^5}\rho'^2. \tag{15}$$

This is the energy density in the image, in the presence of defocusing, represented by the first term, which is a constant, plus astigmatism, coma, and spherical aberration.

4. Energy Centroid for a Circle Sector on the Image

If we divide the circular pupil in circle sectors with almost a triangular shape, the energy centroid on each of these sectors can be calculated as follows. Let us assume that the energy $d\phi$ falling over an extremely small area at the point ρ', θ is

$$\delta\phi = E'dA = E'\rho'\delta\rho'\delta\theta, \tag{16}$$

where θ is illustrated in Fig. 2. Hence, the centroid is located at a radial distance given by

$$\bar{\rho}' = \frac{\int_{\theta-\Delta\theta/2}^{\theta+\Delta\theta/2}\int_0^{\rho'_{\max}} E'\rho'^2 \mathrm{d}\rho'\mathrm{d}\theta}{\int_{\theta-\Delta\theta/2}^{\theta+\Delta\theta/2}\int_0^{\rho'_{\max}} E'\rho'\mathrm{d}\rho'\mathrm{d}\theta}, \tag{17}$$

where $\rho'_{\max}$ from Eq. (7) is given by

$$\rho'_{\max} = \frac{L}{r}\rho_{\max} - 2Br\rho_{\max}\cos[2(\theta-\varphi_a)] - 3Cr\rho_{\max}^2\sin(\theta-\varphi_c) - 4Dr\rho_{\max}^3. \tag{18}$$

Given an image, this value for $\rho'_{\max}$ is not a constant, but is a function of θ in the presence of astigmatism

and/or coma, and $\rho_{\max}$, is the semidiameter of the pupil.

After some algebraic manipulation, it is possible to show that these centroids for the circle sectors are located at a radial distance:

$$\bar{\rho}' = \frac{\left\{\frac{2}{3} + \frac{8Br^2\cos[2(\theta-\varphi_a)]}{3L}\frac{\sin(\Delta\theta)}{\Delta\theta} + \frac{9Cr^3\sin(\theta-\varphi_c)}{2L^2}\frac{\sin(\frac{\Delta\theta}{2})}{\Delta\theta/2}\rho'_{\max} + \frac{32Dr^4}{5L^3}\rho'^2_{\max}\right\}\rho'_{\max}}{1 + \frac{4Br^2\cos[2(\theta-\varphi_a)]}{L}\frac{\sin(\Delta\theta)}{\Delta\theta} + \frac{6Cr^3\sin(\theta-\varphi_c)}{L^2}\frac{\sin(\frac{\Delta\theta}{2})}{\Delta\theta/2}\rho'_{\max} + \frac{8Dr^4}{L^3}\rho'^2_{\max}}. \tag{19}$$

However, because all aberrations are small as compared with the defocusing, and assuming that $\Delta\theta$ is not very large, we may write

$$\bar{\rho}' = \left[\frac{2}{3} + \frac{Cr^3\sin(\theta-\varphi_c)}{2L^2}\rho'_{\max} + \frac{16Dr^4}{5L^3}\rho'^2_{\max}\right]\rho'_{\max}. \tag{20}$$

It is interesting to note that the astigmatism coefficient B is not present in this expression. However, this is to be expected, because the centroid location along the radial direction θ is written here as a function of $\rho'_{\max}$ in the image plane, and this is not a constant, but it describes an ellipse if the astigmatism is present. It is better to write this expression in terms of $\rho_{\max}$, which is the semidiameter of the circular pupil and, hence, it is a constant. Thus, substituting the value of $\rho'_{\max}$ from Eq. (18) and keeping terms only up to order 3, and eliminating terms with the product of two aberrations, we find

$$\bar{\rho}' = \left\{\frac{2L}{3r} - \frac{4}{3}Br\cos[2(\theta-\varphi_a)] - \frac{3}{2}Cr\sin(\theta-\varphi_c)\rho_{\max} - \frac{8}{5}Dr\rho^2_{\max}\right\}\rho_{\max}. \tag{21}$$

5. Retrieval of the Primary Aberration Coefficients from a Defocused Image or from a Hartmanngram

Since $\rho_{\max}$ is a constant equal to the semidiameter of the pupil, we can take this value as the length unit (normalized pupil). Thus, for our purposes, we can write Eq. (21) as

$$\bar{\rho}' = \frac{2L}{3r} - \frac{4}{3}Br\cos[2(\theta-\varphi_a)] - \frac{3}{2}Cr\sin(\theta-\varphi_c) - \frac{8}{5}Dr, \tag{22}$$

where all terms inside of the brackets are constants for a given optical system. The preceding expression can be used to retrieve the primary aberration coefficients from an image of a point object with a large defocusing or from a Hartmanngram, also with a large defocusing.

If the pupil is divided in circle sectors, all with the same angle, the centroids for all these sectors will be distributed on the observation plane around the optical axis. For pure defocusing, pure spherical aberration, or a combination of both, the centroids will be in a centered circle whose radius is a function of the defocusing magnitude and/or the spherical aberration value. For astigmatism, the centroids will be on an ellipse whose orientation and eccentricity depend on the astigmatism magnitude and orientation, respectively. This ellipse has a radius whose magnitude as a function of the angle θ is proportional to $\cos[2(\theta-\varphi_a)]$, where φ_a is the ellipse (astigmatism) orientation. In the presence of defocusing, spherical aberration, and astigmatism, the centroid for the whole image is at the optical axis. In other words, the centroid for the whole image is the centroid of all these centroids for all the circle sectors. However, in the case of coma, the points will be distributed in a figure resembling a decentered distorted circle. It is interesting to note that, if the defocusing term is included, this figure beomes a cardioid. The radius of this figure as a function of the angle θ can be approximately represented by $\sin(\theta-\varphi_c)$, where φ_c is the decentering direction, which can be identified as the coma orientation.

6. Practical Implementation of the Technique

In the case of a defocused image or a Hartmanngram, taken as in Fig. 2, the approximate location of the principal ray on the image has to be determined. If the image has any combination of defocusing, spherical aberration, and astigmatism, without any coma, this point is the centroid of the image. If the image has some coma, the principal ray is not at the centroid. In this case, because the defocusing is assumed to be large as compared with the magnitude of the coma, we can assume that all light rays from the upper half of the pupil arrive at the image plane with a height larger than that of the principal ray. On the other hand, all light rays from the lower part of the pupil arrive at the image plane with a height shorter than that of the principal ray. So, given a defocused image, the location of the principal ray would be approximately given as that for which half of the light rays (or the luminous energy) are above it and half below it. Also, half of the light rays (luminous

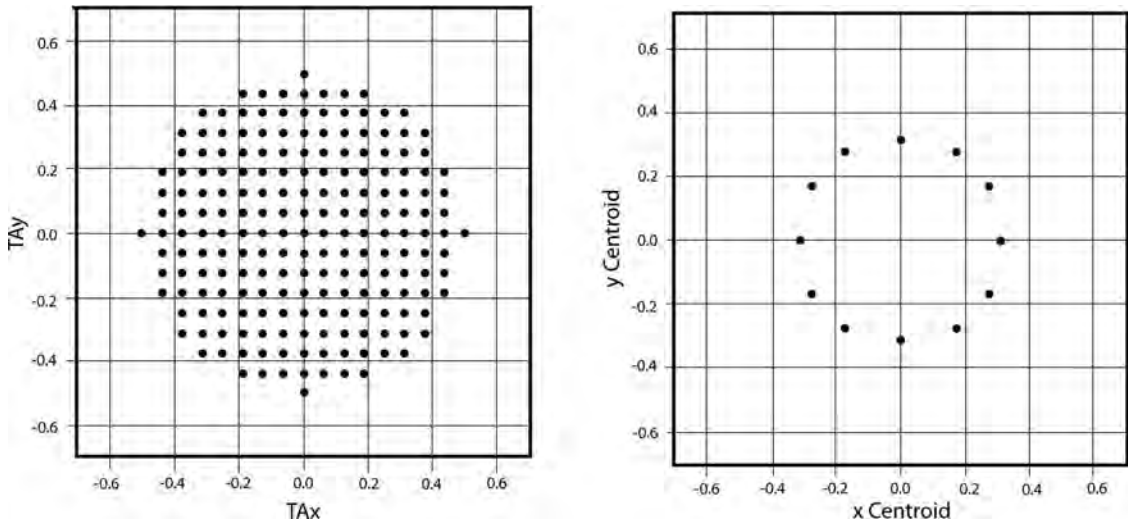

Fig. 3. (left) Computer-generated Hartmanngram with a defocusing $L = 5$. (right) Centroids for the circular sectors. The radial distance for these circular sectors, forming a circle, evaluated from the Hartmanngram, is $\bar{\rho}' = 0.321$. The same distance, calculated from Eq. (20), is equal to 0.33. The unit of length is the semidiameter of the pupil.

energy) are at its left and the other half are at its right.

If the irradiance is measured at many points over the image by means of a CCD detector camera, Eq. (15) can be directly used to estimate the values of the primary aberrations. A two-dimensional polynomial fitting to the irradiance values can be made to obtain the aberration coefficients.

An alternative method can be used once this center (which is the image centroid only if no coma is present) has been located. The image plane is divided in circle sectors with a constant angle. Then, the number of spots in the case of a Hartmanngram or the luminous energy in the case of a defocused image is measured. The second step is to compute the centroids for all the circle sectors, and their locations are plotted.

The next step is to make a least-squares fit of the coordinates (ρ, θ) to a periodic function with a constant, plus the fundamental and the second harmonic. We could make a Fourier fitting by using a discrete Fourier transform. If the points are equally spaced and uniformly distributed, this is possible; otherwise, a least-squares fitting is more appropriate.

7. Numerical Results with Some Computed Generated Hartmanngrams

To estimate the accuracy of Eq. (22), four computer-generated Hartmanngrams were produced with some known values of the primary aberrations, as illustrated in Table 1. It is important to remember that two main considerations were made in the derivation of this expression, i.e., that the number of spots in the Hartmanngram is large and, second, that the defocusing is relatively large compared with the aberrations.

In the four Hartmanngrams in Figs. 3–6, the pupil is normalized, with a semidiameter equal to 1.0. Thus, in all other dimensions, the unit of length is this semidiameter of the pupil. The radius of curvature of the wavefront equal to $r = 10.0$. The defocus displacement is inside of focus, with a value of $L = 5.0$. The circular sectors subtend an angle of 30.0°. The results in Table 1 were obtained.

These results are accurate enough for our applications, as we will describe in Section 8.

8. Possible Applications of this Method and Conclusions

We have two possible applications of this method. One of them is to evaluate the primary aberrations of a defocused image of an optical system, as in, for example, a telescope. This method will allow a quantitative evaluation of the well-known star test (Suiter, [8]).

Another possible application is the automatic evaluation of Hartmanngrams in the presence of primary aberrations. When these aberrations are present in a Hartmanngram, we have two problems. One is that the spots cannot be easily identified in an automatic manner to associate them to the corresponding hole on the Hartmann screen. The typical solution in this case is a human visual identification, making the process slow. The second problem is that the numerical integration of the Hartmann data used to obtain the wavefront deformations might lose

Table 1. Numerical Results for Hartmanngrams in Figs. 3–6 with a Defocusing $L = 5$

Aberration	Value Obtained for $\bar{\rho}'$	
	From Hartmanngram	From Eq. (22)
None	0.321	0.333
Astigmatism $B = -4$	$0.322 - 0.051\cos 2\theta$	$0.333 - 0.053\cos 2\theta$
Coma $C = +4$	$0.326 - 0.055\sin\theta$	$0.333 - 0.060\sin\theta$
Spherical aberration $D = -4$	0.380	0.407

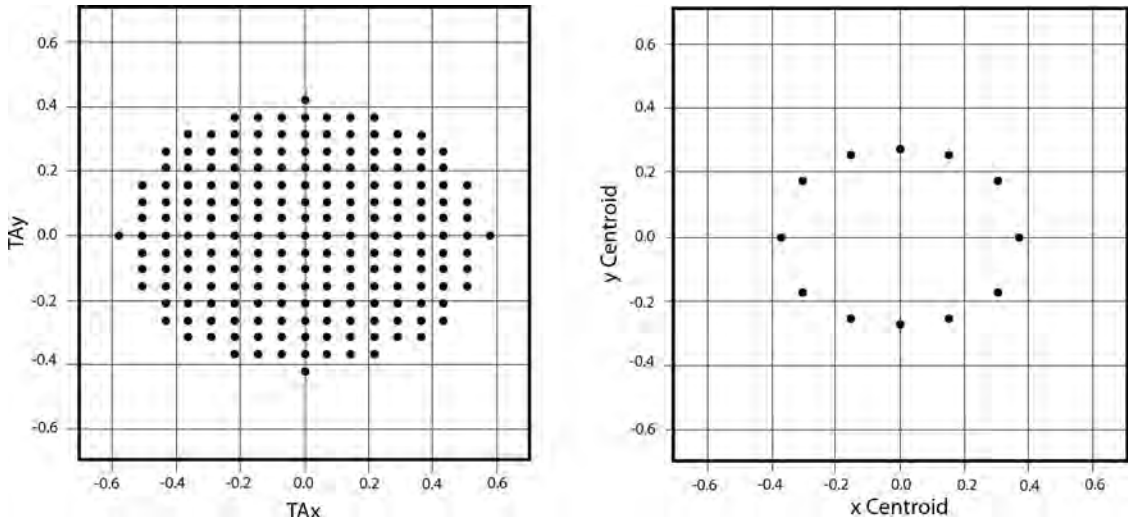

Fig. 4. (left) Computer-generated Hartmanngram with an astigmatism coefficient $B = 4$ and defocusing $L = 5$. (right) Centroids for the circular sectors. These centroids are on an ellipse and, evaluated from the Hartmanngram, $\bar{\rho}' = 0.322 - 0.051 \cos 2\theta$. The same distance, as calculated from Eq. (20), is equal to $\bar{\rho}' = 0.333 - 0.053 \cos 2\theta$. The unit of length is the semidiameter of the pupil.

accuracy, because integration is exact only for a spherical deformation and not when spherical aberration is present.

Both problems can be solved with the method described here.

a. The values of the primary aberrations, mainly spherical aberrations, are calculated from the Hartmanngram to be evaluated, as described here.

b. A synthetic computer-generated Hartmanngram is produced for the primary aberrations just obtained. The corresponding Hartmann screen holes for all of the computed spots are thus known.

c. The image of the Hartmanngram to be evaluated is superimposed over the synthetic generated Hartmanngram. Each of the spots in the first image can be associated with the closest spot in the second image and, hence, the corresponding holes on the Hartmann screen are fully identified.

d. The next step is to compute the transverse aberrations by the usual trapezoidal integration, taking as a reference the spots in the synthetic image.

e. The wavefront thus calculated after trapezoidal integration is added to the wavefront primary aberration calculated in the first step.

f. The total wavefront deformation with respect to the osculating sphere is the sum of the primary aberration wavefront deformations and the wavefront deformations calculated with trapezoidal integration.

Any error in the calculated primary aberration coefficients due to the approximations made is unimportant and does not generate any error in the final

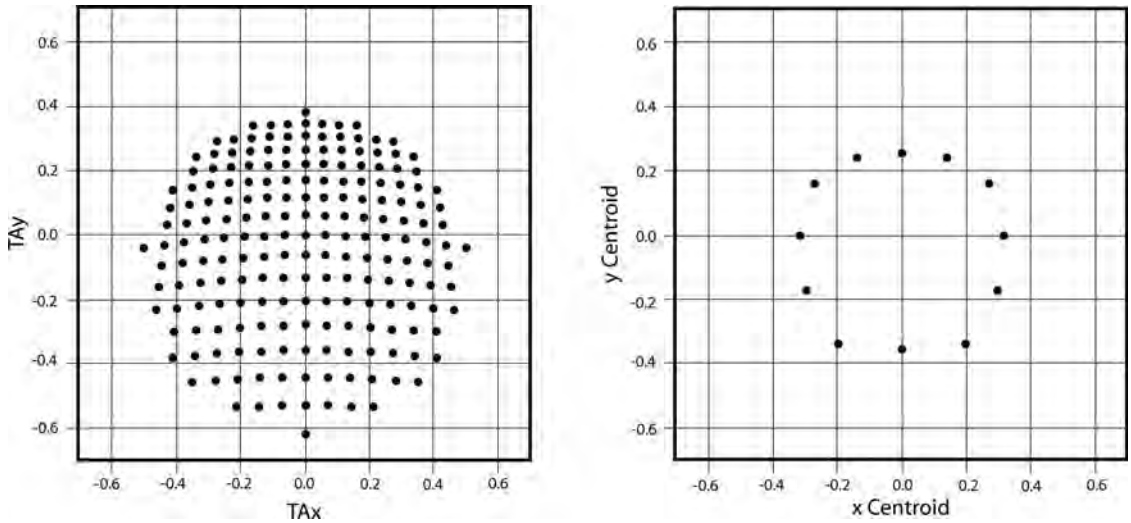

Fig. 5. (left) Computer-generated Hartmanngram with a coma coefficient $C = 4$ and defocusing $L = 5$. (right) Centroids for the circular sectors. The radial distance for these circular sectors, evaluated from the Hartmanngram, is $\bar{\rho}' = 0.326 - 0.055 \sin\theta$. The same distance, calculated from Eq. (20), is equal to $\bar{\rho}' = 0.333 - 0.060 \sin\theta$. The unit of length is the semidiameter of the pupil.

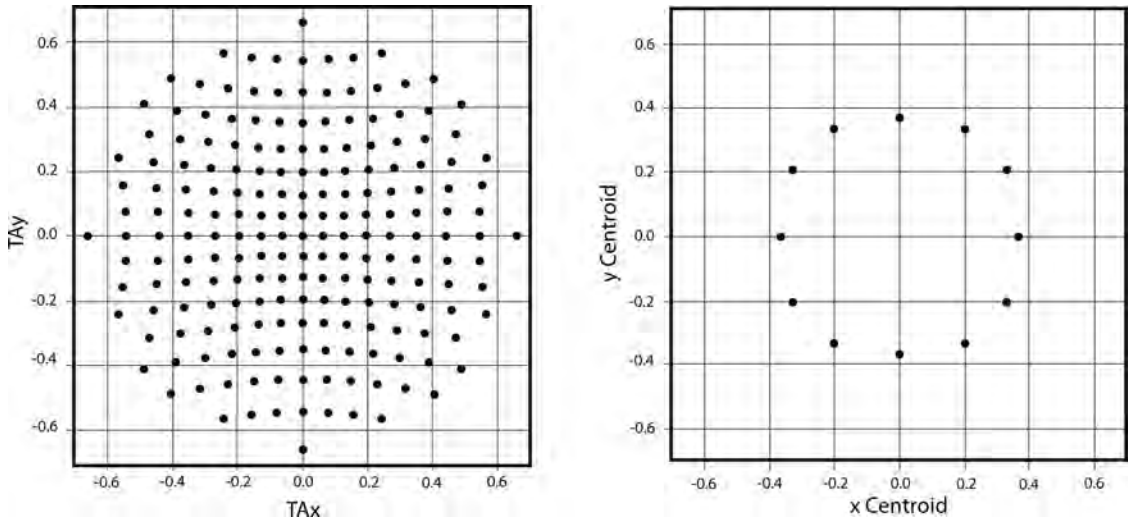

Fig. 6. (left) Computer-generated Hartmanngram with a spherical aberration coefficient $D = -4$ and defocusing $L = 5$. (right) Centroids for the circular sectors. The radial distance for these circular sectors, evaluated from the Hartmanngram, is $\bar{\rho}' = 0.380$. The same distance, calculated from Eq. (20), is equal to 0.407. The unit of length is the semidiameter of the pupil.

result. This is because the reference for the transverse aberration was measured with respect to the synthetic Hartmanngram produced with those aberration coefficients.

The authors wish to thank Consejo Nacional de Ciencia y Tecnología for the financial support.

References

1. R. A. Gonsalves, "Phase retrieval from modulus data," J. Opt. Soc. Am. **66**, 961–964 (1976).
2. R. W. Gerchberg and W. O. Saxton, "A practical algorithm for the determination of phase from image and diffraction plane pictures," Optik (Jena) **35**, 237–246 (1972).
3. P. Artal, J. Santamaría, and J. Bescós, "Retrieval of wave aberration of human eyes from actual point-spread-function data," J. Opt. Soc. Am. A **5**, 1201–1206 (1988).
4. N. Nakajima, "Phase retrieval from two intensity measurements using the Fourier series expansion," J. Opt. Soc. Am. A **4**, 154–158 (1987).
5. G. R. Brady and J. R. Fienup, "Nonlinear optimization algorithm for retrieving the full complex pupil function," Opt. Express **14**, 474–486 (2006).
6. F. Roddier, C. Roddier, and H. Roddier, "Curvature sensing: a new wavefront sensing method," Proc. SPIE **976**, 203–209 (1988).
7. R. Barakat and B. H. Sandler, "Determination of the wavefront aberration function from measured values of the point-spread function: a two-dimensional phase retrieval problem," J. Opt. Soc. Am. A **9**, 1715–1723 (1992).
8. H. R. Suiter, *Star Testing Astronomical Telescopes* (Willmann-Bell, 1994).
9. J. Hartmann, "Bemerkungen uber den Bau und die Justirung von Spektrographen," Zt. Instrumentenkd. **20**, 47 (1900).
10. M. Tscherning, "Die monochrotischen Aberrationen des menschlichen Auges," Z. Psyol. Physiol. Sinn. **6**, 456–471 (1894).
11. D. Malacara-Doblado and I. Ghozeil, "Hartmann, Hartmann-Shack, and other screen tests," in *Optical Testing Shop*, D. Malacara-Hernandez, ed. (Wiley, 2007), pp. 361–397.

ANEXO 7

Hartmann and Shack-Hartmann Tests, Applications and Recent Developments

Daniel Malacara-Hernández and Armando Gómez-Vieyra
Centro de Investigaciones en Optica, A.C.
Loma de Bosque 115
León, Gto. México
dmalacara@cio.mx

Abstract: The Hartmann test dates back from 1904 and it is still widely used in its original configuration, basically using the same principle. Their most popular applications will be described. Techniques to measure the eye aberrations will be described.

OCIS Codes: 120.3930 Metrological Instrumentation.

1. Introduction

The venerable Hartmann test whose history dates back from 1904 Hartmann [1] and has some antecedents in the eye test by Tscherning [2] is still widely used in their original configuration as well as in several other forms, but basically using the same principle. In this talk some of their most popular applications and modifications will be described. Special mention of recent techniques to measure the eye aberrations will be described.

This test, illustrated in Fig. 1 uses a screen with an array of holes placed close to the entrance or exit pupil of the system under test.

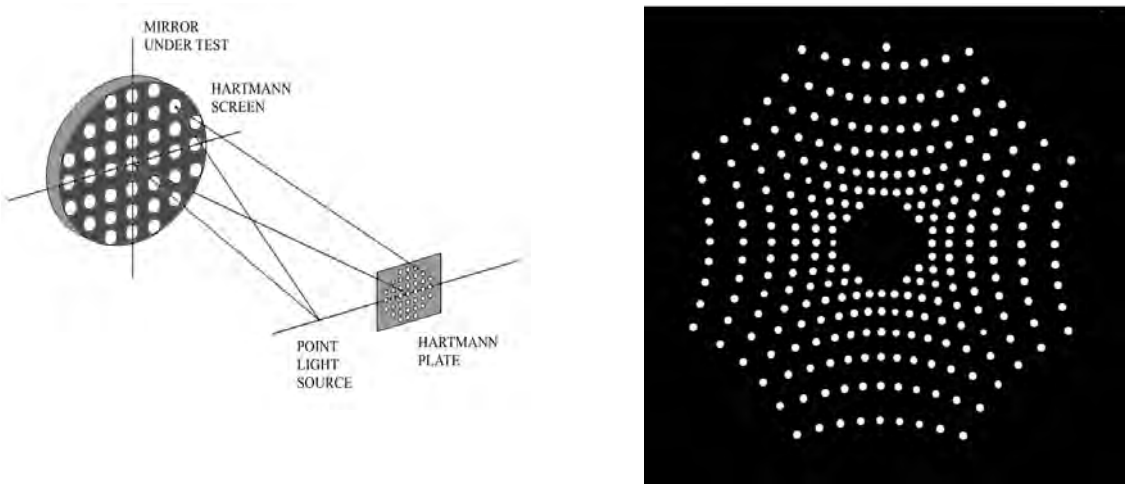

Figure 1.- Hartmann test perspective schematics showing the Hartmann screen over a mirror to be tested, with the spots produced by a parabolic telescope primary mirror.

2. Wavefront or Surface Retrieval

The typical screen is a rectangular array of holes. The wavefront deformations $W(x,y)$ can be retrieved from spots deviations with respect to their ideal positions TA_x and TA_y, related by the expressions:

$$\frac{\partial W(x,y)}{\partial x} = \frac{TA_x(x,y)}{r} \qquad (1)$$

and

$$\frac{\partial W(x,y)}{\partial y} = \frac{TA_y(x,y)}{r} \qquad (2)$$

r is the distance from the pupil of the wavefront to the Hartmann plate. Several different algorithms had been proposed to carry out this calculations, for example, by Ghozeil and Simmons [3] and Southwell [4].

3. Shack- Hartmann Test

Platt and Shack [5] (1971), proposed using a lenticular screen, instead of the screen with holes, as illustrated in Fig. 2. As a result the spot is focused, producing a higher accuracy but reduced dynamic range. Also, this test is for collimated beams instead of convergent beams as in the original test.

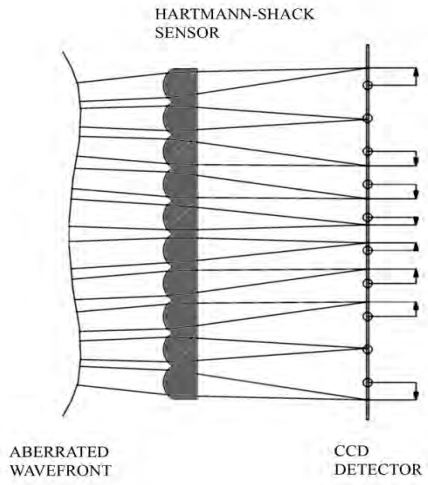

Figure 2.- Hartmann-Shack test using a plate with a rectangular array of lenslets.

This test has been quite successful to measure many different optical systems, but perhaps the most relevant and common one is the measurement of the aberrations of the human eye as described by Liang et. al. [6]. There are several research groups now quite active on this field and had obtained impressive results, for example, the group at the University of Rochester whose leader is David Williams and the group at the Universidad de Murcia with Pablo Artal as its leader.

5. Testing with an Array of Light Sources or Printed Screens

Another modification of the classical Hartmann test is performed by using an array of independent light sources, as illustrated in Fig. 3. The basic principle is the same and there are several possible different configurations, depending on the type of optical element or system to be tested. If the lens is illuminated by a wavefront with a distortion that just matches the spherical aberration, the refracted wavefront will be spherical and thus focused at single focus.

The distance from the ray intersection to the ideal ray intersection in the observation plane can be interpreted as the transverse aberration. It must be noticed that since neither the pinhole nor the light sources are infinitely small, the light spots being observed are not small either. As the classic Hartmann test, the centroid of the spot can be taken. This measurement principle can be used to test lenses or optical surfaces.

A ruled screen, that is, a screen with two rectangular arrays of straight lines drawn on it can be used instead of using arrays of point light sources, as described by López-Ramírez et.al. [7] and shown in Fig. 4.

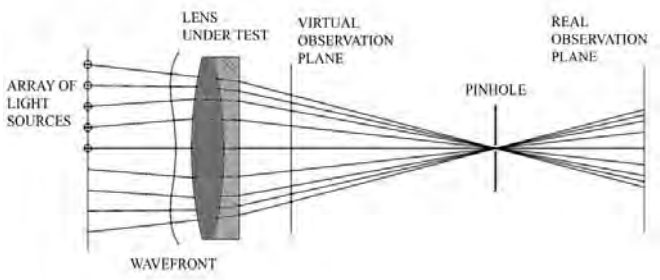

Figure 3.- Testing a convergent lens with an array of light sources in front of the lens. A small stop at the imaging lens selects only the rays that pass through a common focus.

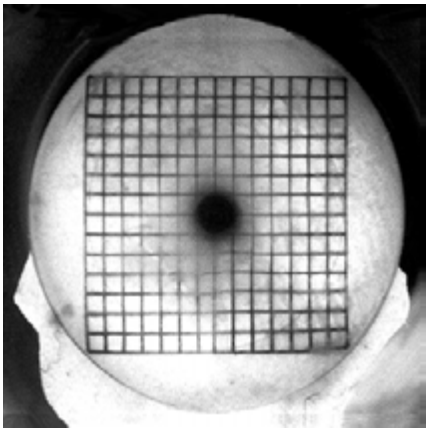

Figure 4.- Testing a convergent lens by observing a ruled screen located at the front focal plane of the lens.

6. References

[1] Hartmann J., "Objektuvuntersuchungen," *Zt. Instrumentenkd.*, **24**, 1 (1904).

[2] Tscherning M., Die monochrotischen Aberrationen des menschlichen Auges, *Z. Psyol. Physiol. Sinn*. **6**, 456-471 (1894).

[3] Ghozeil I. And J. E. Simmons, "Screen Test for Large Mirrors," *Appl. Opt*., **13**, 1773-1777 (1974).

[4] Southwell W. H., "Wave-Front Estimation from Wave-Front Slope Measurements," *J. Opt. Soc. Am.*, **70**, 998 (1980).

[5] Pratt B. C. and R. V. Shack, " Lenticular Hartmann Screen," *Opt. Sci. Newsl..*, **5** , 15-16 (1971),

[6] Liang J., B. Grimm, S. Goelz and J. F. Bille, "Objective Measurements of the Wave Aberrations of the Human Eye with the Use of the Hartmann-Shack Wave-Front Sensor," *J. Opt. Soc. Am.*, **11**, 1949-1957 (1994).

[7] López-Ramírez J. M., D. Malacara-Doblado, and D. Malacara-Hernández, "New Simple Geometrical Test for Aspheric Lenses and Mirrors," *Opt. Eng.*, **39**, 2143 (2000).

ANEXO 8

Methodology for the third order astigmatism compensation in off-axis spherical reflective systems

Armando Gomez-Vieyra[1] and Daniel Malacara-Hernández[1,*]

[1] *Centro de Investigaciones en Óptica A.C, Loma del Bosque 115, C.P. 37000, León, Guanajuato, México*

[*] *Corresponding author: dmalacara@cio.mx*

Abstract

The main constraint of classical off-axis reflecting systems is the third order astigmatism that has long been a research topic of interest. This astigmatism in off-axis spherical reflective imaging systems can be eliminated by the proper configuration. These configurations could be derived from the marginal ray fans equation and they are valid for small angles of incidence. The conditions for the astigmatism compensation in configurations with two and three off-axis mirrors have been derived and analyzed, which has not been reported previously. The expression that defines the conditions for primary astigmatism compensation in a four-mirror system is presented. This shows that the marginal ray fans equation can be used to obtain the condition for astigmatism compensation of a reflective system with any number of mirrors. The developed methodology is verified by ray-tracing analysis of some examples.

OCIS codes: 080.2740, 080.4035, 220.1000.

Introduction

Off-axis reflective systems without rotational symmetry, also known as oblique incidence systems or tilted-decentered systems, have long been a research topic of interest [1-4]. Recently, the optical design of these systems has been applied in laser cavities, spectrographs and retinal adaptive optics imaging systems. It is well known, that the main constraint of classical off-axis reflecting systems is the third order astigmatism, also known as linear or primary astigmatism, which can be eliminated as it will be shown here, by the proper configuration. Rosendahl [5] showed that the Czerney-Turner arrangement of afocal spherical mirror telescope cannot minimize the linear astigmatism for the symmetrical and the antisymetrical cases, if the meridional planes are coplanar. Moreover, he showed that it is possible to compensate the coma for the symmetric configuration. Besides, he compensated the astigmatism with the introduction of two convex mirrors in the array. In recent years, Chang *et al.*[6] eliminated the linear astigmatism in a confocal off-axis conic reflective imaging system with the tilt angles of the image and object planes. However, this introduction of conical surfaces involves an additional cost in these systems. In addition, Web *et al.*[7, 8] described the astigmatism introduced by the off-axis arrangement when reporting the first confocal laser scanning ophthalmoscope, and later by Burns *et al.*[9] in the adaptive optics retinal imaging systems. In his work, Webb *et al.*[7, 8] suggested an off-the-plane perpendicular folding of the optical setup to reduce the astigmatism in the retinal planes. It is based in the marginal ray fans equation as shown by Gómez-Vieyra *et al.* [10] for afocal telescopes. In this work, we present the methodology to reduce the astigmatism in multi-spherical mirror system, with a folding plane of the optical setup or with the combination of convex and concave mirrors, based in the marginal ray fans equation.

Third order astigmatism of a single off-axis spherical mirror

An extension of Gaussian or paraxial optics to off-axis imaging with a fan of rays such that a line going from the center of the pupil to the point where a ray in the beam crosses the pupil, forms an angle θ with the meridional plane [11], for spherical mirrors takes the form:

$$\frac{1}{s_\theta}+\frac{1}{s_\theta'}=\frac{2\cos I}{r(1-\cos^2\theta\sin^2 I)} \tag{1}$$

with I being the angle of incidence of the principal ray onto the mirror, s_θ the object distance, s_θ' the marginal image distance and r the mirror radius of curvature. Rays in all fans are considered to be paraxial in nature and Eq. 1 determined the marginal images along the principal ray. For $\theta=0$ and $\theta=\pi/2$, one recovers the more familiar Coddigton equations [12, 13] that give the positions for the tangential and sagittal images (Fig. 1) as,

$$\frac{1}{s_s}+\frac{1}{s_s'}=\frac{2\cos I}{r}, \tag{2}$$

$$\frac{1}{s_t}+\frac{1}{s_t'}=\frac{2}{r\cos I}. \tag{3}$$

As it will be seen later, sometimes is convenient to rewrite the ray fans equation in terms of vergences $\phi=1/s,$ rather than distances,

$$\phi_\theta+\phi_\theta'=\frac{2\cos I}{r\left(1-\cos^2\theta\sin^2 I\right)}. \tag{4}$$

Then, the difference between the positions (or the vergences) of the sagittal and tangential image is

$$\Delta=s_s'-s_t', \tag{5}$$

which is directly related to the magnitude of astigmatism present in the mirror or in the system.

Thus, for a system with multiple spherical mirrors, the linear astigmatism can be analyzed with Eqs. 2, 3, and 5. We traced the marginal fan rays as commonly performed with thin lenses, considering only that if the meridional planes are common, the sagittal ray fan will propagate obeying Eq. 2 and the tangential ray fan will propagate according to Eq. 3. If any of the meridional mirror planes change of orientation, so do the rest of the marginal planes. For example, in a muti-mirror system, changing the orientation of the meridional plane orientation angle of any component perpendicularly, the sagittal image before the changed plane will become the next tangential object, propagating with Eq. 3. The tangential image before the changed plane will become the next saggital object, propagating with Eq. 2. The relation for astigmatism remains intact.

In the case of arbitrary change of the tangential plane orientation θ, we use Eq. 4, for the new tangential plane, and $\theta + \pi/2$ for the new saggital plane. Using the condition that the difference between the two images (Δ), sagittal and tangential, the entire system is zero, a compensated system of third order astigmatism is obtained. An unconventional reference system is used, such that all distances between are positive, all concave mirrors have positive radii and all concave mirrors have negative radii.

The methodology presented here was previously used by us in a particular case [10]. In the following sections, a generalization and an analysis have been developed for some off-axis spherical multi-mirror system. However, the analysis is not exhaustive, considering that it is enough to appreciate the benefits of the methodology described.

Compensation of third order astigmatism in off-axis two mirror spherical mirror system

Two spherical mirror systems are fully described by six parameters as illustrated in Fig. 2: the angles of incidence I_1 and I_2 of the principal ray onto the mirrors; the mirror radii of curvature r_1 and r_2, and the angle θ between the tangential planes, the separation between the mirrors along the principal ray is d.

As it has been previously introduced, the dominant aberration in these systems is the third order astigmatism. This astigmatism manifests as ray fans passing through different planes that contain the principal ray, focus at different points on it, similar to the case of one mirror off-axis shown in Fig. 1. By an appropriate selection of the system parameters, the astigmatism can be eliminated along the principal ray, by rewriting Eq. 1 as

$$s_\theta' = \frac{r s_\theta \left[\cos^2(\theta)\sin^2(I) - 1\right]}{r - 2 s_\theta \cos(I) - r\cos^2(\theta)\sin^2(I)}, \tag{7}$$

and considering the first mirror as reference. Such, as the first mirror tangential plane orientation $\theta=0$, and the first mirror saggital plane has the orientation $\theta=\pi/2$. The second mirror meridional plane has the orientation $\theta=\theta_2$ and the second mirror saggital plane orientation $\theta=\theta_2+\pi/2$. Substituting the system parameters in Eq. 7 yields

$$s_0' = \frac{r_1 s_0 \left[\sin^2(I_1) - 1\right]}{r_1 - 2 s_0 \cos(I_1) - r_1 \sin^2(I_1)} \tag{8}$$

$$s_{\pi/2}' = -\frac{r_1 s_{\pi/2}}{r_1 - 2 s_{\pi/2} \cos(I_1)} \tag{9}$$

$$s_{\theta_2}' = \frac{r_2 s_{\theta_2} \left[\cos^2(\theta_2)\sin^2(I_2) - 1\right]}{r_2 - 2 s_{\theta_2} \cos(I_2) - r_2 \cos^2(\theta_2)\sin^2(I_2)} \tag{10}$$

$$s_{\theta_2+\pi/2}' = \frac{r_2 s_{\theta_2+\pi/2} \left[\cos^2(\theta_2+\pi/2)\sin^2(I_2) - 1\right]}{r_2 - 2 s_{\theta_2+\pi/2} \cos(I_2) - r_2 \cos^2(\theta_2+\pi/2)\sin^2(I_2)} \tag{11}$$

Substituting $s_0 = s_{\pi/2} = s$, $\theta_2 = \theta_\Delta$, $s_{\theta 2} = s_0' = s_{\theta\Delta}$, and $s_{\theta 2+\pi/2} = s_0' = s_{\theta\Delta+\pi/2}$ into Eqs. 8, 9, 10, and 11, yields

$$s_\Delta' = \left\{ \frac{-2s + r_1 \cos(I_1)}{2ds - (d+s) r_1 \cos(I_1)} + \frac{2\cos(I_2)}{r_2 \left[1 - \cos^2(\theta_\Delta) \sin^2(I_2) \right]} \right\}^{-1} \tag{12}$$

and

$$s_{\Delta+\pi/2}' = \left\{ \frac{-2s\cos(I_1) + r_1}{2ds\cos(I_1) - (d+s) r_1} + \frac{2\cos(I_2)}{r_2 \left[1 - \sin^2(\theta_\Delta) \sin^2(I_2) \right]} \right\}^{-1}, \tag{13}$$

therefore

$$\Delta = -\frac{r_2 \left[-1 + \sin^2(\theta_\Delta) \sin^2(I_2) \right] \left[2ds\cos(I_1) - (d+s) r_1 \right]}{2 \left[2ds\cos(I_1) - (d+s) r_1 \right] \cos(I_2) + r_2 \left[-1 + \sin^2(\theta_\Delta) \sin^2(I_2) \right] \left[2s\cos(I_1) - r_1 \right]} + \frac{r_2 \left[-1 + \cos^2(\theta_\Delta) \sin^2(I_2) \right] \left[2ds\sec(I_1) - (d+s) r_1 \right]}{2 \left[2ds\sec(I_1) - (d+s) r_1 \right] \cos(I_2) + r_2 \left[-1 + \cos^2(\theta_\Delta) \sin^2(I_2) \right] \left[2s\sec(I_1) - r_1 \right]}. \tag{14}$$

For small angles of incidence, Eq. 14 can be expanded in power series of I_1 and I_2 to the first order as

$$\Delta = \frac{2s^2 r_1 r_2^2 I_1^2}{\left\{ 4ds - 2sr_2 + r_1 \left[-2(d+s) + r_2 \right] \right\}^2} + \frac{2 \left\{ \cos(2\theta_\Delta) \left[-2ds + (d+s) r_1 \right]^2 r_2 \right\} I_2^2}{\left\{ 4ds - 2sr_2 + r_1 \left[-2ds + (d+s) r_1 \right] \right\}^2}. \tag{15}$$

As the condition for compensation of third order astigmatism is $\Delta = 0$, then solving Eq. 15 for the angle of incidence I_2 and substituting θ_Δ for θ yields

$$I_2 = \frac{s\sqrt{r_1 r_2} I_1}{(-2ds + (d+s) r_1) \sqrt{-\cos[2\theta]}} \tag{16}$$

The general condition to cancel the astigmatism for different configurations along the principal ray has been met. As result, the four possible general configurations, according to the

mirrors used in the system, are illustrated in Fig. 3. The analysis of the compensation conditions for the general configurations is summarized in Table 1, where, the cases can be subdivided into regions of compensation, according to the configurations. Convex-convex mirror configuration and concave-concave mirror configuration are not compensated in a single saggital plane, following the conditions listed in the Table 1. As for the mixed cases, the compensation can be achieved in a single meridional plane or in a folding less than 45°.

Also, as shown in the Table 1, there are singularities for

$$r_1 = \frac{2ds}{d+s} \tag{17}$$

and

$$|\theta| = 45° \text{and } 135° . \tag{18}$$

Thus, there are values that are not allowed for the compensation of astigmatism, i.e. are values which can not eliminate the astigmatism.

It is possible find all these equations and the equations of the next section in terms of vergence with help of Eq. 4. The notation of the Ec.16 in vergences is

$$I_2 = \frac{\sqrt{r_1 r_2} I_1}{\left(-2d + (d+s) r_1 \phi\right) \sqrt{-\cos[2\theta]}} , \tag{19}$$

which is comfortable to use in configurations where the object is at infinity.

The fact that we do not have a system with only one tangential plane produces a rupture of the symmetry of the system. Consequently, the coma in two directions, the 45° degrees astigmatism, and other asymmetric aberrations are presented in the system.

Compensation of third order astigmatism in off-axis three mirror spherical mirror system

Extending the methodology presented in the previous section, the analysis to the case of a system with three off-axis spherical mirrors will be presented. Three spherical mirror systems are fully described by nine parameters as shown in Fig. 4: the angles of incidence I_1, I_2 and I_3 of the principal ray onto the mirrors; the mirror radii of curvature r_1, r_2, and r_3, the angle θ defined by the folding of the last mirror, and the separation between mirrors along the principal ray is d_1 and d_2. Only one folding has been chosen in order to simplify the analysis.

With the same methodology developed in the preceding section, the general equation for the minimization of the astigmatism in the off-axis three spherical mirror systems has been obtained:

$$I_3 = \frac{r_2 r_3 \sqrt{s^2 r_1 r_2 I_1^2 + \left[-2sd_1 + \left(s + d_1\right) r_1\right]^2 I_2^2}}{\left\{d_1\left(2s - r_1\right)\left(2d_2 - r_2\right) + sr_1 r_2 + d_2\left[-2sr_2 + r_1\left(-2s + r_2\right)\right]\right\}\sqrt{-\cos\left(2\theta\right)}} \quad . \tag{20}$$

Equation 20 has been analyzed for its eight possible system configurations (Fig. 5), and as result, the case conditions for the primary astigmatism compensation have been found, as shown in Table 2. This result has different restrictions, dependent of the folding angle and configuration conditions given by

$$s^2 r_1 r_2 I_1^2 + \left[-2sd_1 + \left(s + d_1\right) r_1\right]^2 I_2^2 , \tag{21}$$

that relates to the amount of astigmatism introduced in the first part of the system.

Also, there are singularities for

$$r d_1\left(2s - r_1\right)\left(2d_2 - r_2\right) + sr_1 r_2 + d_2\left[-2sr_2 + r_1\left(-2s + r_2\right)\right] = 0 \tag{22}$$

and

$$\left|\theta\right| = 45° \text{and } 135° . \tag{23}$$

Thus, there are values that are not allowed for the compensation of astigmatism, i.e. there are values which can not eliminate the astigmatism.

Besides, one could use the same methodology for the configuration of three mirrors but with three different meridian planes. Actually, the analysis will be more complicated and because our objective is to show the methodology, we will not discuss it here.

Compensation of third order astigmatism in off-axis four mirror spherical mirror system

The four off-axis spherical mirror system is fully described by twelve parameters, as shown in Fig. 6: the angles of incidence I_1, I_2, I_3 and I_4 of the principal ray onto the mirrors; the mirror radii of curvature r_1, r_2, r_3, and r_4, the angle θ defined by the folding of the last mirror, and the separation between mirrors along the principal ray is d_1, d_2, and d_3. Solely for the purpose of illustrating the potential of this methodology, the equation that defines the primary astigmatism compensation condition in an arrangement of four off-axis spherical mirrors is:

$$
\begin{aligned}
I_4 = \sqrt{\Bigg\{ -\Big[\sec(2\theta) r_3 r_4 \Big(4s^2 \Big\{ d_1^2 r_2 r_3 I_2^2 + \big[-2d_1 d_2 + (d_1 + d_2) r_2 \big]^2 I_3^2 \Big\} + \\
sr_1 \Big\{ r_2 r_3 \big[sr_2 I_1^2 - 4d_1 (s + d_1) I_2^2 \big] - 4 \big[2d_1 d_2 - (d_1 + d_2) r_2 \big] \\
\big[2(s + d_1) d_2 - (s + d_1 + d_2) r_2 \big] I_3^2 \Big\} + \\
r_1^2 \Big\{ (s + d_1)^2 r_2 r_3 I_2^2 + \big[-2(s + d_1) d_2 + (s + d_1 + d_2) r_2 \big]^2 I_3^2 \Big\} \Big) \Big] \Bigg\} / \\
\Big(d_2 \big[r_1 (2s - r_2) + 2sr_2 \big] (2d_3 - r_3) + sr_1 r_2 r_3 - d_1 (2s - r_1) * \\
\big[d_2 (4d_3 - 2r_3) + r_2 r_3 - 2d_3 (r_2 + r_3) \big] + \\
d_3 \big\{ -2sr_2 r_3 + r_1 \big[-2sr_3 + r_2 (-2s + r_3) \big] \big\} \Big)
\end{aligned}
\tag{24}
$$

As one can see the equation is complicated to be analyzed as above. However, some cases can be of particular interest. For example, the result shown by Rosendahl [5] for the

compensation of astigmatism and coma with four spherical mirrors in only one saggital plane can be found.

Example systems

In this section, the performance of two systems is evaluated. Three mirror system with parameters r_1=1000mm, r_2=2000mm, r_3=1500mm, s=800mm, d_1=1500mm, d_2=1750mm, I_1=3°, I_2=5°, *and* I_3=3.93947°. And four mirror system with r_1=1000mm, r_2=2000mm, r_3=1000mm, r_4=200, s=800mm, d_1=1500mm, d_2=1500mm, d_3=1500mm, I_1=3°, I_2=5°, I_3=4, *e* I_4=14.2842°. They were evaluated with and without primary astigmatism compensation in the image plane respectively (Figs. 7 and 8). The spots diagrams were calculated using the ray tracing software from Zemax Development Corporation (Bellevue, Washington, USA) after correcting for defocus.

In addition, it may be appreciated that although the spots are inside the Airy disk, i.e. the system is limited by diffraction, for the compensated astigmatism case, there are remaining aberrations. The coma in two directions, the 45° degrees astigmatism, and other asymmetric aberrations are presented in the system, as shown in the compensated spots diagrams.

Conclusions

Expressions for minimal astigmatism in image plane applicable to off-axis reflective systems were derived using the marginal ray fan equation. Three simple formulae, Eqs. 16, 20 and 24 for the small angle approximation, were obtained. Discussion of the different general configurations (Figs. 3 and 5) and restriction of these formulae has been presented in Table 1 and 2 for systems with two and three mirrors. More complex configurations can be studied with this methodology. In consequence, the fact that the system does not have only one tangential (or

saggital) plane produces a rupture of the symmetry of the system. Hence, the coma in two directions, the 45° degrees astigmatism, and other asymmetric aberrations are introduced in the system when the system is folded. Two examples have been included to illustrate the results collected throughout the presented work.

References

1. R. A. Buchroeder, “Tilted component optical systems,” Ph.D. dissertation (Optical Sciences Center, University of Arizona, 1976).
2. K. P. Thompson, “Aberration fields in tilted and decentered optical systems,” Ph.D. dissertation (Optical Sciences Center, University of Arizona, 1980).
3. J. R. Rogers, “Vector aberration theory and the design of off-axis systems,” in *International Lens Design Conference,* W. H. Taylor and D. T. Moore, eds., Proc. SPIE **554,** 76–81 (1985).
4. J. M. Sasian, “How to approach the design of a bilateral symmetric optical system,” Opt. Eng. **33,** 2045–2061 (1994).
5. G. R. Rosendahl, “Contributions to the Optics of Mirror Systems and Gratings with Oblique Incidence. III. Some Applications,” J. Opt. Soc. Am. **52**(4), 412–415 (1962)
6. S. Chang, J. H. Lee, S. P. Kim, H. Kim, W. J. Kim, I. Song, and Y. Park, "Linear astigmatism of confocal off-axis reflective imaging systems and its elimination," Appl. Opt. 45, 484-488 (2006)
7. R. H. Webb and G. W. Hughes, "Scanning laser ophthalmoscope," IEEE Transactions on Biomedical Engineering **28**, 488-492 (1981).

8. R. H. Webb, G. W. Hughes, and F. C. Delori, "Confocal scanning laser ophthalmoscope," Appl. Opt. **26**, 1492-1499 (1987).
9. S. A. Burns, R. Tumbar, A. E. Elsner, D. Ferguson, and D. X. Hammer, "Large-field-of-view, modular, stabilized, adaptive-optics-based scanning laser ophthalmoscope," J. Opt. Soc. Am. A 24, 1313-1326 (2007).
10. A. Gómez-Vieyra, A. Dubra, D. Malacara-Hernández, and D. R. Williams, "First-order design of off-axis reflective ophthalmic adaptive optics systems using afocal telescopes," Opt. Express 17, 18906-18919 (2009)
11. A. E. Conrady, *Applied optics and optical design*, part 2 (Dover Publications Inc., New York, 1960), Chap XII.
12. D. Malacara, Z. Malacara, *Handbook of Lens Design*, (Marcel Dekker Inc., New York. 2004), Chap. 5.
13. R. Kingslake, *Lens Design Fundamentals*, (Academic Press, San Diego, 1978), Chap 10.

Acknowledgements

The authors acknowledge the support of the Consejo Nacional de Ciencia y Tecnología de México (CONACYT), through scholar grant No. 170266. The authors are indebted to Ricardo B. Flores for the invaluable comments that have greatly improved the manuscript.

Figure Captions

Figure 1. Gaussian and marginal images formation by an off-axis reflective spherical mirror

Figure 2.- Schematic of general off-axis two spherical mirror system.

Figure 3. Possible configurations for a two spherical mirror system.

Figure 4. Schematic of general off-axis three spherical mirror system with one folding plane.

Figure 5. Possible configurations for a three spherical mirror system.

Figure 6. Schematic for general off-axis four spherical mirror system with one folding plane.

Figure 7. Three mirror system. (r_1*=1000mm,* r_2*=2000mm,* r_3*=1500mm, s=800mm,* d_1*=1500mm,* d_2*=1750mm,* I_1*=3°,* I_2*=5°, and* I_3*=3.93947°*). (a) Spot diagram in image plane without astigmatism correction (θ*=0°*). (b) Spot diagram in image plane without astigmatism correction at θ*=90°*.

Figura 8. Four mirror system (r_1*=1000mm,* r_2*=2000mm,* r_3*=1000mm,* r_4*=200, s=800mm,* d_1*=1500mm,* d_2*=1500mm,* d_3*=1500mm,* I_1*=3°,* I_2*=5°,* I_3*=4, e* I_4*=14.2842°*). (a) Spot diagram in image plane without astigmatism correction (θ*=0°*).(b) Spot diagram in image plane without astigmatism correction at θ*=90°*.

Table 1. Configuration conditions for a two spherical mirror system (Fig. 3)

Mirror 1 (M1)	Mirror 2 (M2)	θ for astigmatism compensation
Concave	Concave (Fig. 3a)	$45° < \|\theta\| < 135$
	Convex (Fig. 3b)	$\|\theta\| < 45°$ and $135° < \|\theta\| < 180°$
Convex	Concave (Fig. 3c)	$45° < \|\theta\| < 135$
	Convex (Fig. 3d)	$\|\theta\| < 45°$ and $135° < \|\theta\| < 180°$

Table 2. Configuration conditions for a three spherical mirror system (Fig. 5)

Mirror 1 (M1)	Mirror 2 (M2)	Mirror 3 (M3)	θ for astigmatism compensation
Concave	Concave	Concave (Fig. 5a)	$45° < \lvert\theta\rvert < 135$
		Convex (Fig. 5b)	$45° < \lvert\theta\rvert < 135$
	Convex	Concave (Fig. 5c)	$45° < \lvert\theta\rvert < 135$ for $s^2 r_1 r_2 I_1^2 + \left[-2sd_1 + (s+d_1) r_1\right]^2 I_2^2 > 0$
			$\lvert\theta\rvert < 45°$ and $135° < \lvert\theta\rvert < 180°$ for $s^2 r_1 r_2 I_1^2 + \left[-2sd_1 + (s+d_1) r_1\right]^2 I_2^2 < 0$
		Convex (Fig. 5d)	$45° < \lvert\theta\rvert < 135$ for $s^2 r_1 r_2 I_1^2 + \left[-2sd_1 + (s+d_1) r_1\right]^2 I_2^2 > 0$
			$\lvert\theta\rvert < 45°$ and $135° < \lvert\theta\rvert < 180°$ for $s^2 r_1 r_2 I_1^2 + \left[-2sd_1 + (s+d_1) r_1\right]^2 I_2^2 < 0$
Convex	Concave	Concave (Fig. 5e)	$45° < \lvert\theta\rvert < 135$ for $s^2 r_1 r_2 I_1^2 + \left[-2sd_1 + (s+d_1) r_1\right]^2 I_2^2 > 0$
			$\lvert\theta\rvert < 45°$ and $135° < \lvert\theta\rvert < 180°$ for $s^2 r_1 r_2 I_1^2 + \left[-2sd_1 + (s+d_1) r_1\right]^2 I_2^2 < 0$
		Convex (Fig. 5f)	$45° < \lvert\theta\rvert < 135$ for $s^2 r_1 r_2 I_1^2 + \left[-2sd_1 + (s+d_1) r_1\right]^2 I_2^2 > 0$
			$\lvert\theta\rvert < 45°$ and $135° < \lvert\theta\rvert < 180°$ for $s^2 r_1 r_2 I_1^2 + \left[-2sd_1 + (s+d_1) r_1\right]^2 I_2^2 < 0$
	Convex	Concave (Fig. 5g)	$45° < \lvert\theta\rvert < 135$
		Convex (Fig. 5h)	$45° < \lvert\theta\rvert < 135$

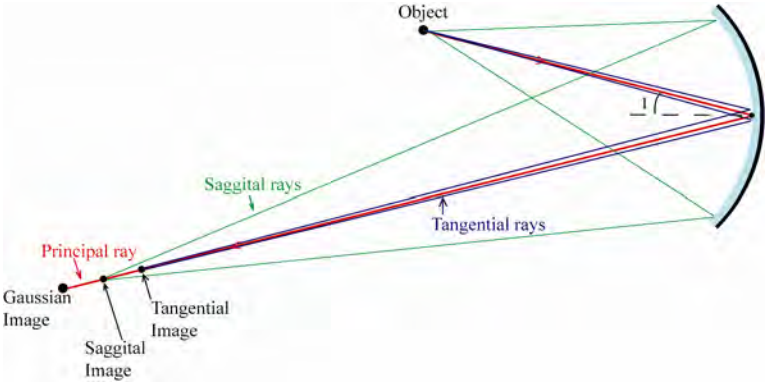

Figure 1.

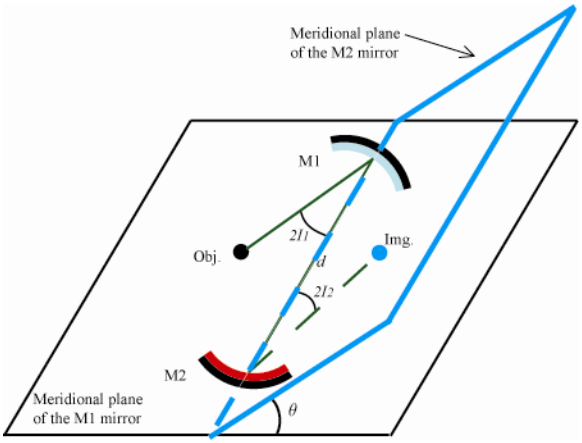

Figure 2.

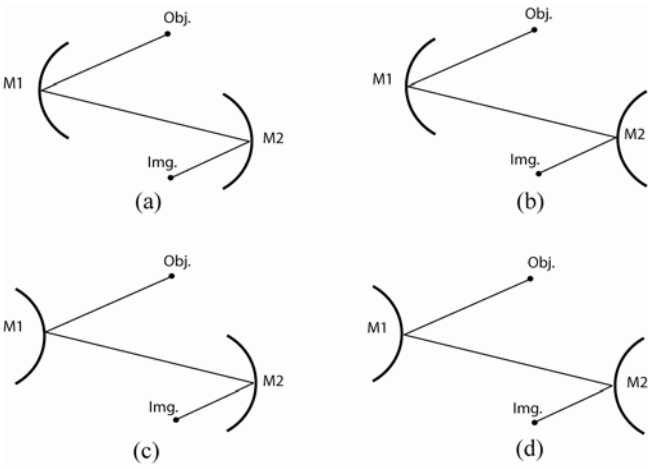

Figure 3.

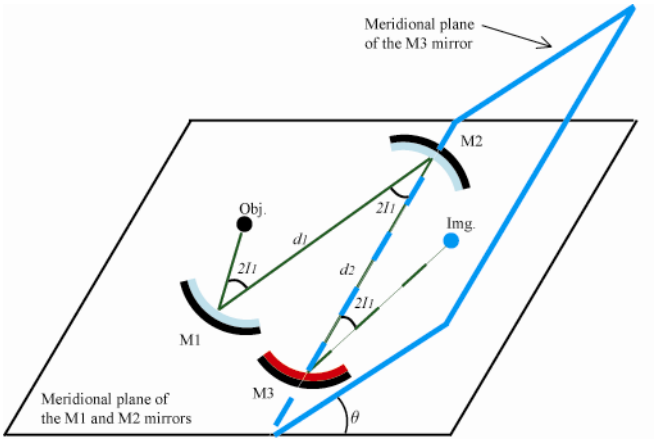

Figure 4.

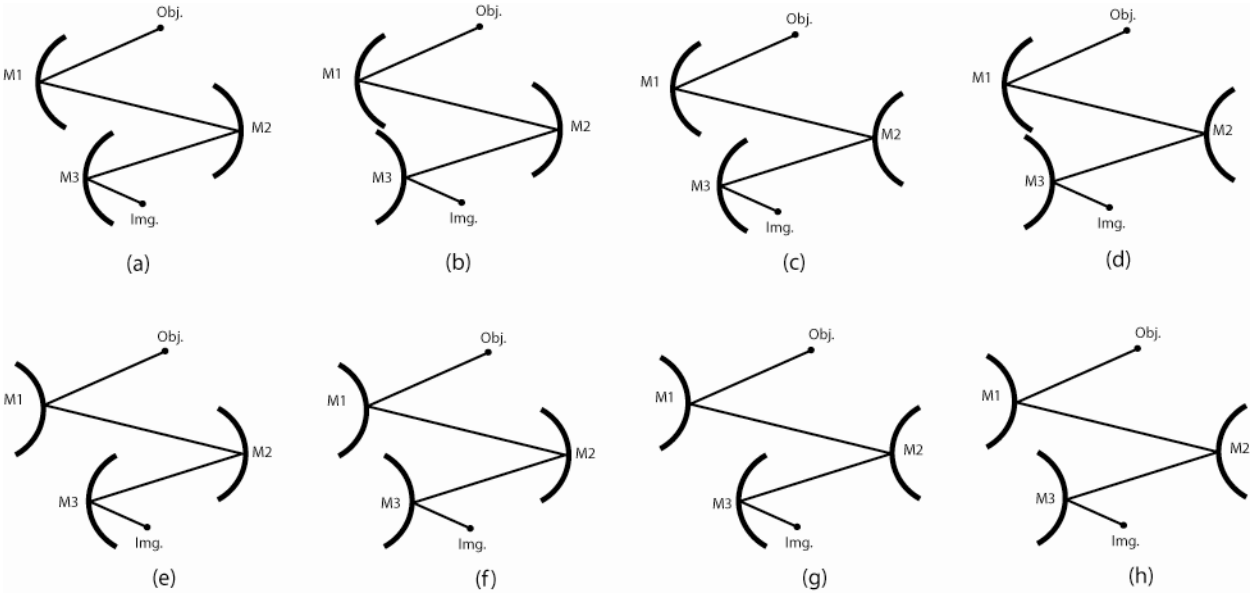

Figure 5

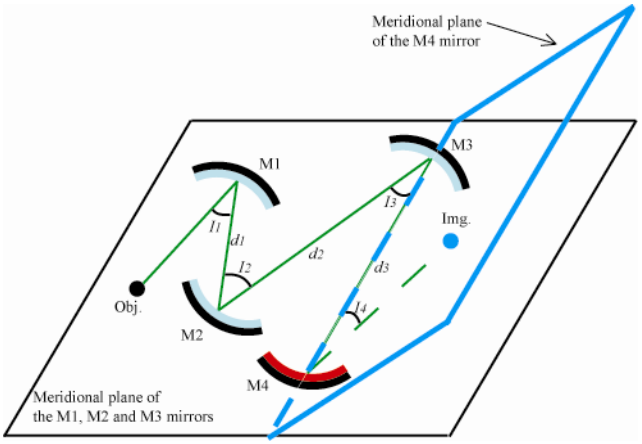

Figure 6.

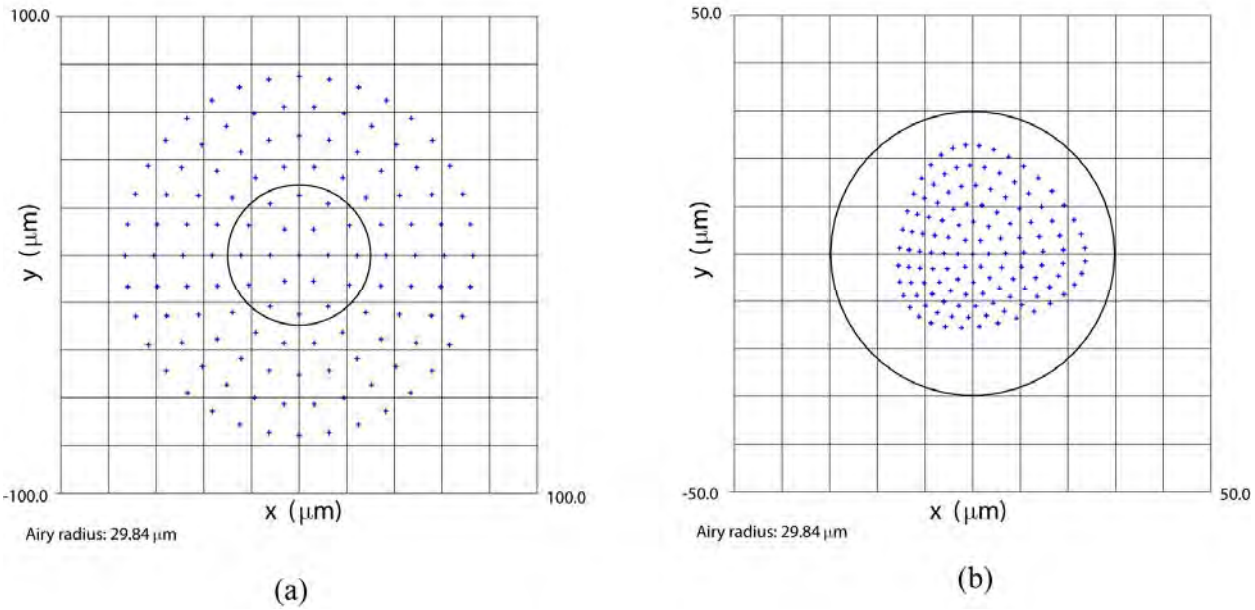

Figure 7.

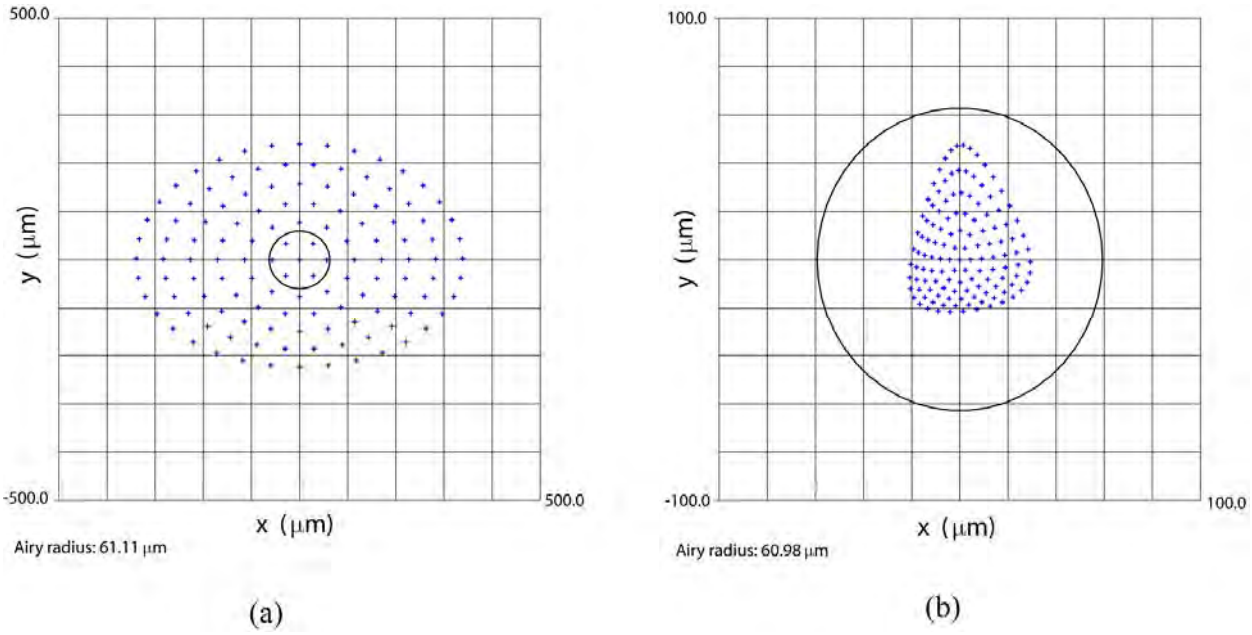
500.0
-500.0
500.0
y (μm)
x (μm)
Airy radius: 61.11 μm
(a)
100.0
-100.0
100.0
y (μm)
x (μm)
Airy radius: 60.98 μm
(b)

Figure 8.